EPFL

Thèse n° 7692

Surface engineering of T cells with polymer nanoparticles to enhance drug delivery to the brain

Présentée le 9 octobre 2020

à la Faculté des sciences et techniques de l'ingénieur
Laboratoire des polymères
Programme doctoral en science et génie des matériaux

pour l'obtention du grade de Docteur ès Sciences

par

Markus SCHUSTER

Acceptée sur proposition du jury

Prof. D. Damjanovic, président du jury
Prof. H.-A. Klok, directeur de thèse
Prof. B. Engelhardt, rapporteuse
Prof. M. Gauthier, rapporteur
Prof. L. Tang, rapporteur

École polytechnique fédérale de Lausanne

2020

The work described in this Thesis has been performed at the École Polytechnique Fédérale de Lausanne from January 2016 until August 2020 under the supervision of Prof. Harm-Anton Klok.

This work was financially supported by the European Commission under a Marie Sklowdowska-Curie Innovative Training Network: BtRAIN – European Brain Barriers Training Network (H2020-MSCA-ITN-2016, n 675619).

Acknowledgments

First of all, I want to thank HAK for supervising my PhD, for giving me helpful advice and letting me persue the scientific questions that I wanted to investigate without any restrictions. Even in times, when research did not go the way, I would have liked, he was always supportive, both professionally and privately. Closely related to that, I also wanted to thank his better half, Eva, for the personal advice she gave me and for all the small coffee chats (in German), that helped me to fight my Bavarian home-sickness. It was an unforgettable time to perform my PhD in your group!

Next, I would like to thank Britta, my second supervisor. For all the issues (and it was a lot of issues) that demanded from me to expand my scope from simple chemistry to biothechnology/biology, she was providing me with the fundamental knowledge of how to tackle them. She also gave life to her baby, “BtRAIN”. Being part of BtRAIN was not only a lot of fun by traveling throughout all of Europe and meeting amazing people, but also helped me scientifically by giving me the chance to perform biological experiments, I would not even have known otherwise. Thank you a lot! By the way, this special thanks also applies to your better half (?!), Urban.

A very special thanks goes to my wife, Tianyu. Before I met her, the scope of my mind barely expanded from Bavaria over two borders to Switzerland. She was literally the key for me to unlock the rest of the world. Her support at home helped me to overcome the darkest times, I had at home and at work, and her liveliness gave me access to the joy of the world. Even in the small flat, we lived in, she found some space for my most beloved pets, Chinchi, Bonbon, and Poppy, which are by now all part of our small family. I could not have done it without you!

Thanks to my former and current office partners, Maxime, Tina, Sabrina and Feng. Even though, I did not see you anymore face-to-face since the Corona-lockdown, I always remember the fun I had with you in our office! I hope you welcome my successor as warmly as you welcomed me. Working with you in one office was unbeatable. Thank you and the whole rest of LP!

A big thanks goes to all the people at the TKI in Berne! Thanks Elisa, for all of the help and practical advice you gave me. Despite, the hard times we had with our in vivo experiments, you always managed to put a smile on my face before I had to take the return train to Lausanne. Thanks Gaby, for your knowledge and experience on IF staining

and for all the stories you told me during my coffee brakes in the incubation times. Even, if working days stretched out to be a bit longer, I could rely on the help and support of both of you!

Last, but not least, a special thanks to my parents and my brother, who enabled me to become what I am today. They supported my under any circumstances and enabled me to pursue all of my goals and dreams without any hesitation. They never lost faith in me and provided me with a safe shelter in my old room at home, whenever I needed it.

List of Abbreviations

^{1}H NMR	proton nuclear magnetic resonance
ADSC	adipose derived stem cell
AMCA	aminomethylcoumarin
APC	antigen presenting cell
API	active pharmaceutical ingredient
bALD	butyraldehyde
BBB	blood-brain barrier
BCA	bicinchoninic acid
BCSFB	blood-cerebrospinal fluid barrier
BMPH	N-ß-maleimidopropionic acid hydrazide
BSA	bovine serum albumin
BSM	bovine submaxillary mucin
BTB	blood-tumor barrier
CAMthiopropanoyl	carbamidomethyl thiopropanoyl
CAT	catalase
CNS	central nervous system
CP	choroid plexus
CPT	camtothecin
cRGD	cyclic Arg-Gly-Asp
CTDR	CellTrackerDeepRed
CTR	CellTrackerRed
CTV	CellTraceViolet
CWB	complete wash buffer
DAPI	4`,6-diamidino-2-phenylindole
DiD	1,1`-dioctadecyl-3,3,3`,3`-tetramethylindodicarbocyanine
DiI	1,1`-dioctadecyl-3,3,3`,3`-tetramethylindocarbocyanine
DiR	1,1`-dioctadecyl-3,3,3`,3`-tetramethylindotricarbocyanine
DLS	dynamic light scattering
DNER	delta and notch-like epidermal growth factor-related receptor
DOGS NTA-Ni	1,2-dioleoyl-sn-glyc-ero-3-[(N-(5-amino-1-carboxypentyl)iminodiacetic acid) succinyl] nickel salt
DOPG	1,2-dioleoylphosphatidylglycerol
DSPE	1,2-distearoyl-sn-glycero-3-phosphoethanolamine
DMSO	dimethyl sulfoxide
DPBS	Dulbecco`s phosphate buffered saline
DTT	1,4-dithiothreitol
EAT	Ehrlich ascites tumor
EPR	enhanced permeation and retention
FACS	fluorescence-activated cell sorting
FND	fusogenic nanodroplet
HBSS	Hank`s balanched salt solution

HCl	hydrochloric acid
H&E	hematoxylin and eosin
HEPES	4-(2-hydroxyethyl)-1-piperazineethanesulfonic acid
$HG2C_{18}$	1.5-dioctadecyl-N-histidyl-L-glutamate
ICAM-1	intercellular adhesion molecule -1
IL-2	interleukin -2
IL-15 Sa	interleukin -15 super-agonist
JAC	lectin jacalin
LC-MSMS	liquid chromatography – tandem mass spectrometry
LFA-1	lymphocyte function-associated antigen -1
MAL	maleimide
MESF	molecular equivalent of soluble fluorophore
MNC	monocyte
MNP	magnetic nanoparticle
MPB-PE	1,2-dioleoyl-sn-glycero-3-phosphoethanolamine-N-[4-(p-maleimidophenyl)butyramide]
MRI	magnetic resonance imaging
MTP	muramyl tripeptide
Mw	molecular weight
MWCO	molecular weight cut-off
NAcCys	N-acetyl cysteine
NaCl	sodium chloride
NaOH	sodium hydroxide
NG	nanogel
NHS-ester	N-hydroxysuccinimide ester
NK	natural killer cells
NP	nanoparticle
PAA	photoactive agent
PAA	poly(acrylic acid)
PAH	poly(allylamine hydrochloride)
PAsp	polyaspartate
PBD	polybutadiene
PBS	phosphate buffered saline
PC	phosphatidyl choline
PDT	photodynamic therapy
PEG	polyethylene glycol
PFA	paraformaldehyde
PGA	poly(glutamic acid)
PHPMA	poly(N-(2-hydroxypropyl) methacrylamide)
PLA	poly(lactic acid)
PLMA	poly(lauryl methacrylate)
PMeSPG	poly(N-3-(methylthio)propyl glycine)
PMPC	poly(2-methacryloyloxyethyl phosphorylcholine)

POPC	1-hexadecanoyl-2-(9Z-octadecenoyl)-sn-glycero-3-phosphocholine
POPE	1-hexadecanoyl-2-(9Z-octadecenoyl)-sn-glycero-3-phosphoethanoleamine
PSar	polysarcosine
PTT	photothermal therapy
PTX	paclitaxel
PVA	poly(vinyl aclohol)
RES	reticuloendothelial system
RM	restimulation medium
RT	room temperature
SDS	sodium dodecasulphate
SM	sphingomyelin
SMCC	succinimidyl 4-(N-meleimidomethyl) cyclohexane-1-carboxylate
SPION	super paramagnetic iron oxide nanoparticle
SVA	succinimidyl valerate
TBS	tris-buffered saline
TCGF	T cell growth factor
TEM	transmission electron microscopy
Tg	glass transition temperature
TGF-β	transforming growth factor β
TGF-βI	transforming growth factor β receptor inhibitor
TNF-α	tumor necrosis factor –α
TRAIL	tumor necrosis factor –α related apoptosis inducing ligand
VCAM-1	vascular cell adhesion molecule -1
WGA	wheat germ agglutinin

Table of Contents

Summary……...1

1. Review on recent developments in cell mediated drug delivery..... 7

1.1. Introduction..... 7

1.2. Cell mediated Drug Delivery 8
1.2.1. Stem Cells 8
1.2.2. Macrophages/Monocytes 8
1.2.3. Neutrophils and Lymphocytes 9

1.3. Strategies for the preparation of nanoparticle loaded cells 9
1.3.1. Trojan horse approach.....10
1.3.2. Covalent cell surface conjugation 16
1.3.3. Non-covalent cell surface immobilization 21

1.4. Conclusions and Outlook..... 30

1.5. References..... 31

2. CD4+ T_{EM}-cell mediated delivery of fluorospheres across the BBB..... 35

2.1. Introduction..... 35
2.1.1. The entry of molecules into the CNS 35
2.1.2. Physiology of the BBB 35
2.1.3. Physiological pathways across the BBB 37
2.1.4. Physiology of the BCSFB.....38
2.1.5. Immunosurveillance of the CNS 38
2.1.6. Hijacking CD4+ TEM cells to deliver model nanoparticles across the BBB.....39

2.2. Experimental Section 40
2.2.1. Materials 40
2.2.2. Methods.....41
2.2.3. Procedures.....42

2.3. Results and Discussion..... 45
2.3.1. Experimental setup of the in vivo experiments 45
2.3.2. Nanoparticle conjugation to CellTracker DeepRed labeled T cells 46
2.3.3. Nanoparticle conjugation to CellTracker Red labeled T Cells.....48
2.3.4. Nanoparticle conjugation to TdTomato transfected T cells 53
2.3.5. Identification of a surface marker for transgenic SJL T cells.....59

2.4. Conclusions..... 59

2.5. References..... 60

3. Conjugation of polymersomes to T cells..... 63

3.1. Introduction..... 63

3.2. Experimental Section 64
3.2.1. Materials 64
3.2.2. Methods.....64
3.2.3. Procedures.....65

3.3. Results and Discussion 70
3.3.1. Preparation and modification of polymersomes 70
3.3.2. Conjugation of polymersomes to Jurkat cells 71
3.3.3. Conjugation of polymersomes to primary T cells (SJL-PLP7) 78
3.4. Conclusions 81
3.5. References 82
3.6. Supporting Information 85

4. Identification of cell surface proteins capable of covalent and non-covalent anchoring of nanoparticles 95

4.1. Introduction 95
4.2. Experimental Section 96
4.2.1. Materials 96
4.2.2. Methods 97
4.2.3. Procedures 97
4.3. Results and Discussion 103
4.3.1. Conjugation of polymersomes to Jurkat cells 103
4.3.2. Confocal microscopy analysis of amine and sialic acid anchored polymersome Jurkat conjugates 107
4.3.3. Key cellular functions of amine and sialic acid anchored polymersome Jurkat conjugates 110
4.3.4. Cellular key functions of amine and sialic acid anchored polymersome SJL/PLP7 conjugates 112
4.3.5. Identification of the surface proteins anchoring the NHS-biotin mediated conjugation of polymersomes to Jurkat cells 117
4.4. Conclusions 120
4.5. References 120
4.6. Supporting Information 122

5. Conclusions and Perspectives 133

Curriculum vitae……..…a

Zusammenfassung

Die Entwicklung Wirkstoffen, die im zentralen Nervensystem (ZNS) aktiv sind, ist eines der herausfordernsten Probleme für Pharmakonzerne. Während die meisten Kandidaten für Wirkstoffe, die im ZNS oder der Tumorumgebung aktiv sind, extrem hohe Bindungskonstanten für deren Ziele aufweisen, können sie keine biologischen Barrieren, wie die Blut-Hirn Schranke oder die Blut-Tumor Barriere überwinden. Dies führt zu einer stark reduzierten Wirksamkeit dieser Medikamente, da sie nur eine kleine Bioverfügbarkeit an deren Zielort aufweisen. Aus diesem Grund werden die meisten Kandidaten für Wirkstoffe von Pharmakonzernen in ersten Screenings ausgeschlossen, nur weil sie deren Ziel nicht erreichen können, selbst wenn sie selber äusserst wirksame Verbindungen darstellen. Eine der neusten Gebiete im Feld des gezielten Transports von Wirkstoffen, der zellvermittelte Transport von Wirkstoffen, wurde etabliert, um diese beiden Probleme zu überwinden. Indem sie eine wirkstoffunabhängige Form zur Erleichterung der Verfügbarkeit von Arzneiwirkstoffen über Barrieren, wie die Blut-Hirn Schranke oder die Blut-Tumor Barriere, hinweg, darstellt, sowie die Bioverteilung von Wirkstoffen im Körper durch eine Kombination verschiedener zielgesteuerter Mechanismen verbessert, zielt diese Disziplin des gezielten Transports von Wirkstoffen darauf ab, eine universelle Methode zur Bereitstellung von Wirkstoffen in Hirn- und Tumorgewebe zu entwickeln, wodurch es uns ermöglicht wäre die schier unendliche Anzahl von bisher ungenutzten ZNS und Tumor aktiven Wirkstoffen zu nutzen.

Kapitel 1 stellt eine Zusammenfassung der neusten Entwicklungen zum gezielten Transport von Wirkstoffen in Hirn- und Tumorgewebe durch einen zellvermittelte Transport dar. Meistens werden dazu Mikro- oder Nanopartikel benutzt, die einen ungezielten, pharmazeutisch aktiven Wirkstoff beinhalten. Durch die Immobilizierung solcher Partikel im Zytosol oder an der Oberfläche von Makrophagen, Lymphozyten, Neutrophilen oder Stammzellen, werden die einzigartigen Eigenschaften dieser Zellen dazu genutzt, den Wirkstoff aktiv und gezielt im Körper zu verteilen. Dieser Effekt wird durch einen selektiven Freisetzungsmechanismus des Wirkstoffes oder des ganzen Partikels am Ziel ergänzt. Die Immobilisierung von Partikeln im Zytosol erfolgt in-vitro, vor der Injektion in den Körper, durch Phagozytose, während die Immobilisierung von Partikeln an der Zelloberfläche in-vitro, durch (nicht) kovalente Bindungen und in-vivo, durch Antikörper vermittelte Bindungen erfolgt.

Kapitel 2 stellt die in-vivo Beurteilung eines zuvor entwickelten Modelsystems dar, das CD4+ T_{EM} Zellen nutzt, die mit bis zu 100 Polystyrene basierten Nanopartikeln durch Maleimid-Thiol-Bindungen, beladen sind. Diese Nanopartikel-T-Zell-Konjugate wurden in früheren Studien erfolgreich genutzt, um Nanopartikel über eine Einzelzellschicht von Hirn-Endothelzellen, welche ein Model der Blut-Hirn Schranke darstellt, zu transportieren. Um deren Potential zu ermitteln, Partikel in das Hirn Parenchyma in-vivo zu transportieren, wurden die Zellen mit verschiedenen Fluoreszenzmarkern im Zytosol markiert, an die Nanopartikel konjugiert und in die Halsschlagader von gesunden Mäusen injeziert. Um Zellen im Parenchyma von Zellen in den Blutgefässen des Hirns zu unterscheieden, wurden die Gehirne in 16µm dicke Schnitte geschnitten, und für Laminin, einem Marker für die endotheliale und parenchymale Basismembran, gefärbt und mittels Fluoreszenzmikroskopie ausgewertet. Kommerziell erhältliche Zytosolmarker reduzierten dabei drastisch die Vitalität der Zellen oder interferierten mit dem Konjugationsprozess der Nanopartikel. Aus diesem Grund wurden selbstfluoreszierende T Zellen, die das Protein TdTomato exprimieren, genutzt, um in weiteren Experimenten den antigenunabhängigen Transport der Nanopartikel in das Hirn-Parenchyma zu beobachten.

Kapitel 3 befasst sich mit verschiedenen Konjugationsstrategieen zur Immobilisierung von biologisch abbaubaren Polymersomen an der Zelloberfläche von T Zellen. Dieses Kapitel stellt den Technologietransfer zu den zuvor in Kapitel 2 erwähnten Polystyrene-Partikeln zu einem pharmazeutisch relevanten System dar, das auf biologisch abbaubaren Polymersomen beruht. Die Oberflächeneigenschaften der Polymersomen, welche eine starke anti-Haftung and biologischen Zellen aufweist, verhindert dabei die kovalente Immobilisierung von Polymersomen an T Zellen. Um dies zu überwinden, wurde diese anti-Haftungseigenschaft durch eine Oberflächenbeschichtung der Polymersomen mit NeutrAvidin aufgehoben. Diese Beschichtung ermöglicht es weiter die Polymersomen durch NeutrAvidin-Biotin Bindung an der Zelloberfläche in einer therapeutisch relevanten Anzahl zu immobilisieren. Die Konjugation von Polymersomen an der T Zelloberfläche ist bis zu 24h stabil, ohne zelluläre Schlüsselfunktionen einzuschränken, wie die Vitalität oder die Fähighkeit der T Zellen an dem Endothelmarker ICAM-1, der die Migration der Zellen vom Blut ins Hirn vermittelt, zu binden.

Kapitel 4 erläutert Methoden, die Membranproteine, die an der Nanopartikel-Zell-Bindung beteiligt sind, zu identifizieren. Dazu wurden Polystyrene Partikel an die Oberfläche von T Zellen durch NeutrAvidin-biotin Bindung immobilisiert. Die Linker

zwischen Nanopartikel und T Zelle, enthielten dabei selektiv spaltpare chemische Gruppen, die es ermöglichen, nach der Spaltung einen Tagg zu hinterlassen, welcher mittels LC-MSMS identifiziert werden kann.

Summary

The development of drugs for the central nervous system (CNS) is one of the most challenging tasks for pharmaceutical industry. While most of the drug candidates acting in the CNS or in the tumor micro-environment show extremely high binding efficiencies to their targets, they cannot cross biological barriers like Blood-Brain Barrier (BBB) and the Blood-Tumor Barrier (BTB). This strongly reduces the efficacy of these drug candidates due to low bioavailability at the target sites. For this reason, a vast majority of drug candidates fail to pass initial screening phases because they simply cannot reach their targets, even though they resemble highly active lead structures. One of the most recent subjects in field of drug delivery, the cell mediated drug delivery, emerged to overcome both of these problems. By providing a drug independent platform to facilitate the trafficking of drug molecules across biological barriers like the BBB or the BTB and by enhancing the biodistribution of the drugs in the body using combinations of different targeting mechanisms, this discipline of drug delivery ultimately aims to develop universal brain and tumor delivery systems that can help to utilize the enormous potential of the immense number of hitherto unused CNS and tumor active drug candidates.

Chapter 1 is a summary of recent approaches for brain and/or tumor delivery of drugs based on cell mediated drug delivery. Most commonly, polymeric nano- or microparticles are utilized to encapsulate a non-targeting active pharmaceutical compound (APC). By immobilizing these particles in the cytosol or on the surface of Macrophages, Lymphocytes, Neutrophils, or Stem Cells, the unique migratory properties of the selected cell type provides part of the active targeting mechanism which is completed by a selective release mechanism of the drug or the whole nano- or microparticle at the target site. The immobilization of the particles in the cytosol of the migrating cells can be accomplished only *in-vitro* before systemic injection into the host utilizing phagocytosis based mechanisms in a Trojan horse approach while the immobilization of the particles on the surface of the migrating cells can be accomplished either in-vitro before systemic injection using covalent or non-covalent immobilization strategies or directly *in vivo* using antibody mediated immobilization strategies in a cellular backpack approach.

Chapter 2 presents the *in vivo* evaluation of a previously developed model system that utilizes CD4+ T_{EM} cells decorated with up to 100 polystyrene based nanoparticles per cell by maleimide thiol conjugation. These nanoparticle T-cell conjugates were previously shown to successfully deliver nanoparticles across a monolayer of brain endothelial cells

in different *in vitro* models of the BBB. To evaluate their particle delivery potential to the brain parenchyma *in vivo*, cells were labeled with different cytosol stains, conjugated to the nanoparticles and injected into the carotid artery of healthy wildtype mice. To distinguish cells that still resided in the brain endothelium and not the brain parenchyma, brains were sectioned into 16µm slices, stained for the parenchymal basement membrane marker laminin and imaged by fluorescence widefield microscopy. As commercially available cytosol stains either drastically reduce cell viability of the T cells or interfere with the nanoparticle conjugation process, intrinsically fluorescent T cells expressing tdtomato were used in further studies to visualize the antigen independent delivery of polystyrene beads to the brain parenchyma.

Chapter 3 explores different conjugation strategies for the immobilization of biodegradable polymersomes onto the surface of T cells. This chapter presents the technology transfer of the previously studied model system which used polystyrene beads to a pharmaceutically relevant carrier system using biodegradable polymersomes. It was shown that the anti-biofouling surface properties of the polymersomes prevented their covalent immobilization on the surface of T cells. However, by surface coating of the particles with NeutrAvidin the surface fouling properties could be improved drastically, enabling the NeutrAvidin-biotin based conjugation of polymersomes to the surface of the T cells in therapeutically relevant amounts. The conjugation of polymersomes to T cells was shown to be stable over 24h without impairing cellular key functions like cell viability or T cell binding to the endothelial inflammatory marker ICAM-1 which mediates the T cell extravasation at the level of the brain endothelium.

Chapter 4 discusses methods to identify the membrane proteins that are utilized throughout the nanoparticle conjugation process to anchor the nanoparticle surface immobilization. Therefore, polystyrene based nanoparticles were conjugated to T cells using NeutrAvidin-biotin based conjugation strategies. The linker between the nanoparticles and the surface proteins was engineered to be selectively cleavable while tagging the proteins for identification by LC-MSMS.

Keywords: Cell mediated drug delivery, cell-surface modification, nanoparticle, polymersome, nanoparticle-cell conjugation, drug shuttle system, brain delivery, BBB, CD4+ T_{EM} cell, extravasation, transendothelial migration, targeted drug delivery.

1. Review on recent developments in cell mediated drug delivery

1.1. Introduction

Targeting of specific tissues and organs is still a major challenge in the field of polymer based drug delivery systems. Targeting strategies can be divided into two major groups, active and passive targeting strategies. The commonly used targeting strategy is the passive targeting using the so called Enhanced Permeation and Retention effect (EPR effect). The EPR effect targets tumor tissue and relies on two factors, firstly, fenestrated capillaries in the tumor microenvironment that are permeable to nanoparticles and secondly, the absence of a lymphatic system in tumor tissue that could drain nanoparticles (NPs) that leaked from the fenestrated capillaries into the extracellular matrix of the tumor tissue. Recent studies, however, reveal that the EPR effect might indeed be efficient in rodents, but is highly heterogeneous in humans because of the inhomogeneous structure of the human tumor microenvironment compared to that of rodents. [1-3] By far, the most prominent example of a FDA-approved drug using the EPR-effect is doxil, a liposomal formulation of doxorubicin. [4] Classical active targeting strategies include the use of antibody and aptamer conjugates [5]. Here, antibodies and aptamers with high binding affinities to the biological target guide the polymer based drug to a close proximity of the target so that the active drug is released in the immediate environment of its action. But despite of their high affinity, these conjugates may still show unsatisfactory biodistributions due to biological barriers. [6-12] To overcome targeting issues as well as biological barriers, circulatory cells with unique migratory properties are used to guide drug loaded nanoparticles to their specific targets. These circulatory cells are highly mobile and show no immunogenicity or toxicity as they usually originate from autologous donors [13]. Pharmaceutically active drugs that are guided by these circulatory cells are typically protected by nanoparticles (NPs), preventing them from metabolic degradation before they reach their target site. This way, the drug delivery system can be additionally tuned to release the drug actively at the target site using trigger responsive NPs, thus minimizing the systemic drug concentration in the body as well as

toxicity as a result of off-target action of the drug. The use of circulatory cells also masks NPs to prevent elimination by the reticuloendothelial system (RES) leading to longer blood half-life times. [14]

The field of cell mediated drug delivery is steadily growing and by now spans over a great variety of different strategies to guide inorganic and organic nanoparticles to most tissues in the body. Therefore, the following review will focus only on the most recent advances (>2015) in the delivery of polymeric nanoparticles and liposomes by circulatory cells like Stem Cells, Monocytes/Macrophages, Neutrophils and Lymphocytes.

1.2. Cell mediated Drug Delivery

1.2.1. Stem Cells

The main advantage of using stem Cells is that they can be very easily loaded with nanoparticles using the Trojan horse approach. [15] Additionally, Stem Cells are typically self-renewable [16] and are relatively easy to harvest and culture as compared to other circulatory cells. [17, 18] They possess strong homing abilities in injured or inflamed tissue [13, 16], where their ability of multi lineage differentiation can positively impact tissue repair and regeneration [18, 19], as well as in (brain) tumors [17, 20-22] where their ability to actively track metastasis opens the possibility to not only target the main tumor but also fight spreading of the tumor via metastases. [13, 23] The main disadvantage of using Stem Cells is the strong rejection of allogeneic transplants, limiting this technology to autologous transplants [19] and a possible induction of tumor formation by the injected Stem Cells. [19] While the later disadvantage is certainly true for the use of embryonal Stem Cells, the use of adult Stem Cells like mesenchymal Stem Cells isolated from adipose tissue (ADSCs) can drastically lower this risk. [16, 19, 22]

1.2.2. Macrophages/Monocytes

Monocytes like Macrophages are Leukocytes that can actively take up nanoparticles by phagocytosis making them the only other cell type to Stem Cells that are typically loaded in a Trojan horse approach. Compared to Stem Cells, they can home in inflamed tissue and tumors [24] and actively track metastases. [25, 26] In fact, Macrophages are the most abundant cell type in the tumor tissue and can make up to 70% of all cells in breast

carcinoma or 40% in glioma. [24, 25] Additionally to Stem Cells, Macrophages possess the ability to migrate across a variety of biological barriers including the Blood-Brain-Barrier (BBB), the Blood-Cerebrospinal Fluid-Barrier (BCSFB), and the Blood-Retina-Barrier (BRB). [27, 28] Common disadvantages of Macrophages are the strong rejection of allogeneic transplants and the high toxicity, even for autologous transplants [29, 30]. In the context of tumor therapies, transplants of Macrophages may promote tumor/metastases growth of several tumors as circulatory Macrophages may get reprogrammed in the tumor microenvironment and start producing tumor growth factors and induce invasive phenotypes of tumors. [24-26, 31, 32]

1.2.3. Neutrophils and Lymphocytes

Neutrophils are the most abundant type of granulophiles and are an essential part of the innate immune system while Lymphocytes are cells of the adaptive immune system that are typically found in the lymphatic system. The three major classes of Lymphocytes used for the cell mediated drug or nanoparticle delivery are Natural Killer cells (NKs), T cells, and B cells. Neutrophils, NKs, and T cells are of special interest in the field of cell mediated delivery as they can home in inflamed tissues and tumors and show enhanced migration properties across biological barriers compared to Macrophages. [28, 33, 34] Typically, Lymphocytes do not phagocytose nanoparticles or take them up by endocytosis and therefore, are commonly loaded using the cellular hitchhiking approach. The only exception to that are NKs, which can be loaded with nanoparticles via adsorptive endocytosis. [35] As a major drawback, Neutrophils and Lymphocytes are relatively hard to isolate and culture *in vitro* [13] and almost exclusively rely on inflammatory signals like cytokines to activate their migration abilities. [36]

1.3. Strategies for the preparation of nanoparticle loaded cells

There are two different strategies for the cell immobilization of nanoparticles. Nanoparticles can be loaded into a cell in a Trojan horse approach or immobilized on the cell surface via non-covalent or covalent interactions in a cellular hitchhiking approach [37]. The following section will discuss each of these strategies in detail and provide a review of the recent research done in the field of cell mediated drug delivery while categorizing the research in one of the following categories.

1.3.1. Trojan horse approach

Named after the infamous Trojan horse in Greek mythology, in this approach nanoparticles are hidden in the interior of a cell similar to the soldiers that were hidden inside the wooden horse during the siege of Trojan. This not only minimizes the contact of the nanoparticles with other cells and prevents premature nanoparticle degradation and offsite toxicity, but also adds another barrier that has to be overcome, once the drug is to be released from the nanoparticle. Typically, this approach is limited to cells that can perform phagocytosis or are able to take up cells using endocytosis [38]. If the uptake is not triggered directly upon adsorptive endocytosis, additional cell penetrating peptides on the surface of the nanoparticles can be used to facilitate their uptake [39, 40]. Table 1 presents an overview of different strategies for the cell immobilization of nanoparticles using the Trojan horse approach that will be discussed further in this chapter.

Table 1: Overview over different strategies for the cell immobilization of nanoparticles using the Trojan horse approach.

Cell Type	*Mechanism*	*Cargo*	*size*	*target*	*Reference*
ADSCs	Endocytosis	SPION loaded PLGA nanoparticles	100nm	astrocytoma	[41]
ADSCs	Endocytosis	Fusogenic nanodroplets	300nm	B16F0 melanoma	[42]
Macrophages	Phagocytosis	PLGA particles	100-200nm	U87 glioma	[43]
Monocytes	BCN-cRGD mediated phagocytosis	Lipid nanoparticles	40nm	4T1 tumor	[39]
Macrophages	MTP mediated phagocytosis	PLA particles	200nm	1205Lu and WM35 melanoma	[40]
Neutrophils	Adsorptive endocytosis	Cationic liposomes	100nm	Postoperative glioma	[35]

In a paper by Huang et al., 100nm sized nanoparticles were formed by the assembly of SPIONs, Cy5.5, Paclitaxel, poly(γ-glutamic acid-co-distearyl γ-glutamate), and PLGA and loaded via endocytosis into ADSCs for the treatment of ALTS1C1 astrocytoma bearing C57Bl/6J mice. [41] The conjugation of the nanoparticles to the ADSCs was shown to shift the biodistribution of the plain nanoparticles from the liver to the brain, where disassembly of the nanoparticles could be achieved by hyperthermia using a high frequency magnetic field acting on the SPION component of the nanoparticles (Figure 1). The treatment with nanoparticle-loaded ADSCs was shown to be superior to control conditions, where a state-of-the-art chemotherapeutic agent (temozolomide) was used, resulting in a 3-fold increase of survival time from 11 to 30 days.

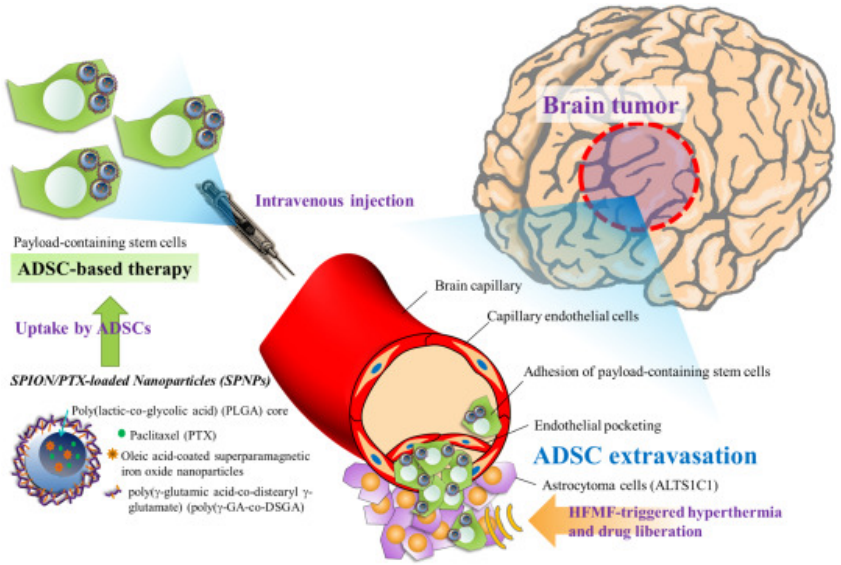

Figure 1: Schematic description of the ADSC-mediated delivery of SPNPs toward brain tumors for dual-modality treatment of orthotopic astrocytoma. Reprinted [41]

Similarly, Ho et al. reported the synthesis of 300nm sized fusogenic nanodroplets (FNDS) by thin-film hydration of a mixture of camptothecin (CTP) with the lipids DOPC, POPE, cholesterol, DiI and DSPE-PEG2000 followed by their endocytotic uptake by ADSCs for the treatment of B16F10 melanoma of C57BL/6JNarl mice. [42] Once the nanoparticle-cell conjugates infiltrated the tumor tissue, the release of CTP was triggered by ultrasonic evaporation of the FNDs (Figure 2). The release of CTP in the tumor micro environment lead to an increased cell death of the tumor cells compared to control tissue, which was confirmed in fluorescence microscopy experiments and hematoxylin and eosin (H&E) stains of the tumor and control tissues.

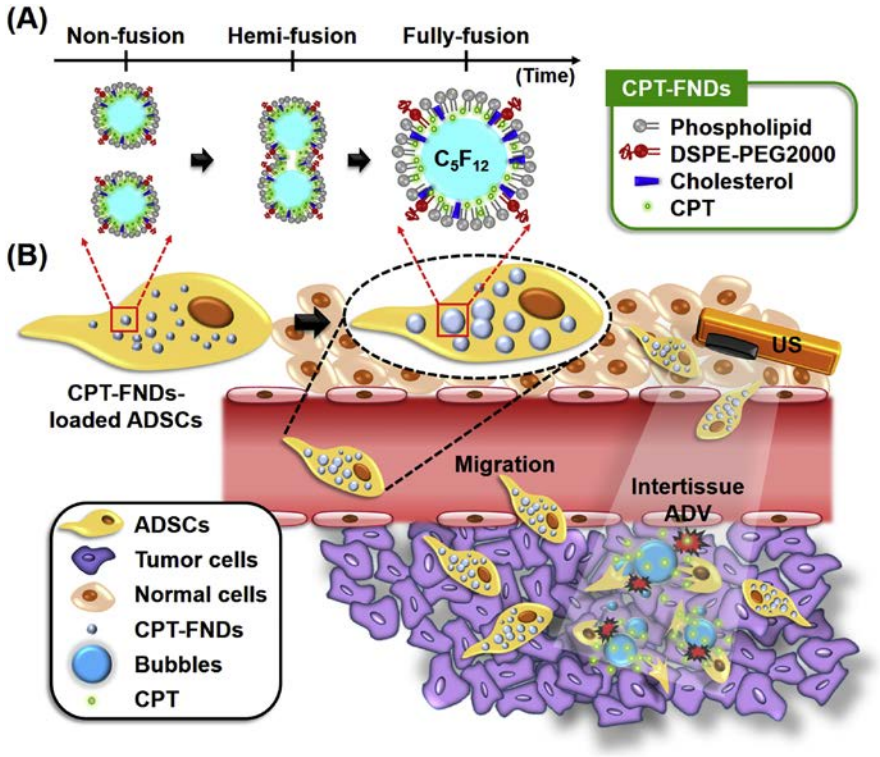

Figure 2: (A) Schematic illustration of CPT-FNDs. (B) Hypotheses for using CPT-FNDs-loaded ADSCs as the tumor-tropic cellular delivery system. The local drug release and physical damage within the tumor were triggered by external US stimulation. Reprinted [42]

Un-mediated phagocytosis was used in the work of Pang et al.. [43] In their work, 100-200nm sized PLGA nanoparticles were formed by the emulsion/solvent evaporation method and loaded with DOX before incubation with RAW264.7 Macrophages (Figure 3). The drug release was achieved by NP degradation in the acidic tumor microenvironment increasing the biodistribution of DOX in the brain of mice with U87 glioma.

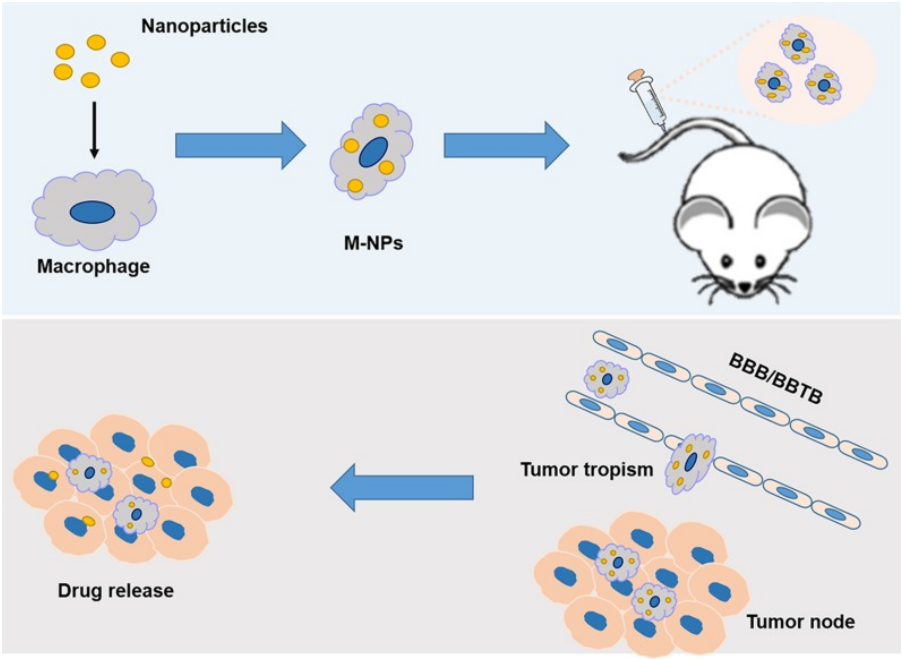

Figure 3: Schematic illustration of the construction of 'Macrophage-NPs' and their targeting delivery into brain tumor. Reprinted [43]

A different approach for nanoparticle uptake of Monocytes was used by Wang et al. [39] In their work, 40nm sized nanoparticles were synthesized by nanoprecipitation of DSPE-PEG2000 and the photoactive agent (PAA) MTD. To enhance the nanoparticle uptake by phagocytosis, Monocytes were consecutively incubated with AC_4ManNAz, an azido-sugar that is used for the metabolic cell surface engineering of the glycocalix with azide groups, and BCN-cRGD, a cyclooctin conjugated version of the cell penetrating peptide cRGD, before co-incubation with the nanoparticles (Figure 4). The pre-treatment of Monocytes with AC_4ManNAz and BCN-cRGD significantly increased the uptake of nanoparticles compared to unmodified Monocytes. To investigate the *in vivo* migration properties of NP-loaded Monocytes, Macrophages from transgenic Luc/GFP mice were isolated, loaded with NPs and injected into 4T1 tumor bearing mice. The Macrophages were tracked by bioluminescence imaging at certain time intervals up to 8d. While the initial bioluminescence was high in liver and spleen at d0, it decreased over time but increased in the tumor with a maximal luminescence at d4. Irradiation of mice with a 660nm laser 5-7d post injection caused a selective temperature increase in the tumor up to 66°C due to the excitation of the PAA leading to a complete inhibition of the tumor growth without additional tumor re-occurrence. The tissue damage was selective for tumor tissue as confirmed by H&E staining.

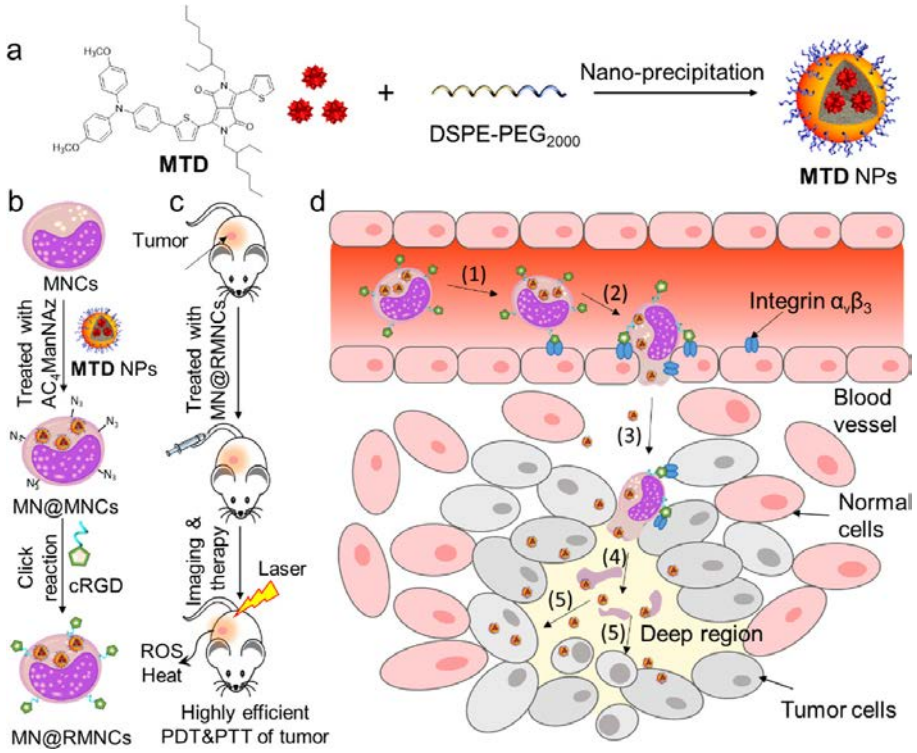

Figure 4: (a) Flow Chart of the Preparation of MTD NPs; (b) Schematic Illustration of the Fabrication of MN@RMNCs; (c) The Therapeutic Strategy of Breast Solid Tumor by Combined PDT and PTT; (d) The Proposed Process of MN@RMNC Delivery into the Tumor Site a(1) MN@MNCs bind with the integrin αvβ3 receptors overexpressed on the surface of cells within tumor tissue, (2) MN@RMNCs move across blood vessel wall and transmigrate into the tumor tissues, (3) MN@RMNCs penetrate and accumulate in the deep regions of the tumors, (4) MTD NPs are released from dead MNCs, (5) MTD NPs are taken up by tumor cells and then produce highly efficient tumor ablation under laser irradiation. Reprinted [39]

Conjugation of Muramyl tripeptide (MTP) to the nanoparticles before incubation with THP-1 Macrophages to enhance their nanoparticle uptake by phagocytosis was used by Xie et. al. [40] In their work, 200nm sized nanoparticles were formed by single emulsion assembly of photoluminescent poly(lactic acid) loaded with the anti-BRAF V600E mutant melanoma specific drug PLX4032 (Figure 5). The nanoparticle cell conjugates were tested only *in vitro* by co-incubation of the conjugates with the two melanoma cell lines 1205Lu (high metastatic) and WM35 (low metastatic). Increasing concentrations of PLX4032 in the NPs as well as increasing numbers of NPs in the Macrophages or NP-loaded Macrophages incubated with melanoma cells showed increasing melanoma cell killing for both cell lines whereas, the viability of the THP-1 cells decreased only minimally.

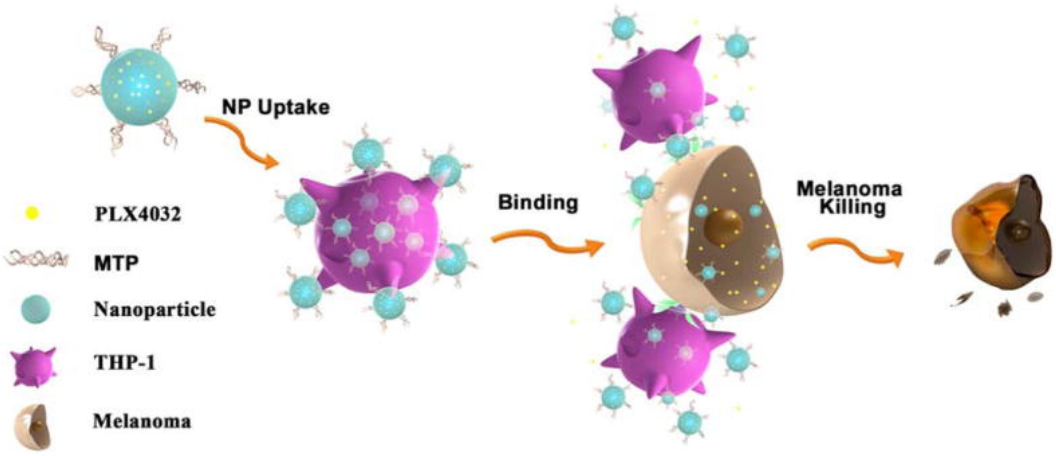

Figure 5: Schematic illustration of the immune cell-mediated nanoparticle (NP) delivery system targeting to cancer cells. Specifically, PLX4032, an anti-BRAF V600E mutant melanoma drug, are loaded within BPLP-PLA nanoparticles. MTP-conjugated BPLP-PLA-PLX4032 nanoparticles bind to THP-1 Macrophages first and they are then delivered to melanoma cells via interactions between THP-1 Macrophages and melanoma cells. The delivered nanoparticles eventually release the PLX4032 drug to kill cancer cells. Reprinted [40]

Another cell type utilizing the Trojan horse approach was used by Xue et al.. [35] In their approach, Neutrophils were loaded by co-incubation with cationic liposomes (CT-NEs) (100nm) exploiting the concept of adsorptive endocytosis (Figure 6). The liposomes were synthesized by thin-film hydration of PC, $HG2C_{18}$ cholesterol, DiR and paclitaxel (PTX) followed by simple coincubation with the Neutrophils. After injection into mice with a surgically removed postoperative glioma, the Neutrophils were recruited by production of pro-inflammatory cytokines (TNF-α and CXCL1/KC) and downregulation of anti-inflammatory cytokines (IL-10) at the operation site as shown by the co-localization of the DiR labeled PTX/CT-NEs with the GFP signal of GFP transfected G422 glioma cells in cryo sections of the brain. Injection of PTX/CT-NEs prevented glioma re-occurrence and drastically increased the 50%-survival time of the mice from 29d of PTX and 38d of PTX-CL (paclitaxel in cationic liposomes) treated mice to 61d.

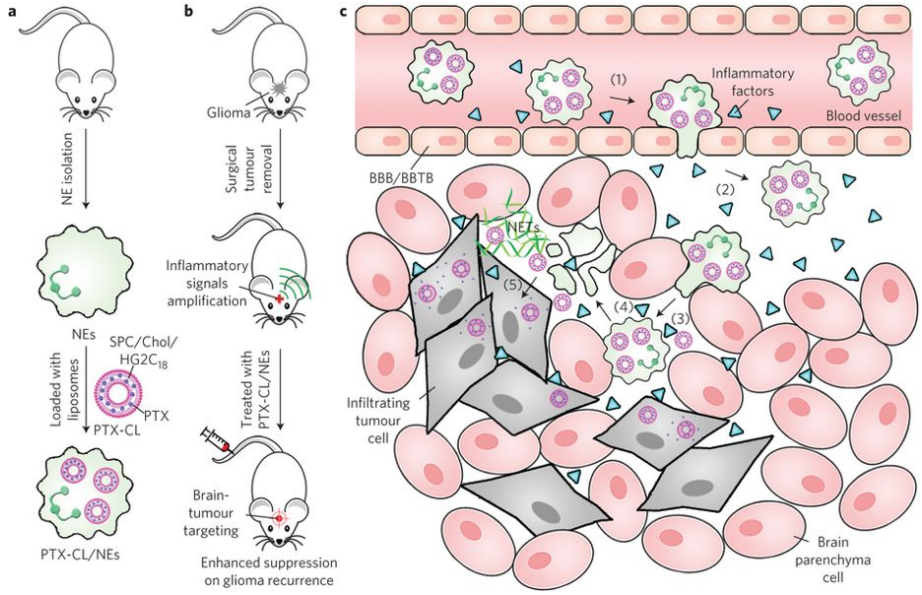

Figure 6: a, Schematic illustration of the preparation of PTX-CL/NEs. SPC, soy phosphatidylcholine; Chol, cholesterol; HG2C18, 1,5-dioctadecyl-N-histidyl-L-glutamate. b, Schematic that shows how PTX-CL/NEs suppress postoperative glioma recurrence in mice. Surgical resection of a tumor amplifies inflammatory signals in the brain, which allows PTX-CL/NEs to target brain tumors, release PTX and suppress glioma recurrence. c, Schematic that shows how PTX-CL/NEs target glioma after intravenous injection into mice whose brain tumor has been resected surgically: (1) inflammatory factors guide the movement of PTX-CL/NEs along the chemotactic gradient; (2) PTX-CL/NEs transmigrate to the inflamed brain across BBB/BBTB; (3) PTX-CL/NEs penetrate the infiltrating tumor cells; (4) PTX-CL/NEs are excessively activated by the concentrated cytokines and release the NETs, which results in a concomitant release of PTX-CL; and (5) PTX-CL delivers PTX into the infiltrating tumor cells to produce an antitumor effect. NETs that primarily consist of DNA from NEs are fibrous extracellular matrices, which were released by NEs on excessive activation by inflammatory cytokines. Reprinted [35]

1.3.2. Covalent cell surface conjugation

In the cellular hitchhiking approach, nanoparticles are immobilized on the cell surface of circulatory cells. In contrast to the Trojan horse approach, the nanoparticles here are exposed to the extracellular micro environment and therefore, can be used for a stimuli-responsive detachment from the cells for example by changes in the pH (e.g. tumor microenvironment) or in the concentration of reactive oxygen species (e.g. inflammatory tissue). One way for the cell surface conjugation of nanoparticles is by covalent reaction between the nanoparticle surface and the cell surface. Typically, this approach utilizes

cell surface amines to conjugate various complementary functional groups like 1) activated carboxy groups via NHS chemistry, 2) carbonyl groups via Schiff base formation or reductive amination, or 3) cell surface thiols via conjugation to Michael acceptor systems like maleimide groups or to pyridylsulfides on the nanoparticle surface [44-46]. Additionally, cell surfaces can be chemically or metabolically modified to enable various bio-orthogonal conjugation approaches. The chemical modification involves oxidation of cell surface alcohols to carbonyl groups enabling the conjugation of amines on nanoparticle surfaces via Schiff base formation and reductive amination or to hydrazine derivatives via hydrazone formation [47-49]. The metabolic modification of the cell surface involves the incubation of cells with acetylated carbonyl- and azido- sugar derivatives of glucose, mannose or galactose [50]. These modified sugar derivatives can be metabolically build into the sialic acid residues present on the cell surface enabling additional bio-orthogonal conjugation to alkyne groups on the nanoparticle surface via copper catalyzed or ring-strain promoted cyclo-addition reactions, or to phosphine groups on the nanoparticle surface via Staudinger ligation [51-53]. In recent years (>2015), however, studies rather focused on the covalent conjugation of cell surface thiols as shown in Table 2, as this strategy is the by far most investigated conjugation strategy already.

Table 2: Overview over different strategies for the cell immobilization of nanoparticles via covalent cell surface conjugation.

Cell Type	*Mechanism*	*Cargo*	*size*	*target*	*Reference*
CD8 T cells	Maleimide-Thiol conjugation	Liposomes and lipid coated PLGA NPs	200nm	EG7-OVA tumors	[45]
CD8 T cells	Maleimide-Thiol conjugation	Liposomes	200nm	TRP SIY prostate tumors	[54]
CD8 T cells	Pyridylsulfide-Thiol conjugation	Liposomes	200nm		[46]

Cell surface thiols were first used for nanoparticle conjugation by Stephan et al. in the group of Prof. Darrel Irvine at MIT. [45] In early studies, they utilized 200nm sized liposomes and lipid coated PLGA NPs that were synthesized from DOPC, DOPG, MPB-PE, DiD and either IL-15 or IL-21 by the emulsion-solvent evaporation method. Conjugation of these NPs to CD8+ T cells (OT-1) was achieved by maleimide-thiol conjugation in order to utilize the IL-15 and IL-21 release in close proximity to the T cells to constantly activate the T cells, increasing the therapeutic effect of the T cells in an adoptive T-cell therapy against EG7-OVA expressing tumors (Figure 7). Nanoparticle-cell conjugation was shown to not impair cellular key functions and infusion of cytokine loaded NP decorated Pmel-1 T cells into mice with B16F10 melanoma successfully prevented tumor growth and increased survival rate of the mice.

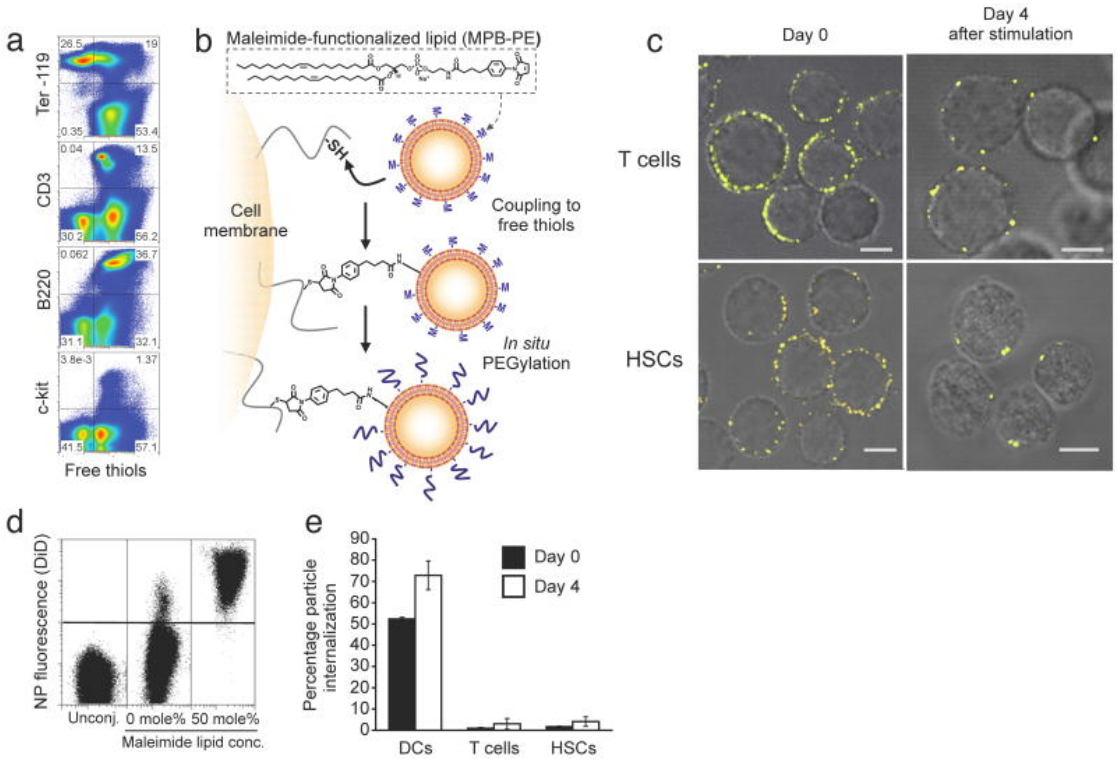

Figure 7: Stable conjugation of nanoparticles (NPs) to the surfaces of T-cells and HSCs via cell-surface thiols. (**a**) Flow cytometry analysis of cell surface thiols on mouse splenocytes detected by fluorophore-conjugated malemide co-staining with lineage surface markers for erythrocytes (Ter-119), T-cells (CD3), B-cells (B220) and hematopoietic Stem Cells (c-kit). (**b**) Schematic of maleimide-based conjugation to cell surface thiols. (**c**) Confocal microscopy images of $CD8^+$ effector T-cells and $lineage^-Sca\text{-}1^+c\text{-}kit^+$ HSCs immediately following conjugation with fluorescent DiD-labeled multilamellar lipid NPs (left panel) and after four day *in vitro* expansion (right panel). Scale bars, 2 μm. (**d**) Flow cytometry analysis of $CD8^+$ T-cells after incubation with

DiD-labeled multilamellar lipid NPs synthesized with or without maleimide-headgroup lipids. (**e**) Quantification of nanoparticle internalization. Immature dendritic cells (DCs), effector $CD8^+$ T-cells, or HSCs were conjugated with carboxyfluorescein-tagged maleimide-bearing liposomes. Extracellular trypan blue quenching was used to differentiate surface-bound and internalized liposomes immediately following conjugation or after four days in culture. Reprinted [45]

Based on these results, liposome-T-cell conjugates for adoptive T-cell therapy were further investigated with regards to the cellular localization of the nanoparticle conjugation. [54] NPs were shown to accumulate at the uropod of T cells after polarization (Figure 8). After co-incubation of the T cells with tumor cells, however, NPs re-localized to the contact zone of tumor cell and T cell, called the immunological synapse, without interfering target cell killing or cytokine release (Figure 9). Blockade of the immunological synapse by encapsulating Shp inhibitors in the NPs blocked the suppressive signals of the tumor cell towards the T cell allowing T cell expansion in the tumor leading to a reduced tumor burden and an average of 14d survival advantage in mice with TRP-SIY prostate tumors as shown in *in vivo* bioluminescence imaging. Further, cell surface capture methods and proteomics were used to identify CD45, $\alpha_L\beta_2$ integrin and CD97 as main surface proteins involved in the conjugation reaction.

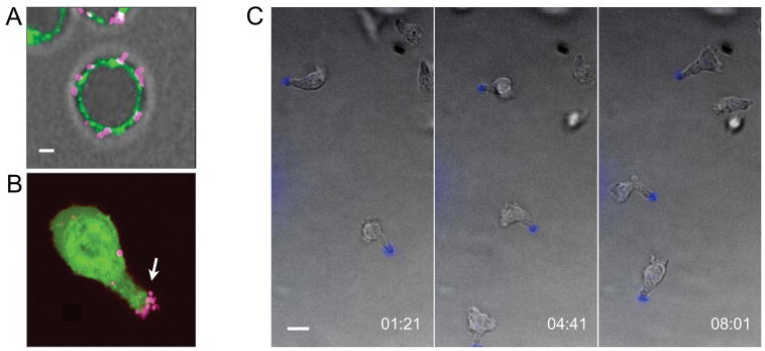

Figure 8: Surface-linked nanoparticles cluster at the uropod of migrating T cells (A, B) Confocal micrographs of lipid NP-conjugated CD8+ effector T cells. Shown are T-cells (surface-stained with FITC-cholera toxin, green) immediately after surface-conjugation of fluorescent NPs (magenta) (A), or CFSE-labeled T-cells (green) conjugated with particles (magenta) migrating on an MS1 endothelial cell monolayer towards a chemoattractant (B). Scale bar 2 µm. (C) Time-lapse confocal images illustrating the polarization of surface-linked NPs (blue) towards the uropod on effector T cells migrating within a 3D collagen matrix. Scale bar: 10 µm. Times are shown in elapsed min:sec. Reprinted [54]

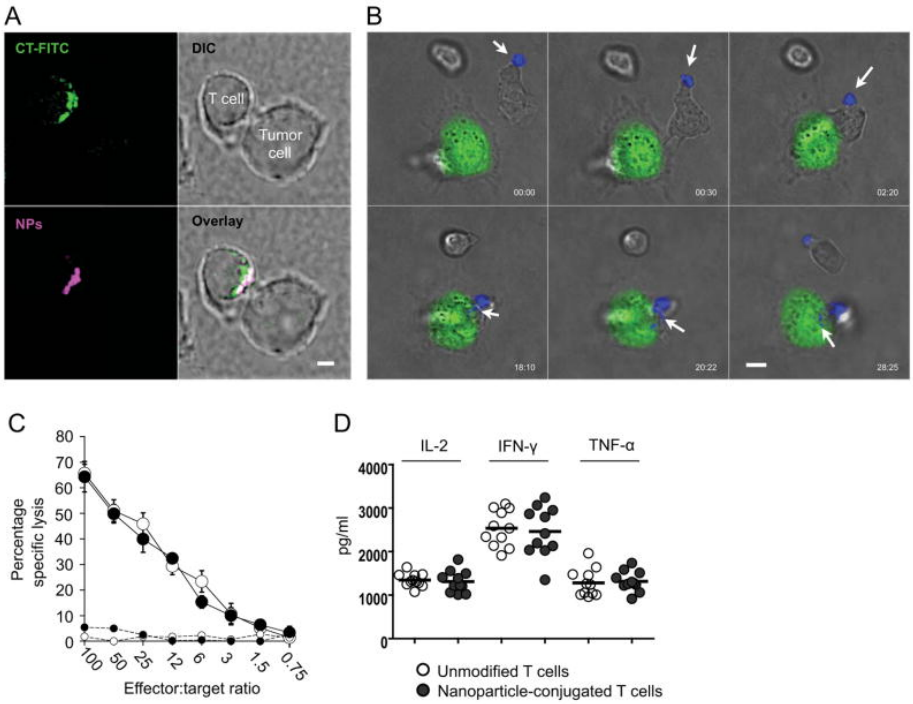

Figure 9: Nanoparticles redistribute from the uropod into the T-cell/tumor cell contact zone without disturbing key synapse functions. (A) 2C CD8+ effector T-cells conjugated with MLVs were incubated with SIY-target peptide-expressing TRAMP tumor cells for 20 min, then fixed and stained with FITC-cholera toxin to mark lipid rafts known to accumulate at the IS. Shown are confocal images of a T-cell forming a synaptic contact with a tumor cell. Nanoparticles were fluorescently labelled with rhodamine-conjugated lipid (magenta). Scale bar: 2 μm. (B) Time-lapse images illustrating the redistribution of nanoparticles (blue) from the uropod of 2C effector T cells towards the nascent synapse following TRAMP-SIY tumor target (green) recognition. Scale bar 4 μm; elapsed time shown in min:sec. (C) Standard 4 hour 51Cr release assay comparing cytotoxicity of unmanipulated (○) and particle-conjugated (●) 2C effector CD8+ T cells targeting TRAMP-SIY (large symbols) or control TRAMP (small symbols) tumor cells. (D) ELISA analysis of IL-2 (at 24 hrs), IFN-γ and TNF-α (at 48 hrs) secreted by NP-decorated 2C effector T-cells seeded on an irradiated TRAMP-SIY tumor cell monolayer. Reprinted [54]

Additionally, in order to achieve a trigger responsive release of the nanoparticles from the T cell surface, Wayteck et al. utilized pyridylsulfide conjugation to immobilize liposomes of similar lipid composition on the surface of OT-1 T cells via a disulfide bond (Figure 10) [46]. This strategy enabled the reductive cleavage of whole NP from T cells in the tumor micro environment and was used for the delivery of lipid coated si-RNA hydrogels

as a model for si-RNA delivery to induce sequence specific silence of disease related target genes of the tumor cells without impairing tumor cell killing. [46]

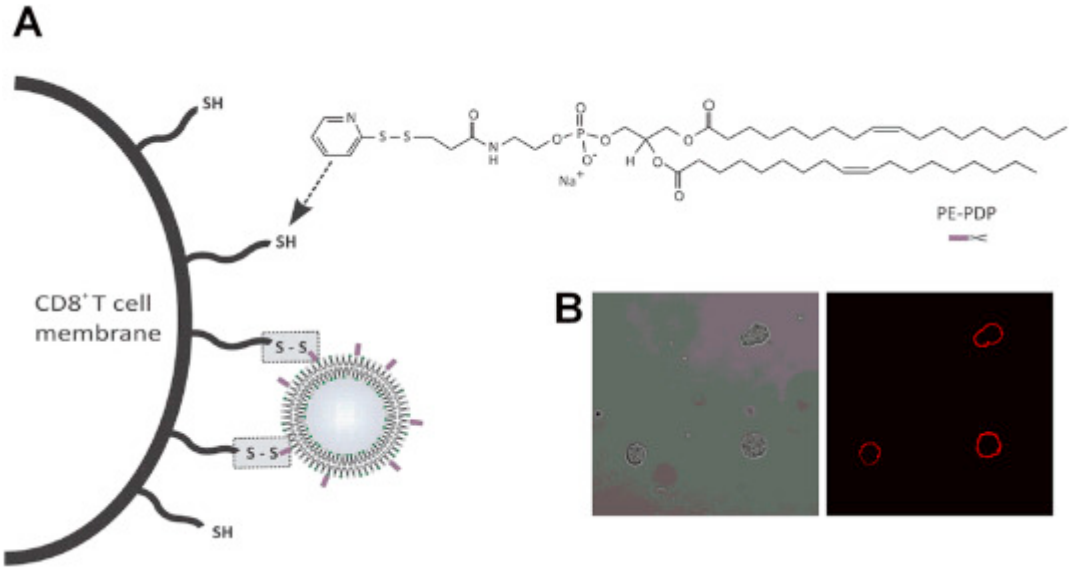

Figure 10: Schematic representation of the formation of a disulfide bond between PDP-functionalized lipids that are incorporated into the liposome bilayer and reduced exofacial thiol groups, present at the cell surface. (B) Transmission and confocal fluorescence images of non-activated murine OT-I CD8+ T cells incubated with Cy5-labeled maleimide. Reprinted [46]

1.3.3. Non-covalent cell surface immobilization

Another way to achieve a cellular hitchhiking approach is by non-covalent cell surface immobilization. This can be achieved either by exploiting hydrophobic or electrostatic interactions between the cell surface and the nanoparticle surface or by decoration of the nanoparticles with cell surface specific antibodies or aptamers [55-57]. While covalent cell surface conjugation or cell immobilization via hydrophobic interactions are limited to *in vitro* conjugation conditions, non-covalent cell surface immobilization using antibodies and aptamers can theoretically also be achieved *in vivo*, as free nanoparticles can still bind to circulatory cells after injection, in this case. Table 3 represents the recent advances in the field of nanoparticle mediated delivery using non-covalent cell surface immobilization strategies.

Table 3: Overview over different strategies for the cell immobilization of nanoparticles via non-covalent cell surface immobilization.

Cell Type	*Mechanism*	*Cargo*	*size*	*target*	*Reference*
CD45 leucocytes	E-selectin	liposomes	100nm	Prostate tumor	[58]
NK cells	E-selectin	liposomes	100nm	SW620 tumor	[59]
CD8 T cells	Various antibodies	IL-2 nanogels	100nm	B16F10 melanoma	[60] [61]
Macrophages	Anti-CD11b antibody	phagocytosis-resistant backpacks	7-10µm	Brain	[55]

Wayne et. al. utilized liposomes decorated with E-selectin, a surface marker that can specifically bind to several ligands on the surface of different leukocytes, for the cell surface immobilization on an undefined mix of CD45+ leucocytes. [58] First, they synthesized 100nm sized liposomes by thin-film hydration of a lipid mix of PC, SM, cholesterol, and DOGS NTA-Ni. DOGS NTA-Ni was used for the conjugation of His tagged TRAIL (TNF-related apoptosis-inducing ligand), an apoptosis ligand that can rapidly clear viable cancer cells from the blood circulation. SM was used for the conjugation of E-selectin to the liposome surface, enabling the *in vivo* conjugation of the liposomes to random mix of CD45 leukocytes. The anti-tumor efficiency of the ES/TRAIL decorated liposomes was then investigated in a tumor model in which DU145-luc-mcherry prostate cells were orthotopically injected into the prostate of NOD-SCID mice (Figure 11). Injection of ES/TRAIL liposomes cleared the primary tumor to undetectable limits, as determined by whole body bioluminescence imaging, by induction of the apoptosis of circulatory tumor cells. A 5% reduction in the count of circulatory tumor cells in the blood could be achieved, additionally reducing the formation of blood borne metastases.

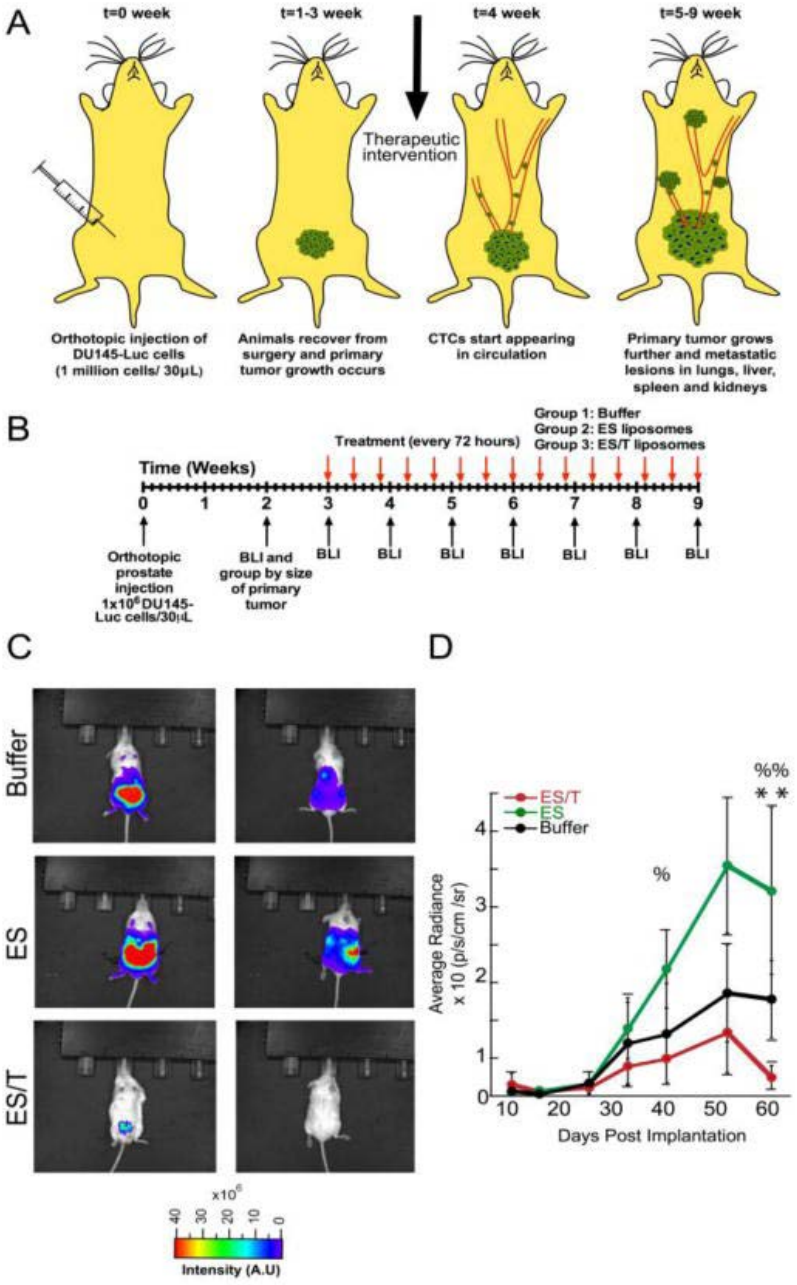

Figure 11: Test of ES/TRAIL liposomes to prevent metastasis in an orthotopic model of prostate cancer (A) Schematic of orthotopic xenograft model for metastatic prostate cancer progression. (B) Timeline for ES/T liposome efficacy trial in tumor-bearing mice. (C) Whole animal BLI of the ventral (left) and dorsal (right) side of representative animals from each treatment group at the end of the trial (week 9) (D) Average radiance from the primary tumor. Comparisons were made via one-way ANOVA with Tukey posttest. Error bars represent the mean ± SD at each timepoint. ES vs ES/TRAIL: %=($p < 0.05$) %%=($p<0.01$). Buffer vs ES/TRAIL: **=($p<0.05$). Reprinted [58]

Similarly, Chandrasekaran et al. used TRAIL decorated liposomes for the antibody-mediated conjugation to NK cells. [59] They formed 100nm sized liposomes by thin-film hydration of PC, cholesterol, DSPE-mPEG2000, and DSPE-mPEG2000-maleimide and conjugated TRAIL and anti-NK1.1 to the liposomes by maleimide-thiol conjugation (Figure 12). Their binding towards different subsets of Leukocytes was investigated *in vitro* verifying a specific binding of the liposomes to NK cells over B cells, T cells, dendritic cells, and Macrophages. Injection of the TRAIL/Anti-NK1.1 liposome into a SW620 mouse tumor model cleared the primary tumor of the luciferase expressing SW620 cells to undetectable limits and prevented the formation of metastases in the tumor draining lymph nodes, as determined by whole body bioluminescence imaging. While H&E staining of lymph nodes showed tissue abnormalities with glands, clusters, and sheets of neoplastic cells surrounded by fibrous tissue for the control groups of the tumor model, lymph nodes of mice injected with TRAIL/Anti-NK1.1 liposomes did not show any abnormalities compared to healthy lymph node tissue.

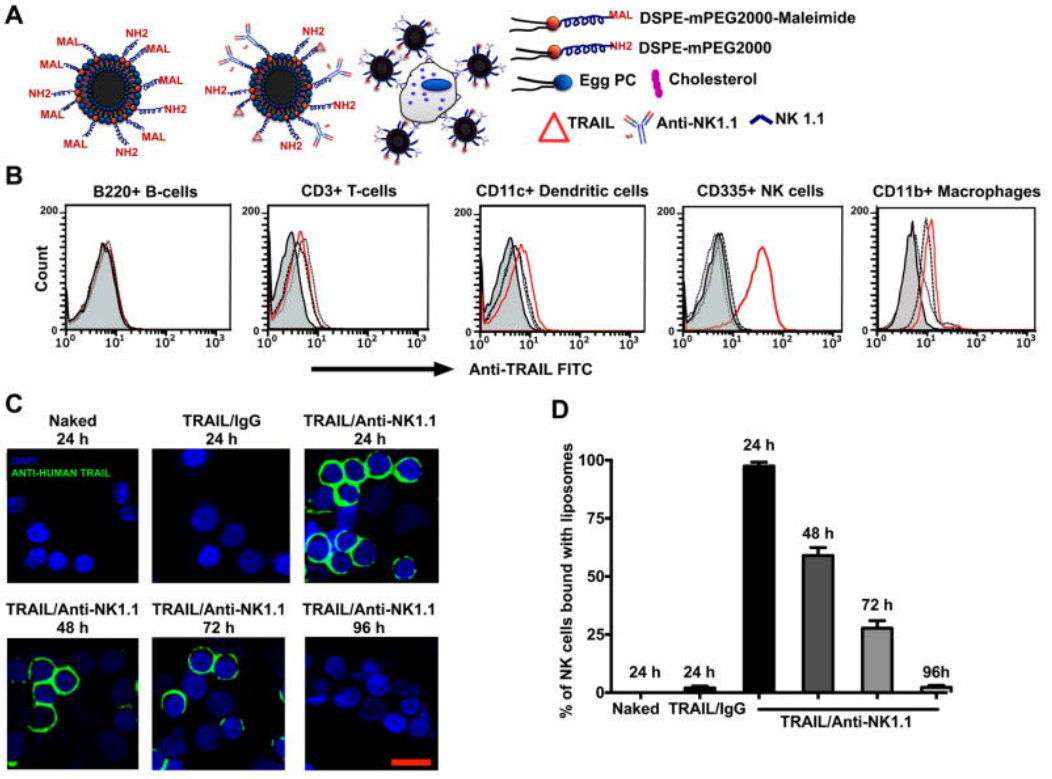

Figure 12: Pharmacokinetics of TRAIL/Anti-NK1.1 liposomes (A) Schematic of liposome formulation used in the study. Liposomes were decorated with TRAIL and Anti-NK1.1 proteins via maleimide-thiol chemistry. Anti-NK1.1 on liposome mediates conjugation of liposomes to

NK1.1 expressing natural killer (NK) cells to form "super" natural killer cells. (B) Flow cytometric analysis of the interaction of liposomes with different kinds of cells within the lymph nodes. Shown are histograms from liposome fluorescence (FITC conjugated anti-human TRAIL) from B220+ B-cells, CD3+ T-cells, CD11c+ dendritic cells, CD335+ NK cells and CD11b+ Macrophages from the inguinal lymph nodes of mice injected with buffer (filled), naked liposomes (– – – – – – – – –), TRAIL/IgG liposomes (⋯⋯⋯⋯) or TRAIL/Anti-NK1.1 liposomes (_____) 24 hr post-injection. (C) Representative fluorescent confocal micrographs of NK cells isolated from the inguinal lymph nodes of mice subcutaneously injected with naked (t=24 hr), TRAIL/IgG (t=24 hr) or TRAIL/Anti-NK1.1 liposomes (t=24, 48, 72 and 96 hr) labeled with nuclear stain DAPI and anti-human TRAIL on the liposome surface. Scale bar=20μm. (D) Numerical quantification of the percentage of NK cells bound with liposomes with different functionalizations. Bars represent the mean and standard deviation from 10 different confocal images for each time point. Reprinted [59]

The early work of Irvine et al. on CD8 T cells, discussed above was further developed by Tang et al. to immobilize traceless-degradable cytokine nanogels on CD8 T cells via antibody conjugation for adoptive T cell therapy.[60] To avoid the low loading capacities, liposomes were replaced by crosslinked IL-15 nanogels via a traceless reductively-cleavable linker. As maleimide-thiol and NHS-amine conjugation of the nanogels to the CD8 T cells lead to internalization, the cell surface markers CD2, CD8, CD11α, CD90 (=Thy1.1) and CD45 were screened for antibody mediated conjugation of the nanogels to the T cells (Figure 13). The highest retention on cell surface was achieved for anti-CD45, a rather unspecific surface marker for different groups of leucocytes. The highest nanogel internalization was achieved for the immobilization via anti-Thy 1.1. Injection of the nanogel decorated T cells in mice with B16F10 tumors resulted in an increased T cell expansion (CD4+, CD8+, NK cells) and an increased therapeutic window compared to systemically injected IL-15.

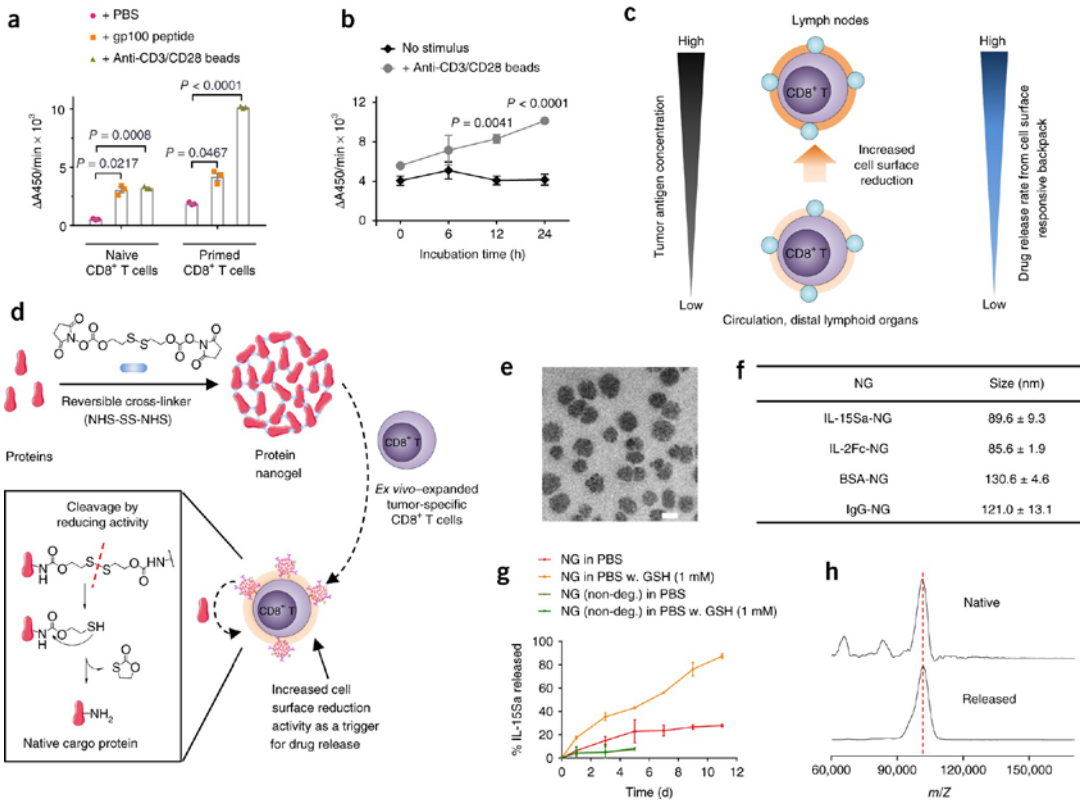

Figure 13: (**a**) Measurement of WST-1 cell-surface reduction activity rate in the presence of an intermediate electron acceptor for 1 h at 37 °C after naive or con-A-primed $CD8^+$ T cells were incubated in the presence of gp100 peptide (10 μg/ml) or anti-CD3/CD28 beads for 24 h. (**b**) Cell surface reduction activity rate in con-A-primed $CD8^+$ T cells that were incubated in the presence of anti-CD3/CD28 beads. Data in **a**,**b** represent the mean ± s.e.m. (*n* = 3 biologically independent samples per group), and *P* values were determined by one-way analysis of variance (ANOVA) and Tukey's tests. (**c**) Proposed strategy for linking increased surface redox activity of activated $CD8^+$ T cells to accelerated drug release kinetics from a redox-responsive backpack. (**d**) Scheme for protein NG synthesis and for release of protein in response to reducing activity in the local microenvironment. (**e**) Representative transmission electron microscopy image of NGs prepared from IL-15Sa (*n* = 3 independent experiments). Scale bar, 50 nm. (**f**) Hydrodynamic sizes of different NGs, as determined by dynamic light scattering (*n* = 3 independent samples). Data are mean ± s.d. (**g**) Release kinetics of cytokines from redox-responsive or nondegradable IL-15Sa-NGs in PBS with or without added glutathione (GSH) as a reducing agent. Data are mean ± s.d. (*n* = 3 independent experiments). (**h**) Representative MALDI mass spectrometric analysis of released and native cytokines (*n* = 2 independent experiments).

With these observations, they further compared the performance of TGF-βI (an inhibitor for the tumor growth factor β) loaded liposomes after antibody-mediated immobilization

on the internalizing receptor CD90/Thy1.1 and the non-internalizing receptor CD45 for the treatment of B16F10 melanoma (Figure 14). [61]. Immobilization on CD45 resulted in a higher immobilization capability and outperformed the immobilization on Thy1.1 in experiments where T cells are loaded *ex vivo*. Under *in vivo* conjugation conditions, however, when antibody decorated liposomes were injected systemically, immobilization on Thy1.1 showed far superior results, as CD45 is a common surface antigen for all T cells. Thus, Thy1.1 can be seen as a specific surface marker for the CD8 T cells, however, under *in vivo* conjugation conditions, this is not the case any more for CD45.

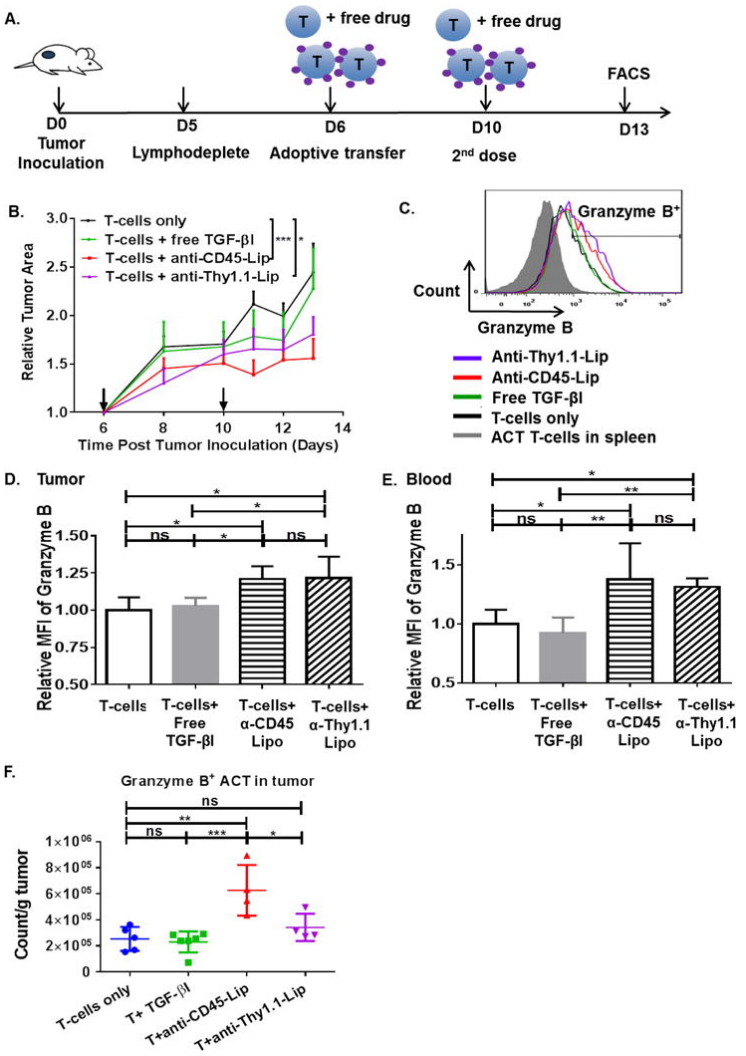

Figure 14: Pre-loading T-cells with SB liposomes targeting non-internalizing CD45 receptor leads to greater tumor infiltration by donor T-cells and enhanced therapeutic efficacy of ACT. Thy1.2^{+} C57Bl/6 mice were injected with B16F10 tumor cells (0.5×10^{6}) subcutaneously day 0, sublethally lymphodepleted by irradiation on day 5, and received i.v. adoptive transfer of 8×10^{6}

activated pmel-1 Thy1.1$^+$ CD8$^+$ T-cells on day 6, when tumors had a mean size of 17±4 mm^2. T-cells were either conjugated with anti-CD45 liposomes or anti-Thy1.1 liposomes encapsulating TGF-βI before adoptive transfer. Other groups of mice either receive equivalent dose of systemic free TGF-βI (1 μg) in addition to T-cells or T-cells alone. After four days, animals in respective groups were boosted with 12×10^6 activated T-cells and 1.5 μg TGF-βI either in liposomes or free form, and sacrificed for analysis by flow cytometry on day 13. (A) Experimental timeline. (B) Relative average tumor growth normalized to day 6 tumor areas. *, $p<0.05$, by two-way ANOVA followed by Sidak's multiple comparison test (against T-only group) on tumor size on day 13. (C) Sample histograms of granzyme B expression of tumor infiltrating adoptively transferred T-cells. (D, E) Mean fluorescence intensities of granzyme B expression for ACT T-cells in tumors (D) and blood (E). (F) Quantification of number of granzyme B$^+$ CD8$^+$ Thy1.1$^+$ T-cells per gram of tumor. *, $p<0.05$; **, $p<0.01$, ***, $p<0.001$, by one-way ANOVA followed by Tukey's multiple comparison test. Reprinted [61]

Rather unconventional for a cellular hitchhiking approach, Klyatchko et al. used antibody-mediated nanoparticle cell conjugation by immobilizing phagocytosis resistant backpacks on the cell surface of Macrophages by CD11b mediated antibody conjugation, for delivery of catalase to the brain in lipopolysaccharide-induced encephalitis. [55] The 7-10μm sized backpacks were produced via layer-by-layer assembly of bovine submaxillary mucin (BSM)/lectin jacalin (JAC), poly(allylamine hydrochloride) (PAH), magnetic nanoparticles, catalase, poly(acrylic acid) (PAA), and biotinylated PAH (Figure 15). Brain delivery of the backpacks was visualized on brain cryo sections, however, cells resident in the brain endothelium and in the brain parenchyma were not distinguished by any marker (Figure 16).

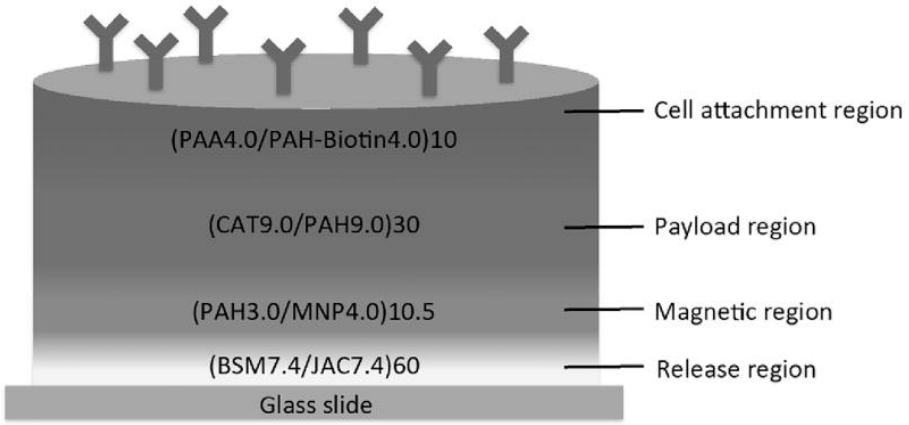

Figure 15: Scheme showing the catalase containing backpack structure. From bottom to top: Release region is composed of 60 bilayers of bovine submaxillary mucin (BSM) and lectin jacalin

(JAC); Magnetic region made of 10.5 bilayers of poly(allylamine hydrochloride) (PAH) and magnetic nanoparticles (MNP); Payload region containing 30 bilayers of PAH and catalase from bovine liver (CAT); Cell attachment region comprised of 10 bilayers of poly(acrylic aid) (PAA) and biotinylated PAH (PAH-biotin). Backpacks are topped with CD11b antibodies for macrophage conjugation. Reprinted [55]

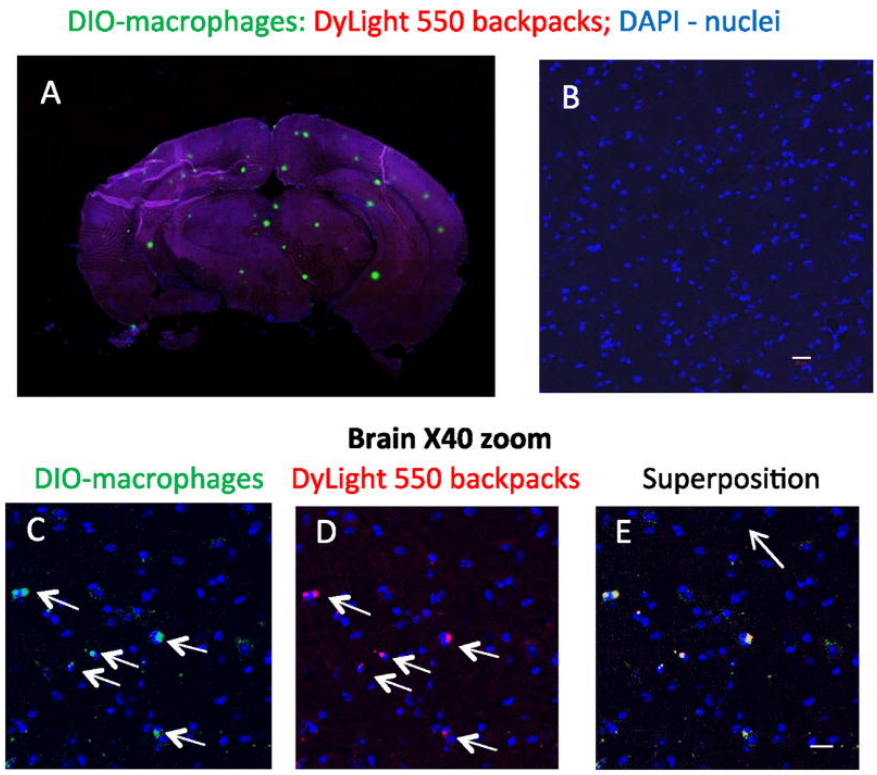

Figure 16: Recruitment of Macrophages with the attached backpacks to the brain in LPS-intoxicated mice. Fluorescently-labeled DiO-Macrophages (green, 2 × 106 cells/ml) loaded with fluorescently-labeled backpacks (red, NeutrAvidin 550) attached. Cell-backpacks (5 × 106 cells/mouse in 100 µl) were injected into C57/BL mice (5 mice/group) with brain inflammation (A, C–E). Fourteen hours later, mice were sacrificed, and brain slides were examined by confocal microscopy (A: whole brain, B–E: 40× magnification). LPS-intoxicated mice injected with backpacks alone (no cell-carriers, 5 mice/group) were used as a control group (B). Co-localization of fluorescently-labeled Macrophages (green, C) and backpacks (red, D) manifested in yellow staining (E) confirmed that Macrophages delivered considerable amount of backpacks to the inflamed brain (shown by arrows). No fluorescence was found in the inflamed brain when backpacks were injected alone (without cell-carriers, B) indicating that systemically administered Macrophages facilitated transport of backpacks across the BBB in the presence of brain inflammation. The representative images from three independent experiments. The bar: 20 µm. Reprinted [55]

1.4. Conclusions and Outlook

The conjugation of drug loaded NPs to circulatory cells with specialized migratory properties, opens up opportunities to a variety of new drug delivery systems with outstanding *in vitro* and *in vivo* properties. Cell-mediated drug delivery systems were successfully shown to act as primary treatment (delivery of chemotherapeutics exploiting specialized migratory properties) as well as supportive treatment (continuous delivery of interleukins close to the surface of T cells to boost adoptive T cell therapy). However, commonly used cells are restricted to autologous donors (Stem Cells/Macrophages/Neutrophils/cytotoxic T Lymphocytes), which limits the clinical use of these cells, as they have to be isolated from the patient before each use and fully characterized before each reinjection. This additional work would be reflected in prolonged synthesis time, which might be unfavorable for late stage cancer patients, and can potentially increase input and hence, price of the therapies. Therefore, it is important to establish *ex vivo* conjugation strategies combined with *in vivo* studies and transfer results to a system that can be used in allogenic transplants or to a system that utilizes *in vivo* conjugation. One solution to this drawback might be the identification of specific surface proteins that do not interfere with the functionality of the cells. These proteins can then be targeted in antibody-based conjugation approaches or can be screened for selectively binding peptides and aptamers that do not activate/inactivate the target proteins using phage display and cell selex. [62, 63] Despite all the efforts in the field of nanoparticle delivery systems, three major issues remain and require further investigation. Firstly, all the work done on Monocytes and Leucocytes relies on cells in which migratory properties are fully dependent on inflammatory signals and therefore can be only used in certain pathogenic setups. Secondly, the nanoparticles used for cell conjugation were either solid core nanoparticles or liposomes, both of which reflect rather old nanoparticle architectures. Nanoparticles like polymersomes, so far, are not reported to be successfully conjugated to cell surfaces although they are superior to liposomes in the sense that they can encapsulate higher quantities of hydrophilic and hydrophobic drugs at the same time and can be engineered to show a trigger responsive release of their cargo. Lastly, most investigations are focused on the nanoparticle immobilization on cells using one distinct chemistry or conjugation method followed by their application, but no study has been published yet that systematically compares the impact of different conjugation chemistries on the functionality and viability of the nanoparticle-cell

conjugates comparing these different strategies to each other. Each of these questions will be discussed in the three main chapters of this thesis.

1.5. References

1. Fang, J., H. Nakamura, and H. Maeda, *The EPR effect: Unique features of tumor blood vessels for drug delivery, factors involved, and limitations and augmentation of the effect.* Advanced Drug Delivery Reviews, 2011. **63**(3): p. 136-151.
2. Danhier, F., *To exploit the tumor microenvironment: Since the EPR effect fails in the clinic, what is the future of nanomedicine?* Journal of Controlled Release, 2016. **244, Part A**: p. 108-121.
3. Maeda, H., et al., *Tumor vascular permeability and the EPR effect in macromolecular therapeutics: a review.* Journal of Controlled Release, 2000. **65**(1–2): p. 271-284.
4. Barenholz, Y., *Doxil® — The first FDA-approved nano-drug: Lessons learned.* Journal of Controlled Release, 2012. **160**(2): p. 117-134.
5. Ray, P., et al., *Application of Aptamers for Targeted Therapeutics.* Archivum Immunologiae et Therapiae Experimentalis, 2013. **61**(4): p. 255-271.
6. Chen, Y. and L. Liu, *Modern methods for delivery of drugs across the blood–brain barrier.* Advanced Drug Delivery Reviews, 2012. **64**(7): p. 640-665.
7. Lundy, D.J., et al., *Inducing a Transient Increase in Blood–Brain Barrier Permeability for Improved Liposomal Drug Therapy of Glioblastoma Multiforme.* ACS Nano, 2019. **13**(1): p. 97-113.
8. Kreuter, J., *Drug delivery to the central nervous system by polymeric nanoparticles: What do we know?* Advanced Drug Delivery Reviews, 2014. **71**: p. 2-14.
9. Zhang, T.-T., et al., *Strategies for transporting nanoparticles across the blood-brain barrier.* Biomaterials Science, 2016. **4**(2): p. 219-229.
10. Saraiva, C., et al., *Nanoparticle-mediated brain drug delivery: Overcoming blood–brain barrier to treat neurodegenerative diseases.* Journal of Controlled Release, 2016. **235**: p. 34-47.
11. Wohlfart, S., S. Gelperina, and J. Kreuter, *Transport of drugs across the blood–brain barrier by nanoparticles.* Journal of Controlled Release, 2012. **161**(2): p. 264-273.
12. Upadhyay, R.K., *Drug Delivery Systems, CNS Protection, and the Blood Brain Barrier.* BioMed Research International, 2014. **2014**: p. 37.
13. Su, Y., et al., *Design Strategies and Applications of Circulating Cell-Mediated Drug Delivery Systems.* ACS Biomaterials Science & Engineering, 2015. **1**(4): p. 201-217.
14. Chambers, E. and S. Mitragotri, *Prolonged circulation of large polymeric nanoparticles by non-covalent adsorption on erythrocytes.* Journal of Controlled Release, 2004. **100**(1): p. 111-119.
15. Gao, Z., et al., *Mesenchymal stem cells: a potential targeted-delivery vehicle for anti-cancer drug loaded nanoparticles.* Nanomedicine: Nanotechnology, Biology and Medicine, 2013. **9**(2): p. 174-184.
16. Wagers, A.J. and I.L. Weissman, *Plasticity of Adult Stem Cells.* Cell, 2004. **116**(5): p. 639-648.

17. Feng, Y., et al., *Hypoxia-cultured human adipose-derived mesenchymal stem cells are non-oncogenic and have enhanced viability, motility, and tropism to brain cancer.* Cell Death &Amp; Disease, 2014. **5**: p. e1567.

18. Mizuno, H., M. Tobita, and A.C. Uysal, *Concise Review: Adipose-Derived Stem Cells as a Novel Tool for Future Regenerative Medicine.* STEM CELLS, 2012. **30**(5): p. 804-810.

19. Stuckey, D.W. and K. Shah, *Stem cell-based therapies for cancer treatment: separating hope from hype.* Nature Reviews Cancer, 2014. **14**: p. 683.

20. Pendleton, C., et al., *Mesenchymal Stem Cells Derived from Adipose Tissue vs Bone Marrow: In Vitro Comparison of Their Tropism towards Gliomas.* PLOS ONE, 2013. **8**(3): p. e58198.

21. Lamfers, M., et al., *Homing properties of adipose-derived stem cells to intracerebral glioma and the effects of adenovirus infection.* Cancer Letters, 2009. **274**(1): p. 78-87.

22. Josiah, D.T., et al., *Adipose-derived Stem Cells as Therapeutic Delivery Vehicles of an Oncolytic Virus for Glioblastoma.* Molecular Therapy, 2010. **18**(2): p. 377-385.

23. Studeny, M., et al., *Mesenchymal Stem Cells: Potential Precursors for Tumor Stroma and Targeted-Delivery Vehicles for Anticancer Agents.* JNCI: Journal of the National Cancer Institute, 2004. **96**(21): p. 1593-1603.

24. Mantovani, A., et al., *Role of tumor-associated macrophages in tumor progression and invasion.* Cancer and Metastasis Reviews, 2006. **25**(3): p. 315-322.

25. Qiu, S.-Q., et al., *Tumor-associated macrophages in breast cancer: Innocent bystander or important player?* Cancer Treatment Reviews, 2018. **70**: p. 178-189.

26. Qian, B.-Z., et al., *CCL2 recruits inflammatory monocytes to facilitate breast-tumour metastasis.* Nature, 2011. **475**: p. 222.

27. Corraliza, I., *Recruiting specialized macrophages across the borders to restore brain functions.* Frontiers in Cellular Neuroscience, 2014. **8**(262).

28. Bauer, M., et al., *β₁ integrins differentially control extravasation of inflammatory cell subsets into the CNS during autoimmunity.* Proceedings of the National Academy of Sciences, 2009. **106**(6): p. 1920-1925.

29. Brynskikh, A.M., et al., *Macrophage Delivery of Therapeutic Nanozymes in a Murine Model of Parkinson's Disease.* Nanomedicine (London, England), 2010. **5**(3): p. 379-396.

30. Dou, H., et al., *Macrophage delivery of nanoformulated antiretroviral drug to the brain in a murine model of neuroAIDS.* Journal of immunology (Baltimore, Md. : 1950), 2009. **183**(1): p. 661-669.

31. Zheng, H., et al., *Murine RAW264.7 cells as cellular drug delivery carriers for tumor therapy: a good idea?* Cancer Chemotherapy and Pharmacology, 2018.

32. Lewis, C.E. and J.W. Pollard, *Distinct Role of Macrophages in Different Tumor Microenvironments.* Cancer Research, 2006. **66**(2): p. 605.

33. Engelhardt, B. and R.M. Ransohoff, *Capture, crawl, cross: the T cell code to breach the blood–brain barriers.* Trends in Immunology, 2012. **33**(12): p. 579-589.

34. Ransohoff, R.M. and B. Engelhardt, *The anatomical and cellular basis of immune surveillance in the central nervous system.* Nat Rev Immunol, 2012. **12**(9): p. 623-635.

35. Xue, J., et al., *Neutrophil-mediated anticancer drug delivery for suppression of postoperative malignant glioma recurrence.* Nat Nano, 2017. **12**(7): p. 692-700.

36. Adams, D.H. and A. Rlloyd, *Chemokines: leucocyte recruitment and activation cytokines.* The Lancet, 1997. **349**(9050): p. 490-495.

37. Anselmo, A.C. and S. Mitragotri, *Cell-mediated delivery of nanoparticles: taking advantage of circulatory cells to target nanoparticles.* Journal of controlled release : official journal of the Controlled Release Society, 2014. **190**: p. 531-541.

38. Anselmo, A.C. and S. Mitragotri, *Cell-Mediated Delivery of Nanoparticles: Taking Advantage of Circulatory Cells to Target Nanoparticles.* Journal of controlled release : official journal of the Controlled Release Society, 2014. **0**: p. 531-541.

39. Wang, P., et al., *Engineered Cell-Assisted Photoactive Nanoparticle Delivery for Image-Guided Synergistic Photodynamic/Photothermal Therapy of Cancer.* ACS Applied Materials & Interfaces, 2019. **11**(15): p. 13935-13944.

40. Xie, Z., et al., *Immune Cell-Mediated Biodegradable Theranostic Nanoparticles for Melanoma Targeting and Drug Delivery.* Small, 2017. **13**(10): p. 1603121.

41. Huang, W.-C., et al., *Tumortropic adipose-derived stem cells carrying smart nanotherapeutics for targeted delivery and dual-modality therapy of orthotopic glioblastoma.* Journal of Controlled Release, 2017. **254**: p. 119-130.

42. Ho, Y.-J., et al., *Camptothecin-loaded fusogenic nanodroplets as ultrasound theranostic agent in stem cell-mediated drug-delivery system.* Journal of Controlled Release, 2018. **278**: p. 100-109.

43. Pang, L., et al., *Exploiting macrophages as targeted carrier to guide nanoparticles into glioma.* Oncotarget, 2016. **7**(24): p. 37081-37091.

44. Xie, Y.-Q., et al., *Redox-responsive interleukin-2 nanogel specifically and safely promotes the proliferation and memory precursor differentiation of tumor-reactive T-cells.* Biomaterials Science, 2019. **7**(4): p. 1345-1357.

45. Stephan, M.T., et al., *Therapeutic cell engineering with surface-conjugated synthetic nanoparticles.* Nat Med, 2010. **16**(9): p. 1035-1041.

46. Wayteck, L., et al., *Hitchhiking nanoparticles: Reversible coupling of lipid-based nanoparticles to cytotoxic T lymphocytes.* Biomaterials, 2016. **77**: p. 243-254.

47. Holden, C.A., et al., *Surface engineering of macrophages with nanoparticles to generate a cell-nanoparticle hybrid vehicle for hypoxia-targeted drug delivery.* International journal of nanomedicine, 2010. **5**: p. 25-36.

48. Zeng, Y., et al., *High-efficiency labeling of sialylated glycoproteins on living cells.* Nature methods, 2009. **6**(3): p. 207-209.

49. Yang, Y., et al., *Enhanced imaging of glycan expressing cancer cells using poly(glycidyl methacrylate)-grafted silica nanospheres labeled with quantum dots.* Analytica Chimica Acta, 2020. **1095**: p. 138-145.

50. Mahal, L.K., K.J. Yarema, and C.R. Bertozzi, *Engineering Chemical Reactivity on Cell Surfaces Through Oligosaccharide Biosynthesis.* Science, 1997. **276**(5315): p. 1125-1128.

51. Xu, L., et al., *Click hybridization of immune cells and polyamidoamine dendrimers.* Advanced healthcare materials, 2014. **3**(9): p. 1430-1438.

52. Bernardin, A., et al., *Copper-Free Click Chemistry for Highly Luminescent Quantum Dot Conjugates: Application to in Vivo Metabolic Imaging.* Bioconjugate Chemistry, 2010. **21**(4): p. 583-588.

53. Saxon, E. and C.R. Bertozzi, *Cell Surface Engineering by a Modified Staudinger Reaction.* Science, 2000. **287**(5460): p. 2007-2010.

54. Stephan, M.T., et al., *Synapse-directed delivery of immunomodulators using T-cell-conjugated nanoparticles.* Biomaterials, 2012. **33**(23): p. 5776-5787.

55. Klyachko, N.L., et al., *Macrophages with cellular backpacks for targeted drug delivery to the brain.* Biomaterials, 2017. **140**: p. 79-87.

56. Anselmo, A.C., et al., *Delivering Nanoparticles to Lungs while Avoiding Liver and Spleen through Adsorption on Red Blood Cells.* ACS Nano, 2013. **7**(12): p. 11129-11137.

57. Swiston, A.J., et al., *Surface Functionalization of Living Cells with Multilayer Patches.* Nano Letters, 2008. **8**(12): p. 4446-4453.

58. Wayne, E.C., et al., *TRAIL-coated leukocytes that prevent the bloodborne metastasis of prostate cancer.* Journal of Controlled Release, 2016. **223**: p. 215-223.

59. Chandrasekaran, S., et al., *Super natural killer cells that target metastases in the tumor draining lymph nodes.* Biomaterials, 2016. **77**: p. 66-76.

60. Tang, L., et al., *Enhancing T cell therapy through TCR-signaling-responsive nanoparticle drug delivery.* Nature Biotechnology, 2018.

61. Zheng, Y., et al., *Enhancing Adoptive Cell Therapy of Cancer through Targeted Delivery of Small-Molecule Immunomodulators to Internalizing or Noninternalizing Receptors.* ACS Nano, 2017. **11**(3): p. 3089-3100.

62. Sefah, K., et al., *Development of DNA aptamers using Cell-SELEX.* Nat. Protocols, 2010. **5**(6): p. 1169-1185.

63. Molek, P., B. Strukelj, and T. Bratkovic, *Peptide phage display as a tool for drug discovery: targeting membrane receptors.* Molecules (Basel, Switzerland), 2011. **16**(1): p. 857-887.

2. CD4+ T_{EM}-cell mediated delivery of fluorospheres across the BBB

2.1. Introduction

2.1.1. The entry of molecules into the CNS

The entry of drugs or nanocarriers from the blood to the brain parenchyma is prevented by 2 major barriers, the BBB, and the BCSFC. Together, they provide homeostasis to the brain enabling the correct and efficient functionality of the brain while protecting it from external forces or infections. Importantly, these barriers are not static but show high plasticity, opening and closing frequently under inflammatory but also under healthy conditions [1].

2.1.2. Physiology of the BBB

The BBB is a physical barrier blocking the diffusion of molecules across the brain endothelium [2, 3]. While adherent junctions are formed by cadherin's and establish the adhesive contacts between endothelial cells, tight junctions are formed by claudins and additionally harbor occluding and Junctional Adhesion Molecules (JAMs). These tight junctions provide physical barrier properties to the brain endothelium excluding the exchange of polar solutes between the blood and the brain (Figure 1) [4]. Astrocytes and pericytes surrounding the endothelium form the parenchymal basement membrane separating a defined space between the perivascular space that additionally contains immune cells and APCs and the parenchyma that contains the neurons. Astrocytes and pericytes increase the barrier functions of the BBB and can regulate the opening and closing of the tight junctions under healthy conditions [5]. Together with the endothelium and the neurons, they form the neurovascular unit (Figure 2). In addition to the physical barrier functions, the BBB also enables metabolic barrier functions. Potentially harmful molecules are excluded from the brain by transporters on the luminal and abluminal site of the endothelial cells, which actively pump molecules from the perivascular space to the

blood and by metabolic enzymes that metabolize these harmful molecules in the brain parenchyma.

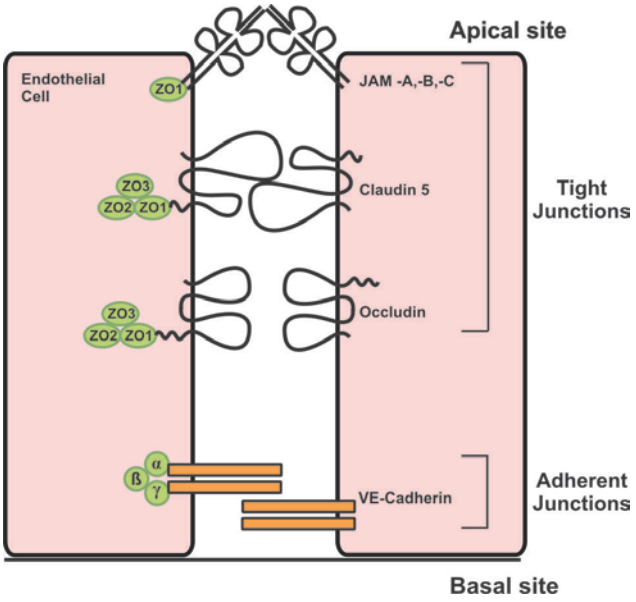

Figure 1: Intercellular junctions of brain endothelial cells. Adherent junctions formed by PECAM and VE-Cadherin provide the structural integrity of the endothelium while the tight junctions formed by the junctional adhesion molecules (JAM –A, -B, -C), Claudin 5 and Occludin physically block the diffusion of polar solutes from the apical to the basal site. Adherent junctions are associated to the cytoskeleton by a complex of α, ß and γ catenin. Tight junctions are associated to the cytoskeleton by a complex of ZO-1, ZO-2 and ZO-3.

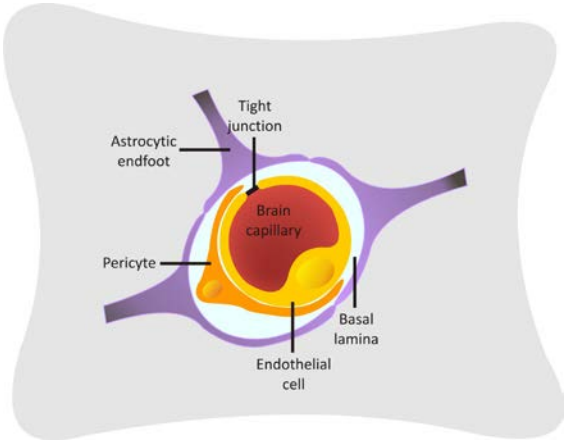

Figure 2: Neurovascular unit: Brain endothelial cells are linked by tight junctions that prevent the diffusion of polar solutes from the blood to the brain. Pericytes are closely associated to the endothelial cells. Astrocytes surrounding the endothelial cells deposit the parenchymal basement membrane. Together with the astrocytic endfeet this barrier is referred to as *glia limitans.*

2.1.3. Physiological pathways across the BBB

To provide salts, nutrients, and other special molecules like proteins and hormones to the brain, there are 4 different physiological pathways across the BBB (Figure 3) [2, 3]. These include the paracellular aqueous pathway, the transcellular lipophilic pathway, transport proteins, and receptor-mediated or adsorptive transcytosis. Due to reduced pinocytotic activity at the brain endothelium, small-molecule CNS drugs are designed to cross the BBB via the transcellular lipophilic pathway (Lipinski Rule of 5) [6, 7]. CNS drugs conjugated to carriers mostly rely on highly invasive methods like intraventricular delivery or disruption of the BBB or entry via adsorptive or receptor mediated transcytosis [8, 9]. Additionally, bulky lipophilic or amphiphilic drugs are substrates for efflux pumps like ABCs that actively remove these molecules from the CNS [10].

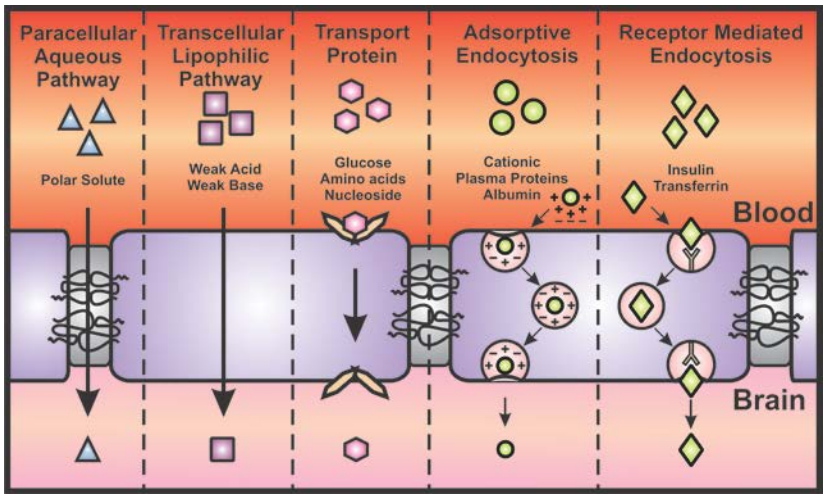

Figure 3: Scheme of brain endothelial cells linked by tight junctions to form the blood-brain barrier (BBB). Molecular trafficking across the BBB relies on A) the paracellular aqueous pathway that describes the diffusion of polar solvents between two endothelial cells, B) the transcellular lipophilic pathway that describes the diffusion of the neutral species of weak acid or bases across the lipophilic cell membrane of endothelial cells, C) transport proteins that facilitate the transport of essential nutrients like glucose, amino acids and nucleosides to the brain, D) adsorptive endocytosis which is triggered by association of cationic plasma proteins like albumin to the anionic lipid bilayer of the cell membrane and E) receptor mediated endocytosis which is triggered by receptors binding certain proteins and hormones like insulin and transferrin. As the paracellular aqueous pathway is blocked by the tight junctions under normal conditions, molecular trafficking mostly relies on pathway B)-E), while most pharmaceuticals acting in the brain resemble weak acids and bases that enter the brain via pathway B).

2.1.4. Physiology of the BCSFB

The Cerebrospinal Fluid (CSF) surrounds the brain in direct contact. It contains nutrients and protects the brain from traumata. The CSF is formed by 4 distinct structures in the brain that are each called choroid plexus [11-14]. These structures filter water and nutrients from the fenestrated endothelium through an additional epithelial layer with tight junctions, which forms the Blood Cerebrospinal Fluid Barrier (BCSFB) (Figure 4).

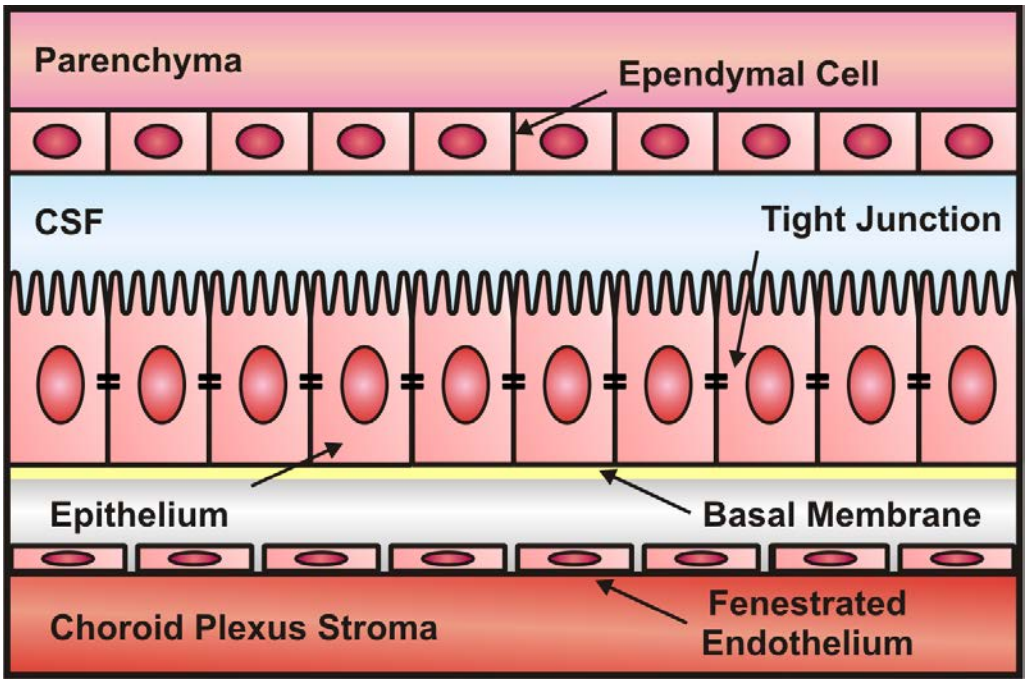

Figure 4: Blood Cerebrospinal Fluid Barrier (BCSFB): Epithelial cells linked by tight junctions filter the fluid from the choroid plexus stroma to produce the cerebrospinal fluid (CSF) that embeds the brain.

2.1.5. Immunosurveillance of the CNS

For reasons of immune surveillance, CD4+ T cells can cross the BBB. [15, 16] They extravasate from the brain endothelium to sample the perivascular space for APCs. In case they get reactivated by inflammatory signals, they produce inflammatory markers to recruit other immune cells and migrate further to the brain parenchyma [17]. The extravasation can be divided into 3 steps [18, 19]. First, T cells get recruited on the endothelium by integrin recognition of the endothelial inflammatory markers ICAM-1

and VCAM-1 [20]. In a second step, T cells start to crawl against the blood flow mediated by the markers ICAM-1 and ICAM-2. Finally, T cells undergo diapedesis by opening tight junctions and migrating in between 2 endothelial cells (paracellular pathway) or by forming "tunnels" through a single endothelial cell (transcellular pathway) [21]. As ICAM-2 and VCAM-1 are constitutively expressed on the brain endothelium, T cell migration can also occur in the absence of neuroinflammation.

2.1.6. Hijacking CD4+ TEM cells to deliver model nanoparticles across the BBB

The special migrating properties of CD4+ T_{EM} cells can be exploited to deliver drug loaded NPs across the BBB in an antigen independent manner, meaning independently of healthy or inflammatory conditions (Figure 5). The nanoparticle delivery properties of fluorosphere conjugated encephalitogeneic SJL-PLP7 cells were previously investigated *in vitro* by our group regarding their capability to carry these model nanoparticles across a monolayer of brain endothelial cells under static and flow conditions. The following chapter presents a first proof-of-concept study to demonstrate the antigen independent nanoparticle delivery potential of nanoparticle conjugated CD4+ T_{EM} cells across the BBB *in vivo* utilizing the same polystyrene based model nanoparticles. This model system represents the first step in developing an antigen independent drug delivery system for the efficient delivery of CNS active drugs across the BBB.

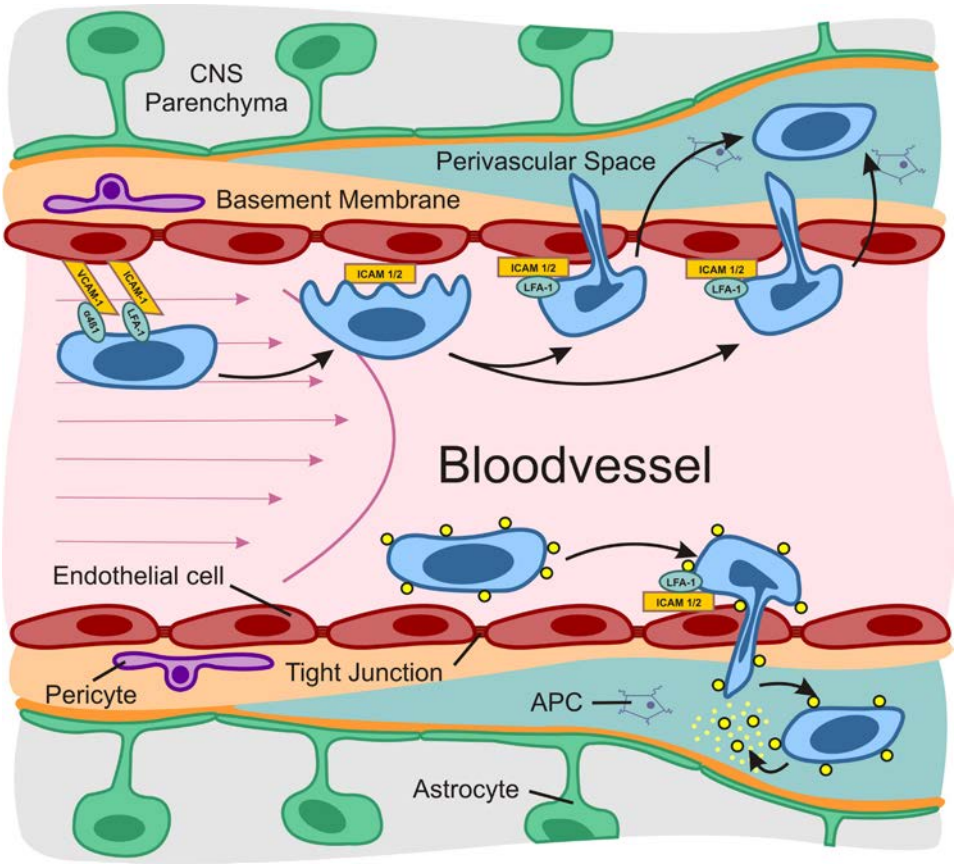

Figure 5: Migration of CD4+ T cells at the brain endothelium. T cells arrest at the endothelium as result of integrin recognition of ICAM-1 and VCAM-1. After polarization T cells crawl against the blood flow and undergo trans- or paracellular diapedesis to sample the perivascular space for antigen presenting cells (APCs). Drug loaded nanoparticles can be immobilized on the surface of these T cells in a cellular backpack approach to be carried across the BBB. Active or passive triggering release mechanisms can be used to release the NP cargo in the perivascular space or the CNS parenchyma.

2.2. Experimental Section

2.2.1. Materials

All chemicals were used as received unless described otherwise. The polymers Methoxy poly(ethylene glycol)$_{5000}$-SVA (mPEG-SVA) and maleimide- poly(ethylene glycol)$_{5000}$-SVA (Mal-PEG-SVA) were purchased from LaysanBio Inc. (Alabama, USA). Amine modified Fluospheres (F8764, 200 nm, Yellow-green), AnnexinV – AlexaFluor647, CellTracker Red CMTPX, CellTracker DeepRed, 4’,6-diamidino-2-phenylindole (DAPI),

Staurosporin and wheat germ agglutinin, Texas Red-X conjugate (WGA-TexasRed) were purchased from FischerScientific. N-Acetyl cysteine and poly(L-Lysin) (84 kDA, 0.01%) was purchased from SigmaAldrich.

PRIMARY ANTIBODIES

Name	***Host***	***Manufacturer***	***Order-Nbr***
Anti-pan Laminin	Rabbit	DAKO	Z0097
Anti-CD4	Rat	Pharmingen	L3T4
Anti-ICAM I	Rat	TKI	20081017
Anti-MHC-I	Rat	BMA Biomedicals	ER-MP 42, T2104
Anti-PECAM I	Rat	TKI	Mec13.3
Anti-TCR Vα3.2 PE	Rat	BioLegend	135406
Anti-TCR Vß1.1 PE	Rat	BioLegend	553198
Anti-TCR Vß6 PE	Rat	BioLegend	140003
Anti-VCAM I	Rat	TKI	19970723

ISOTYPE CONTROLS

Name	***Host***	***Manufacturer***	***Order-Nbr***
IgG	Rabbit	R&D Systems	AB-105-C
Anti-9B5	Rat	TKI	20180603RR

SECONDARY ANTIBODIES

Name	***Host***	***Manufacturer***	***Order-Nbr***
Anti-Rat AF488	Donkey	Invitrogen	A21208
Anti-Rat Cy3	Donkey	Biolegend	712-165-153
Anti-Rabbit AMCA	Goat	Jackson	111-156-045

2.2.2. Methods

Sizes, size distributions and zeta-potentials of nanoparticles were determined using a zetasizer (NANO-ZS, Malvern, UK) at a scattering angle of 173° using back-scattering

detection. Briefly, 2 µL of fluosphere suspension was diluted in 998 µL MilliQ water at pH=7.4 for measurement of the size distribution or in 998 µL NaCl solution (1 mM) at pH=7.4 for measurement of the ζ-potential. All measurements were carried out at 25°C. Cell conjugation experiments were performed in clear u-shaped 96well-plates with a cell repellent surface purchased from Greiner Bio-One GmbH. Flow cytometry measurements were performed in FACS buffer (1 mM NaN_3 in DPBS supplemented with 2%FBS) on a Beckman Coulter Gallios instrument equipped with 3 lasers (405 nm, 488 nm, 640 nm) and 10 detectors (450/50, 550/40, 525/40, 575/25, 620/20, 695/30, 755LP, 660/20, 725/20, 755LP) and analyzed with FlowJo (V10.6.1) if not stated otherwise. Confocal microscopy images were taken on an inverted Zeiss LSM700 equipped with a Plan-Apochromat 63x/1.40 DIC oil objective and reconstructed and analyzed with Imaris.

2.2.3. Procedures

Surface modification of Fluospheres with mPEG-SVA/ MAL-PEG-SVA: Amine modified fluospheres (100 µL) were centrifuged (5 min, 30.000 g) and resuspended in MilliQ water (400 µL) followed by 2 washes in MilliQ water (400 µL, 5 min, 30.000 g) and sonication for 10-15 min. mPEG-SVA/MAL-PEG-SVA in MilliQ water (40 mg/100 µL) was added to the nanoparticles for 1 h under gentle shaking on an orbital shaker. PEG modified nanoparticles were centrifuged (30 min, 30.000 g) and resuspended in MilliQ water (400 µL) followed by 2 washes in MilliQ water (400 µL, 5 min, 30.000 g) and sonicated for 10-15 min. Fluospheres were kept at 4°C until use and diluted in MilliQ water/DPBS just before use.

Cell lines and cell cultures

Encephalitogenic CD4+ effector/memory proteolipid protein (PLP) peptide aa139-153 specific T cells (line SJL/PLP7, TKI Bern) [22] were cultured in RPMI 1640 glutamax medium (Gibco) supplemented with 10% fetal bovine serum (FBS) (Gibco), 1% penicillin/streptomycin (Gibco), 1% non-essential amino acid (Gibco), 1% Na-pyruvate (Gibco), 0.4% β-mercaptoethanol (Gibco), and 1% IL-2 supernatant (self-made) at 37°C and 5%CO_2. Cells were typically used for modification and in functional assays at day 3 after restimulation.

CellTracker Red labeling of Cells: CellTracker Red in DMSO (50 µg/1 vial in 10 µL) was diluted in DPBS (29 mL, 2.5 µM) and preheated at 37°C to prepare the CTR labeling solution. T cells were washed 2 times in 10 mL DPBS and resuspended in CTR labeling

solution at a concentration of 1 x10^6 cells/mL. The cell suspension was incubated for 30min at 37°C (+5% CO_2). Cells were pooled and washed 2 times in full cell culture medium (20 mL) and incubated for 10min at 37°C (+5% CO_2) before further use.

CellTracker DeepRed labeling of Cells: CellTracker DeepRed in DMSO (15 µg/1 vial/ in 20 µL) was diluted in DPBS (40 mL) and preheated at 37°C to prepare the CTDR labeling solution. T cells were washed 2 times in 10 mL DPBS and resuspended in CTDR labeling solution at a concentration of 1 x10^6 cells/mL. The cell suspension was incubated for 20 min at 37°C (+5% CO_2), added to 5 volume equivalents of full cell culture medium and incubated for another 10min at 37°C (+5% CO_2). Cells were pooled and washed 2 times in full cell culture medium (20 mL) and incubated for 10 min at 37°C (+5% CO_2) before further use.

Cell surface modification of T cells with maleimide modified Fluospheres: T cells were washed 2 times in 10 mL DPBS and resuspended in DPBS at a concentration of 30 x10^6 cells per mL. An equal volume of maleimide modified fluospheres in MilliQ water (1.50 x10^{11} NPs/mL) was added to the cell suspension and incubated at 37°C with gentle mixing every 10 min. After 30 min, 1 mM NAcCys in PBS (20 µL) was added to the reaction mixture and incubated at 37°C for 10 min to quench the reaction. The suspension was washed 3 times in 10 mL DPBS to remove unbound particles from the cells. The particle-cell conjugates were resuspended in NaN_3 (1 mM) and FBS (2%) supplemented DPBS at a cell concentration of 1 x10^6 cells/mL and analyzed by flow cytometry.

Viability assay: Viability assays were performed using AnnexinV – Alexa647 as indicator for apoptosis and DAPI as indicator for necrosis. Briefly, (un-)modified cells were washed once with DPBS (10 mL) and 0.3 x10^6 cells were resuspended in Annexin binding buffer (300 µL) containing DAPI (1 µg/mL). AnnexinV-Alexa647 conjugate (15 µL) was added and the suspension was kept for 15 min in the dark. Subsequently, 500 µL Annexin binding buffer was added directly followed by analysis of the cells by flow cytometry. As a positive control, 1 x10^6 cells were incubated with 1 µM Staurosporin for 24 h to induce apoptosis. Freshly biotinylated and non-biotinylated cells were used as a negative control. All controls were kept in full cell culture medium/DPBS at 37°C until analysis with the actual sample. Staurosporin treated cells were used to gate the cell populations as followed: Viable cells (Q4), apoptotic cells (Q3) and necrotic cells (Q1,Q2)

Preparation of slides for confocal microscopy: Nanoparticle conjugated and/or cell body labeled cells were washed 2 times in 10 mL DPBS and resuspended at a cell concentration of 0.5 x10^6 cells/mL. WGA-Texas Red (1 mM, 50 µL) was added to 1 mL of cell suspension for 30 min at RT. Glass cover-slips were coated with Poly(L-Lysine) for 10 min at RT and cells were immobilized onto the cover slips by centrifugation at 200 g for 3 min. After 2 washes in 1 mL DPBS cells were fixed in PFA-solution (4% in DPBS, 1 mL) for 10 min and washed again in 1 mL DPBS. Finally, the fixed particle-cell conjugates were mounted on ProLong Diamond mounting medium and the microscopy slides were kept at 4°C until analysis by confocal microscopy. Nanoparticles were counted automatically in Imaris by recognition of green fluorescent spheres with minimal dimensions of 150 nm x 150 nm x 250 nm in the deconvoluted image sets.

Injection of nanoparticle modified T cells into the carotid artery of mice: Mice were housed in individually ventilated cages under specific pathogen-free conditions at 22 °C with free access to chow and water. Animal procedures executed were approved by the Veterinary office of the Canton Bern (permission number 31/17.) T cells were labeled with CellTracker Red/ CellTracker DeepRed 0-1 d before injection and conjugated to nanoparticles directly before injection using the protocols described above. CellTracker Red/CellTracker DeepRed labeled T cells (8.5 x10^6), CellTracker Red/CellTracker DeepRed labeled T cells conjugated to nanoparticles (8.5 x10^6) and free nanoparticles in DPBS (1.05 x10^9 NPs) were injected into the carotid artery of C57/Bl6 mice (n=1, female, 8weeks old) using the following protocol. Mice were injected with TNF-α (1 µg, ip) at least 4h before surgery and with Buprenorphine (7.5 µg, ip) at least 30 min before surgery. Directly before surgery, mice were anaesthetized in a flow chamber using isoflurane (4.5%, 600 mL/min). Anesthesia was maintained during the surgery using isoflurane (3%, 220 mL/min). The eyes were protected with Lacrinorm® and 0.9% NaCl (1 mL, ip) was injected to prevent dehydration of the mice. The carotid artery was assessed via a 0.5 cm incision at the trachea and isolated using 3 sutures (1 close knot on the cranial side, 1 wire to stop the blood flow and the heart side, 1 loose knot to secure the catheter). A catheter was inserted in a small incision at the carotid artery, the blood flow was opened by loosening the heart side wire and the knot on the cranial side and samples were slowly applied using the catheter. The catheter was flushed with 0.9% NaCl (50 µL), removed together with all wires and the skin was closed with 2-3 sutures. Mice were allowed to recover from anesthesia, sacrificed after 3-5 h and perfused with PFA

(1%, 10mL). Brain, liver and spleen were collected, embedded in OCT resin and frozen at -80°C.

Immunofluorescence staining of tissue sections: For fluorescence imaging, tissue sections (16-20µm) were cut on a cryostat at -20°C, mounted on SuperFrost Plus® microscopy slides (Thermo Scientific) and dried overnight in the dark. The area around the dried sections was restricted using a DAKO Pen®. Sections were post fixed using PFA (2%, 150 µL) for 10 min at room temperature. The PFA was discarded and sections were washed 3x for 5 min with TBS (50 mM Trizma Base, 150 mM NaCl, 1 mM $CaCl_2x2H_2O$, pH= 7.4). After incubation of the sections with blocking buffer (150 µL) (TBS, 5% w/V skimmed milk, 0.3% V/V Triton X-100, 0.04% w/V NaN_3) for 20 min at room temperature, a mix of anti-pan Laminin and a second primary antibodies in blocking buffer (150 µL, 10 µg/mL) was applied for 1 h at room temperature. Unbound primary antibodies were removed by 3 washes with TBS for 5 min and a mix of anti-rabbit AMCA and a second secondary antibodies in blocking buffer (150 µL, 10 µg/mL) was applied for 1h at room temperature. Unbound secondary antibodies were removed by 3 washes with TBS for 5min and sections were mounted on MOWIOL® and dried overnight before imaging.

2.3. Results and Discussion

2.3.1. Experimental setup of the in vivo experiments

Nanoparticle (un-)modified T cells were injected into the carotid artery of TNF-α pretreated C57Bl6 mice (wt) to evaluate the impact of nanoparticle conjugation on the *in vivo* migration properties of the T cells. Treatment of the mice with TNF-α is necessary as it activates the brain endothelium leading to a faster T cell migration to the brain parenchyma. However, it does not influence the qualitative migration behavior of the T cells compared to unpathogenic conditions. To unambiguously distinguish injected T cells from native T cells, cells were labeled with amine and thiol reactive fluorescent dyes before nanoparticle conjugation and injection into the mice. Mice were sacrificed 5 h and 20 h post injection, brain, liver and spleen were harvested and embedded into OCT® resin (Figure 1).

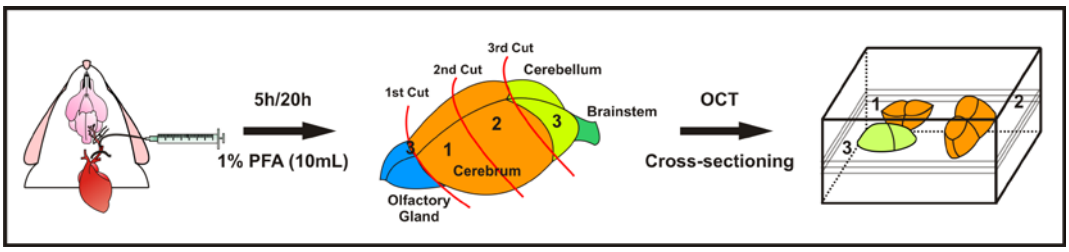

Figure 1 Schematic representation of the experimental setup. Cells are injected into the carotid artery of C57Bl6 mice. After 5 or 20 h, mice are perfused with 1% PFA (10mL), the brain is harvested cut into 3 equal pieces and embedded into OCT resin. This tissue block is used to cut 16µm thick tissue sections on a cryostat at -25°C.

The frozen tissue blocks were sliced into 16 µm thick tissue sections, mounted on microscopy slides and stained for laminin, a marker for the endothelial and parenchymal basement membrane. Cells co-localizing with the laminin stain are already adhering to the endothelium, but did not yet undergo diapedesis to reach the brain parenchyma. On the contrary, cells outside of the laminin stain in contrast are fully resident in the CNS parenchyma. Due to the use of green fluorescent nanoparticles and the use of a secondary antibody for the laminin labeled with AMCA, cell labeling was limited to red or far red fluorescent dyes.

2.3.2. Nanoparticle conjugation to CellTracker DeepRed labeled T cells

First, the impact of the amine reactive fluorescent dye CellTracker DeepRed (CTDR) on the viability and proliferation of the T cells was evaluated using an AnnexinV/DAPI based viability assay and a 3H-Thymidin proliferation assay. AnnexinV acts as an indicator for cell apoptosis as it binds to phosphatidyl serine, a lipid that is only relocated to the outer cell surface upon early cell apoptosis. DAPI acts as marker for cell necrosis, as it is cell membrane impermeable and only gets fluorescent once it is intercalated into the DNA. To directly measure cell proliferation, cells are incubated with 3H-Thymidin. This radioactively labeled nucleotide is taken up by healthy cells to be incorporated into the DNA over time. The radioactive 3H-Thymidin can be detected using a ß-counter. While the radioactivity will be maximal for untreated cells, the signal will decrease if cells took up less 3H-Thymidin as a result of a reduced growth or proliferation resulting from the CTDR labeling. While incubation of the T cells with CTDR (0.25-2.5 µM) seemed to have no impact on apoptosis and necrosis of the cells (Figure 2C),

concentrations higher than 0.5 µM of CTDR were shown to significantly decrease cell proliferation (Figure 2B). Analysis of the nanoparticle labeled T cells by flow cytometry and confocal microscopy revealed that incubation of the cells with CTDR did not compromise the efficiency of the nanoparticle conjugation (Figure 3). Consecutive labeling of T cells with the amine reactive CTDR and the thiol reactive nanoparticles resulted in a drastic increase of cell death (96.5%) after nanoparticle conjugation. This increase is attributed to the increased cell stress resulting from the consecutive chemical modification of two different chemical moieties on the cell surface and cytoplasm (amines and thiols) as compared to the modification of only thiols on the cell surface alone.

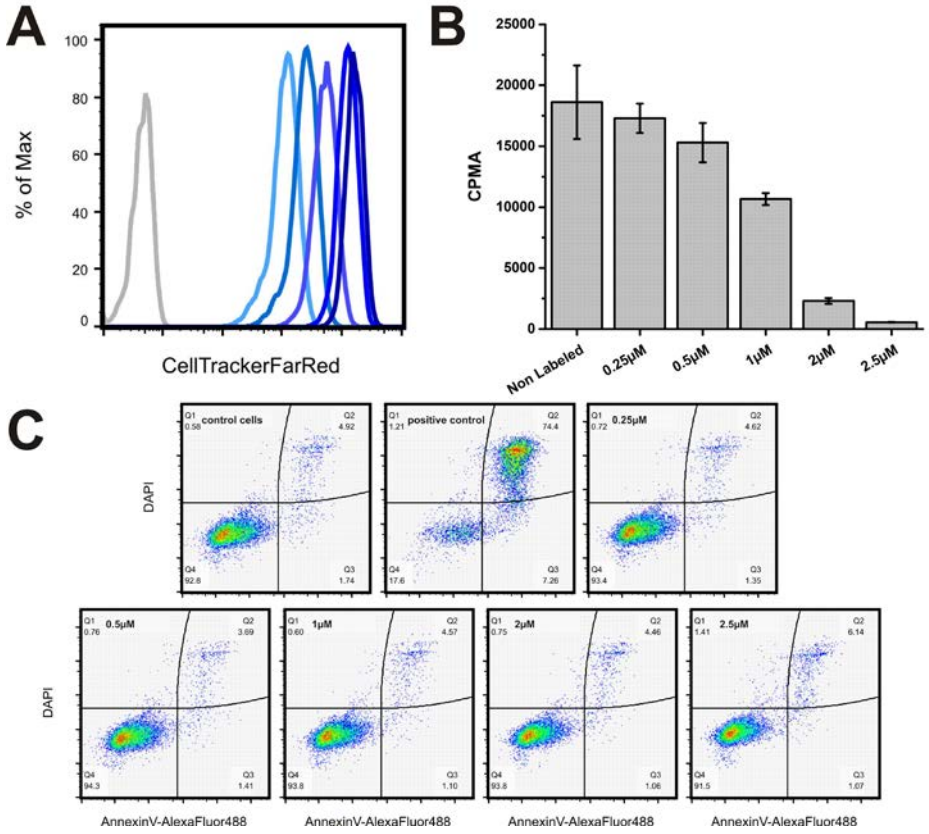

Figure 2 (A) Flow cytometry histogram of unmodified SJL-PLP7 cells (grey) and SJL-PLP7 cells incubated with 0.25 µM, 0.5 µM, 1 µM, 2 µM and 2.5 µM CTDR (light blue –> dark blue). (B) Radioactive count of unmodified SJL-PLP7 cells and SJL-PLP7 cells incubated with 0.25 µM, 0.5 µM, 1 µM, 2 µM and 2.5 µM CTDR after incubation with 3H-Thymidin. (C) Flow cytometry dot plots of unmodified SJL-PLP7 cells (control cells) SJL-PLP7 cells incubated with staurosporin (positive control) and SJL-PLP7 cells incubated with 0.25 µM, 0.5 µM, 1 µM, 2 µM and 2.5 µM CTDR incubated with AnnexinV-AlexaFluor488 and DAPI. AnnexinV acts as marker for cell apoptosis, DAPI as marker for necrosis.

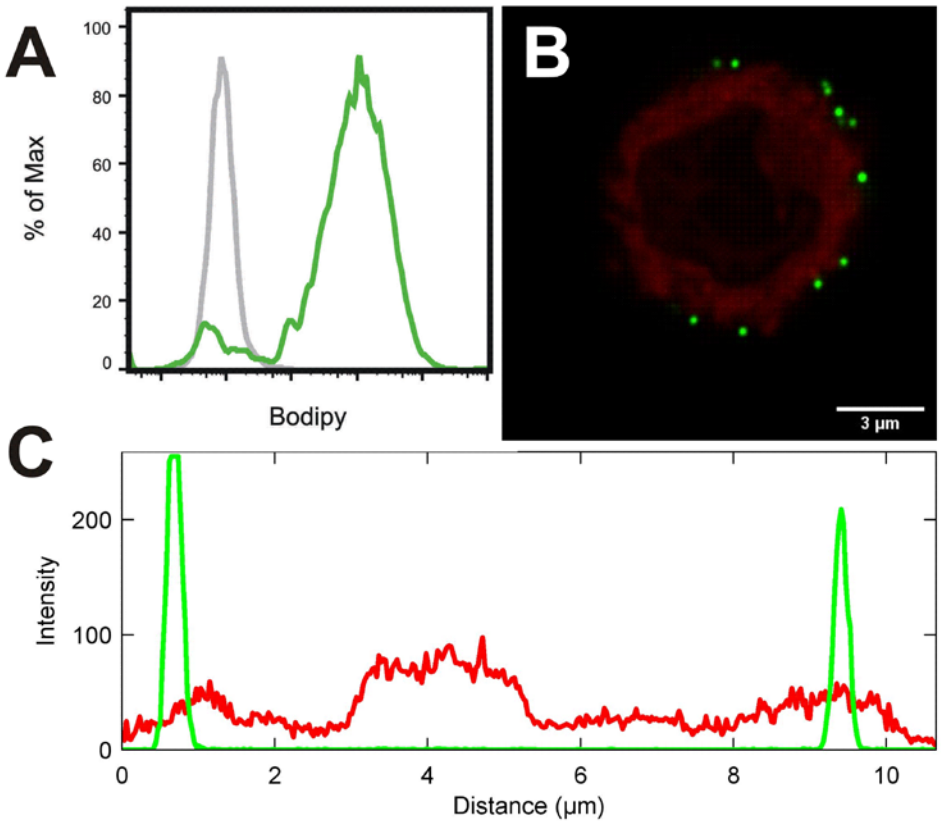

Figure 3 Flow cytometric analysis (A) representative cross section of confocal images (B) and profile plot of confocal images (C) of SJL-PLP7 cells labeled with 0.5 µM CellTracker DeepRed. The Bodipy associated channel shows the fluorescence intensity of CellTracker DeepRed labeled cells on day 4 before (grey) and after (green) conjugation to nanoparticles. The reconstructions of confocal images visualize the absolute number of nanoparticles (green) on the surface of CellTracker Red labeled T cells (red). The average amount of nanoparticles per cell (n = 10) was 48 ± 7.5 nanoparticles/cell.

2.3.3. Nanoparticle conjugation to CellTracker Red labeled T Cells

To avoid the labeling of the T cells with chemistries targeting two different chemical groups on the cell surface and cytoplasm, cells were labeled with the thiol reactive fluorescent dye CellTracker Red (CTR). Comparable to CTDR, CTR did not induce apoptosis or necrosis of the cells upon incubation with the cells as determined in an AnnexinV/DAPI viability assay (Figure 4B). Additionally, no significant difference in the proliferation of cells could be observed in a 3H-Thymidin assay upon incubation of the cells with CTR (0.25-2.5 µM) (Figure 4C).

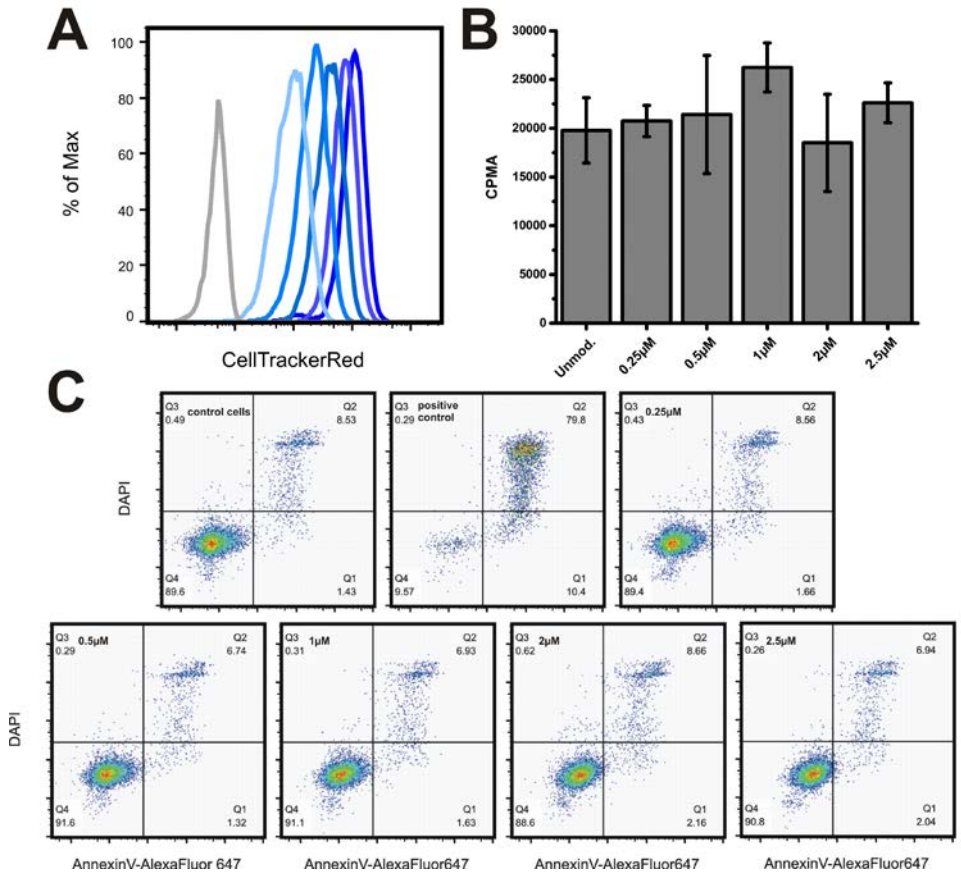

Figure 4 (A) Flow cytometry histogram of unmodified SJL-PLP7 cells (grey) and SJL-PLP7 cells incubated with 0.25 µM, 0.5 µM, 1 µM, 2 µM and 2.5 µM CTR (light blue –> dark blue). (B) Radioactive count of unmodified SJL-PLP7 cells and SJL-PLP7 cells incubated with 0.25 µM, 0.5 µM, 1 µM, 2 µM and 2.5 µM CTR after incubation with 3H-Thymidin. (C) Flow cytometry dot plots of unmodified SJL-PLP7 cells (control cells) SJL-PLP7 cells incubated with staurosporin (positive control) and SJL-PLP7 cells incubated with 0.25 µM, 0.5 µM, 1 µM, 2 µM and 2.5 µM CTR incubated with AnnexinV-AlexaFluor488 and DAPI. AnnexinV acts as marker for cell apoptosis, DAPI as marker for necrosis.

Flow cytometry was used to monitor the two-step chemical modification process of the cellbody labeling with CTR and the nanoparticle conjugation and the average number of nanoparticles per cell was evaluated using confocal microscopy (Figure 5). Figure 5A-C present the results that were obtained when T cells were first stained with 2.5 µM CellTracker Red and then modified with the maleimide functionalized nanoparticles at a ratio of 5000 particles / cell. In a second experiment (Figure 5D-F), cells were stained with 1 µM CellTracker Red and then surface modified with the nanoparticles. Analysis of the confocal images indicated that the former reaction conditions result in 4.2 ± 2.3

nanoparticles/cell while the latter generates T cells that carry 12.0 ± 3.7 nanoparticles/cell. These results suggest that nanoparticle conjugation to the cells after cell labeling with CTR is inhibited, as both labeling processes depend on thiol reactive chemistries. Therefore, cells that are labeled with a decreased concentration of CTR can be conjugated to a linearly increasing amount of nanoparticles. To facilitate the identification of diapedesed T cells in the brain sections with fluorescence microscopy (*vide infra*), for the *in vivo* experiments T cells were used that were stained with 2.5 µM CellTracker Red prior to nanoparticle surface conjugation.

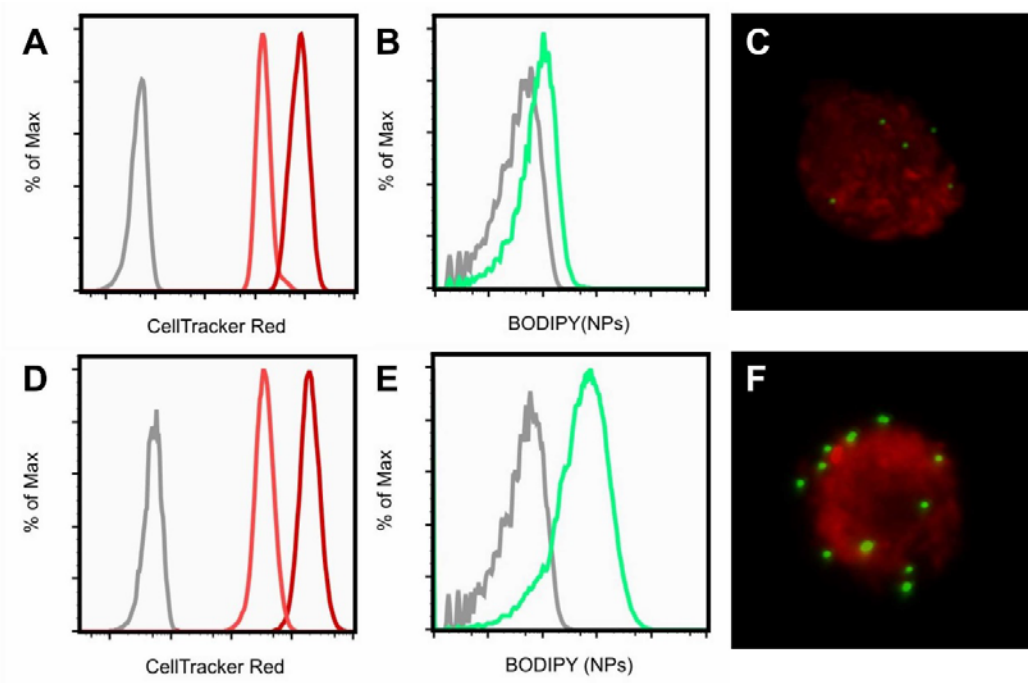

Figure 5 Flow cytometric analysis and representative 3D reconstructions of confocal images of SJL-PLP7 cells labeled with 2.5 µM (A-C) and 1 µM (D-F) CellTracker Red. The CellTracker Red associated channel shows the fluorescence intensity of unmodified control cells on day 3 (grey), cells labeled with CellTracker Red on day 3 (red) and cells labeled with CellTracker Red on day 4 (pale red). The Bodipy associated channel shows the fluorescence intensity of CellTracker Red labeled cells on day 4 before (grey) and after (green) conjugation to nanoparticles. The reconstructions of confocal images visualize the absolute number of nanoparticles (green) on the surface of CellTracker Red labeled T cells (red). The average amount of nanoparticles per cell (n = 5) was 4.2 ± 2.3 nanoparticles/cell (C) and 12.0 ± 3.7 nanoparticles/cell (F)

The ability of the T cells to transport nanoparticles to the CNS *in vivo* was studied in TNF-α pretreated C57Bl6 mice. In these experiments, 8.5 x 10^6 CellTracker Red stained and nanoparticle-loaded T cells in DPBS were administered via the carotid artery. For controls, mice were given 8.5 x 10^6 CellTracker Red stained T cells as well as ~ 1.050 x 10^6 mPEG modified nanoparticles. After 5 h, mice were sacrificed and their brain, liver, and spleen was collected. Migration of T cells and nanoparticles to the CNS was assessed by fluorescence microscopy analysis of brain sections. Figure 6 presents representative images of brain sections that were analyzed for each of the three different experiments. Analysis of these brain sections demonstrates T cell migration to the CNS both in case of administration of non-surface modified, control T cells as well as nanoparticle-decorated T cells.

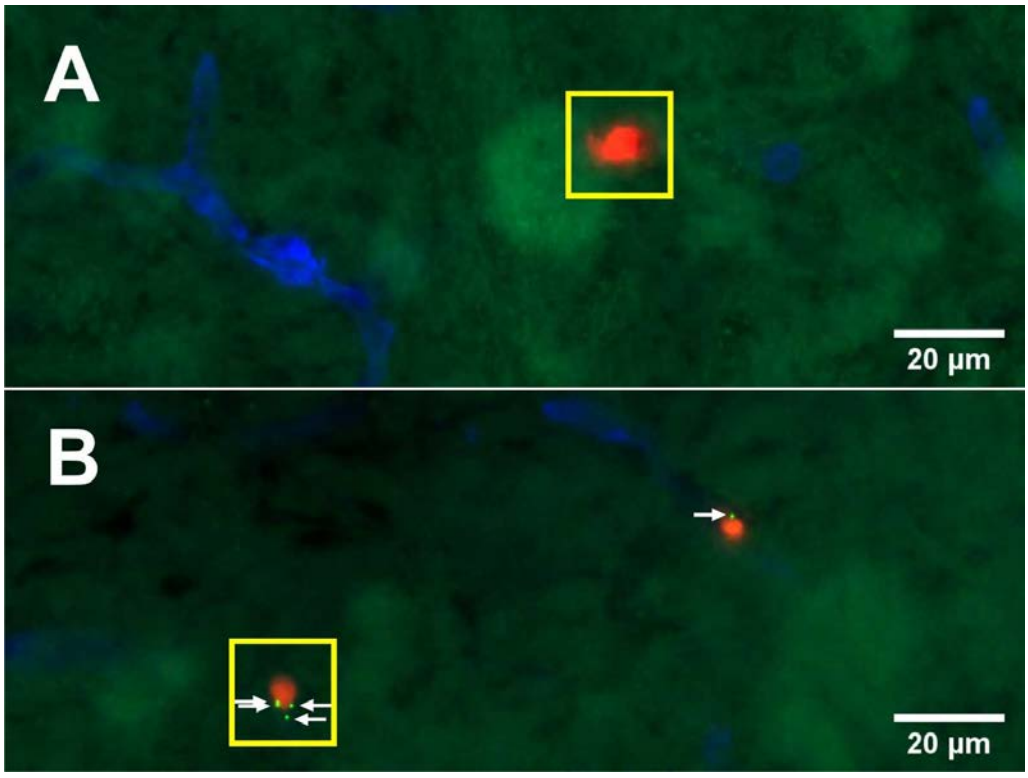

Figure 6: Widefield microscopy images of the brain parenchyma of mice after injection of CTR labeled SJL-PLP7 cells (A) and after injection of CTR labeled SJL-PLP7 cells conjugated to thiol reactive nanoparticles (B). The parenchymal basement membrane was stained for laminin (blue). Cells were labeled with 2.5 µM CTR (red) and conjugated to thiol reactive nanoparticles (green). T cells resident in the brain parenchyma are marked by a yellow box. White arrows indicate the presence of nanoparticles on the cell surface.

In contrast, however, in the experiment where only nanoparticles were administered, the fluorescence micrographs did not provide any evidence for nanoparticle migration to the brain and CNS (Figure 7 A-B). Generally, in both cases (after injection of nanoparticle modified and unmodified CellTracker Red labeled cells) a comparable high number of elongated T cells could be found in the brain endothelium (Figure 7 C-D). These cells strongly adhere to the endothelium via ICAM/integrin recognition, but fail to undergo diapedesis. The shear of the blood flow then results into elongated structures if cells do not detach from the endothelium. As this effect is observable equally after injection of CellTracker Red labeled cells with and without nanoparticle modification, it is most likely a result of CellTracker Red induced cellular stress but not the subsequent nanoparticle modification.

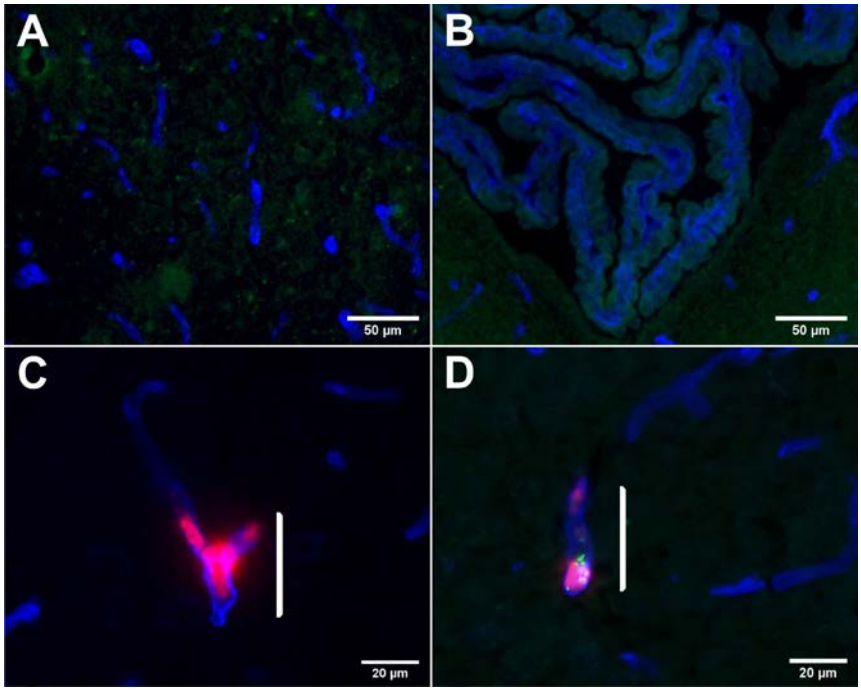

Figure 7: (A) Widefield microscopy image of the brain parenchyma of a mouse after injection of free NPs. (B) Widefield microscopy image of the choroid plexus of a mouse after injection of free NPs. (C-D) Widefield microscopy images of the brain parenchyma of mice after injection with CTR labeled SJL-PLP7 cells with and without conjugated NPs demonstrating T cells that adhere to the endothelium but cannot migrate to the parenchyma. The parenchymal basement membrane was stained for Laminin (blue). Cells were labeled with 2.5 µM CTR (red) and conjugated to thiol reactive fluorospheres (green). Elongated cells that adhere to the endothelium but failed to migrate to the parenchyma are marked with white bars.

To quantify these analyses, for each experiment, the average number of T cells per section, the number of CNS residing T cells as well as the number of nanoparticle-carrying T cells was determined. The results of these analyses, summarized in Table 1, revealed the presence of 195 ± 48 and 134 ± 25 T cells/section respectively for mice that were administered nanoparticle-decorated or non-surface modified control T cells. From the total number of T cells, 4.9 %, resp 3.0 % were found to reside in the CNS. When nanoparticle-decorated cells were injected, 27% of the T cells that were found in the CNS still carried a nanoparticle payload. These cells carried 2.5 ± 2.3 nanoparticles per cell.

Table 1. Quantitative analysis of brain sections of C57Bl6 mice after injection of CellTracker Red labeled SJL-PLP7 T cells with and without surface immobilized nanoparticles (n = 5).

Condition	*CTR labeled cells without nanoparticles*	*CTR labeled, nanoparticle-modified cells*
Average number of T cells per section	130 ± 25	195 ± 48
% of CNS resident T cells	3.0	4.9
Total Σ over all sections of CNS resident T cells	20	48
Total Σ over all sections of CNS resident T cells that carry NPs	-	13
Average number of NPs on the surface of all CNS resident T cells that carry NPs	-	2.5 ± 2.3

2.3.4. Nanoparticle conjugation to TdTomato transfected T cells

To avoid the necessity to label T cells with two chemistries that either target two different chemical moieties on the cell or compete with each other, transgenic CD4+ T cells expressing TdTomato (AI14 heterocygote TCR-MOG/2D2 cells) were conjugated to nanoparticles and injected in TNF-α pretreated C57Bl6 mice to monitor their migration

properties to the CNS within 5 and 20 h. These cells carry a significantly increased number of nanoparticles without losing their red fluorescence that results from the TdTomato fluorescence as determined by flow cytometry and confocal microscopy (Figure 8).

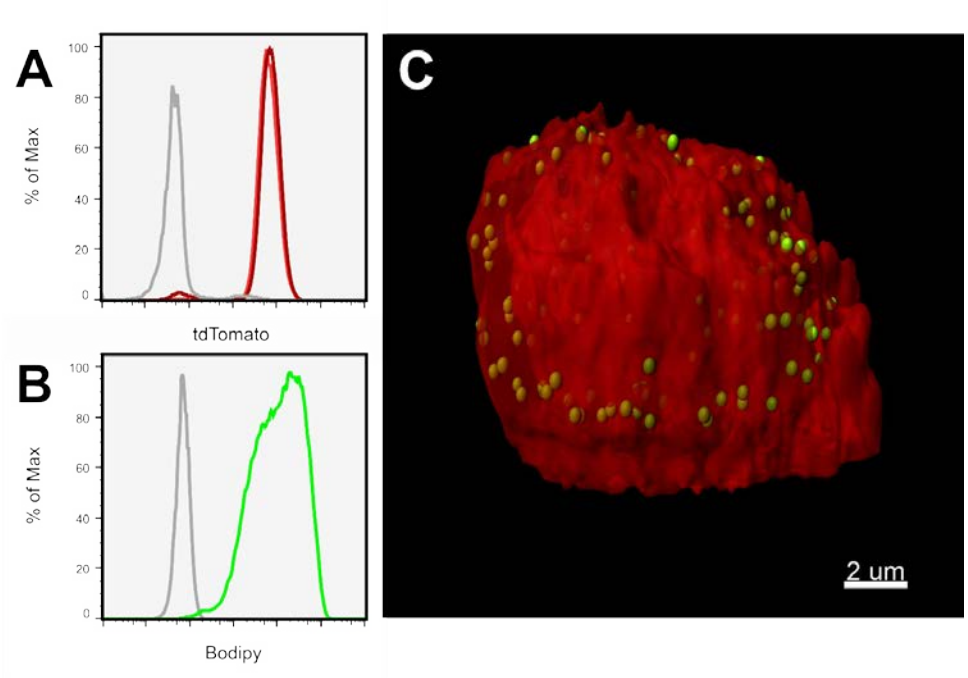

Figure 8 Flow cytometric analysis and representative confocal microscopy reconstruction of tdTomato transfected TCR-MOG (2D2) cells. (A) tdTomato associated fluorescence before (dark red) and after (light red) conjugation to nanoparticles. The FACS plot is calibrated on the unfluorescent cell debris (grey). (B) Bodipy associated fluorescence before (grey) and after conjugation to fluospheres (green). (C) Reconstructions of confocal images visualizing the absolute number of nanoparticles (green) on the surface of tdTomato transfected T cells stained with WGA-AlexaFluor647 (red). The average amount of nanoparticles per cell (n = 5) was 156.2 ± 16.2 nanoparticles/cell.

No T cells could be observed in the microscopy section of the mouse brains, liver or spleen after staining for laminin in both cases, whether nanoparticle modified or unmodified cells were injected. This fact lead to the conclusion that T cells lost their TdTomato associated fluorescence after injection and indeed, if sections were stained additionally for the alpha or beta chain of the transgenic T cell receptors (TCR Vα3.2, TCR Vß1.1), T cells could be visualized in high numbers in the liver and the spleen (Figure 9A-B), however only in negligible numbers in the brain. (Figure 10)

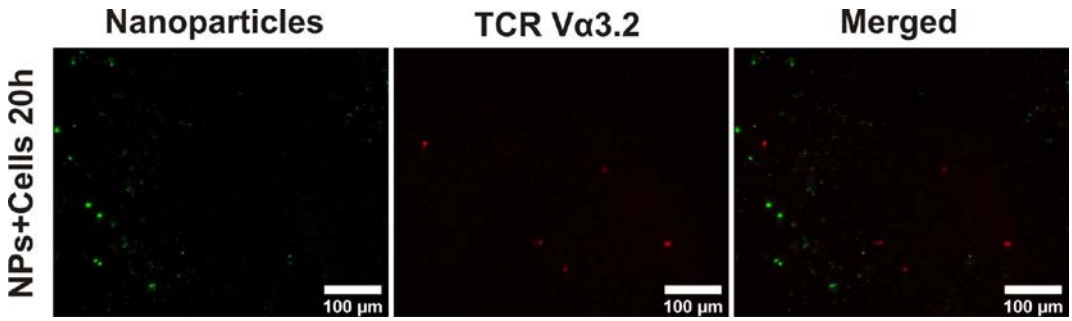

Figure 9 Widefield microscopy image of spleen sections of a mouse after injection of nanoparticle modified tdTomato transfected TCR-MOG cells. The parenchymal basement membrane was stained for Laminin (blue). Cells were stained with anti-TCR-Vα3.2 (red) and conjugated to thiol reactive fluorospheres (green).

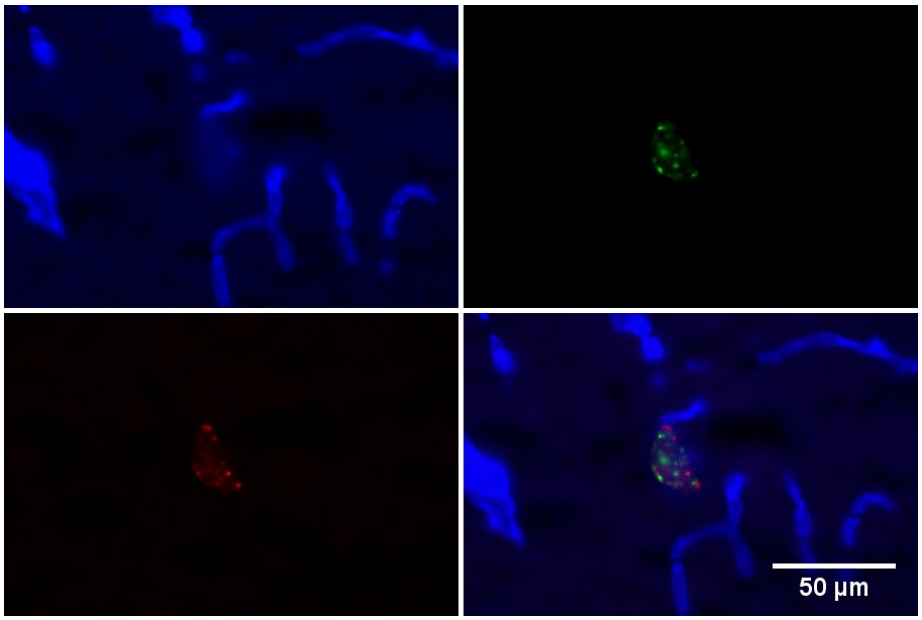

Figure 10 Widefield microscopy image of the brain parenchyma of a TNF-α pretreated mouse after injection of nanoparticle modified tdTomato transfected TCR-MOG cells. The parenchymal basement membrane was stained for Laminin (blue). Cells were stained with anti-TCR-Vα3.2 (red) and conjugated to thiol reactive fluorospheres (green).

This profound contrast in the migration behavior between these cells and the previous cell line can be explained by the fact that two completely different kinds of cells were used. The previously used SJL-PLP7 cells were a cell line specifically created to induce encephalogeneic response in the CNS after injection into SJL mice and therefore, show a

very strong migration behavior, while the TCR-MOG cells that were used now are direct, primary isolated cells of 2D2 mice that were vaccinated against the MOG peptide. Additionally, brain sections of mice in both experiments were stained for the inflammatory markers ICAM-1 and VCAM-1, to compare the inflammatory state of the brain endothelium in both cases (Figure 11-12). Figure 14-15 show the drastic difference of the TNF-α induced inflammation of the brain endothelium, which was significantly stronger in the first experiment.

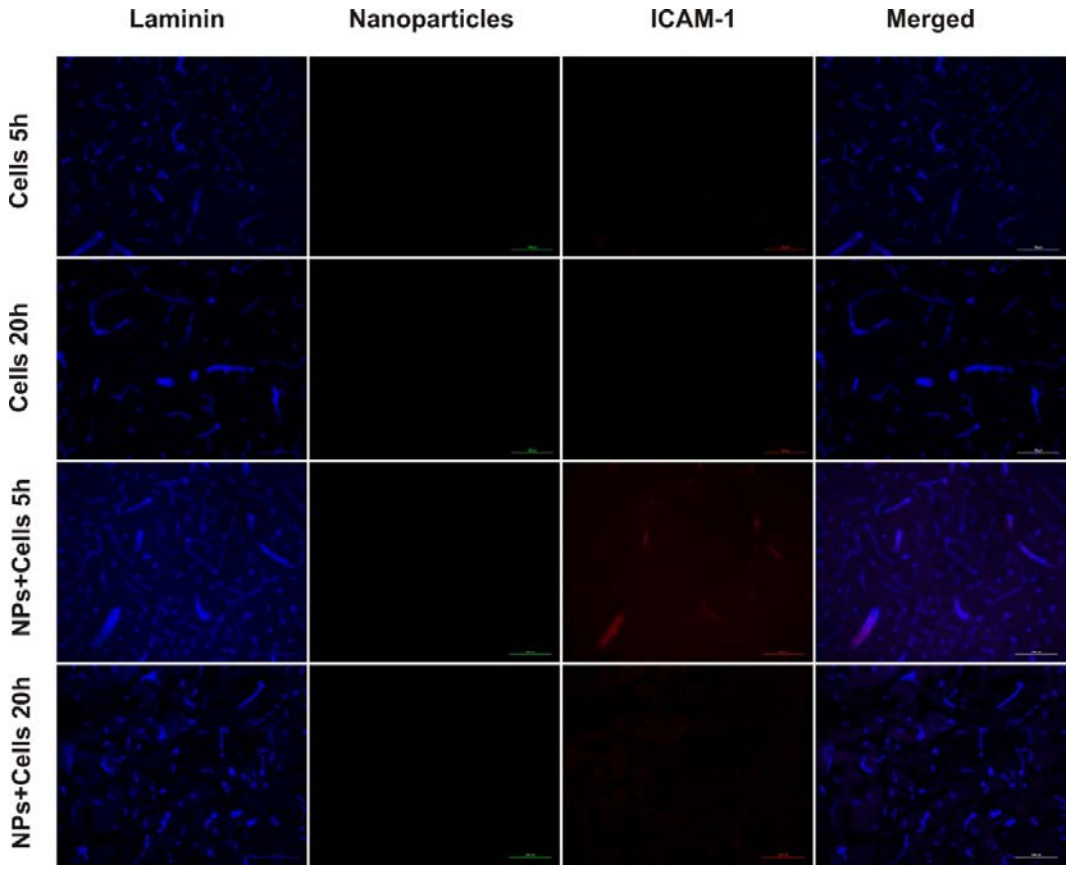

Figure 11 Widefield microscopy images of brain sections (20 µm) after immunofluorescence staining for laminin (AMCA, blue) and ICAM-1 (PE/Cy3, red) of mice treated with unmodified T cells and nanoparticle conjugated T cells for 5h/20h. Nanoparticle fluorescence is associated to Bodipy (green). (Scale bar= 100 µm)

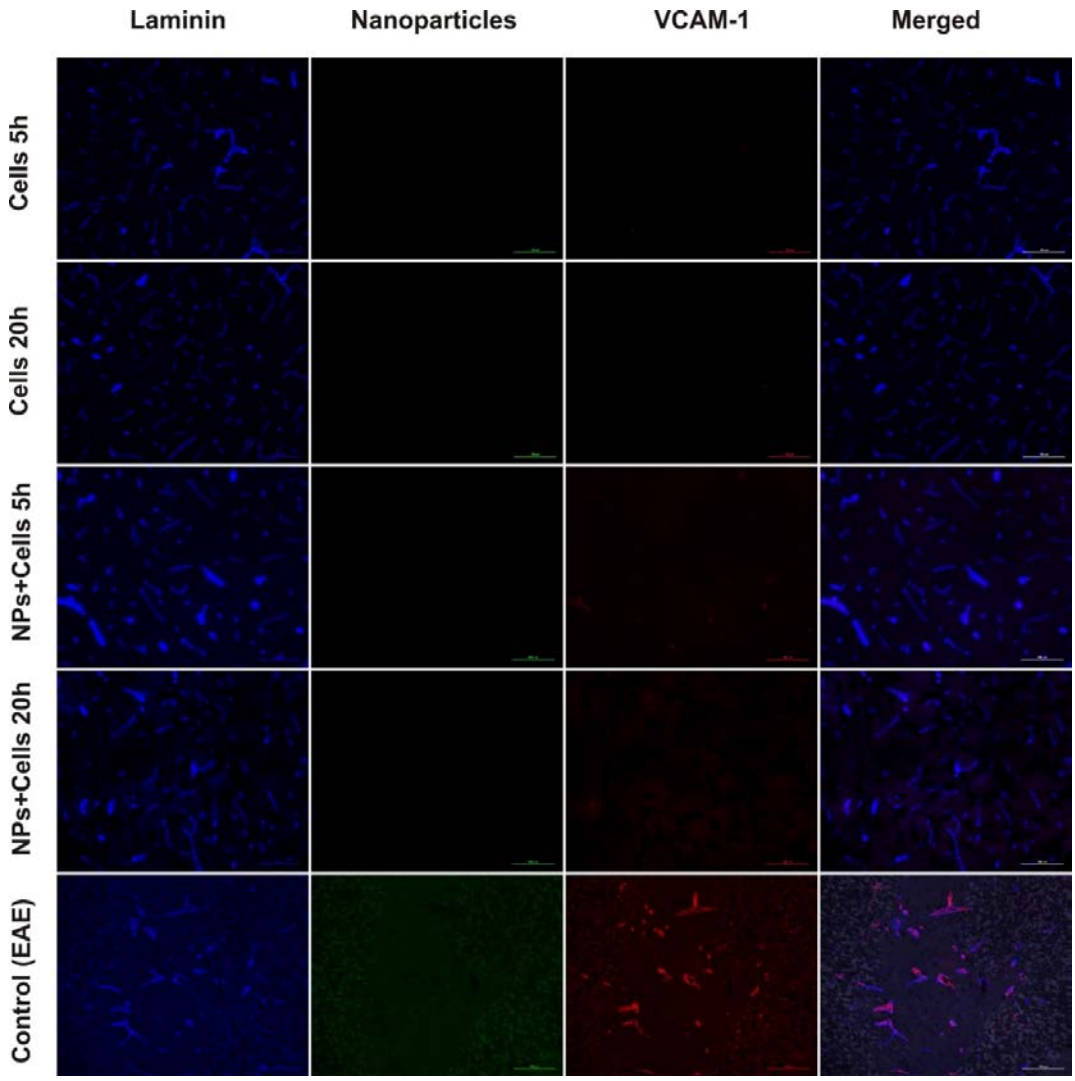

Figure 12 Widefield microscopy images of brain sections (20µm) after immunofluorescence staining for laminin (AMCA, blue) and VCAM-1 (PE/Cy3, red) of mice treated with unmodified T cells and nanoparticle conjugated T cells for 5h/20h. Nanoparticle fluorescence is associated to Bodipy (green). (Scale bar= 100 µm).

To increase the migration of unmodified control cells, in further studies mice were not pretreated with TNF-α but instead mice with acute experimental autoimmune encephalomyelitis (aEAE) were used. The use of mice with aEAE does qualitatively effect the T cell migration to the brain parenchyma compared to untreated wildtype mice as this animal model resembles the pathogenic immune response leading to multiple sclerosis in humans. Additionally to improve the migration properties of nanoparticle modified cells, cells were conjugated to a smaller amount of nanoparticles (29±5.8

NPs/cell). Nanoparticle un-/modified transgenic TCR-MOG cells expressing TdTomato (Ai14 homozygote) were injected into C57Bl6 mice to evaluate the impact of nanoparticle conjugation on the T cell migration to the CNS. This time, homozygote TCR-MOG mice were used to increase the TdTomato associated fluorescence as cells in the last experiment lost their red fluorescence after injection. However, this was also the case for the homozygote cells and tissue sections had to be stained again for TCR Vα3.2 or TCRß1.1 to identify the injected T cells. This staining revealed that in average (n=10 sections) only a small number of the unmodified T cells per brain section adhered to the brain endothelium (9.1±5.7) or migrated to the brain parenchyma (0.4±0.7). These numbers were even smaller for nanoparticle conjugated T cells with an average of 0.5±0.7 cells adhering to the brain endothelium and 0.4±0.7 cells entering the brain parenchyma (Figure 13). Additionally, all nanoparticle modified cells entering the brain parenchyma completely lost their nanoparticle cargo during the migration.

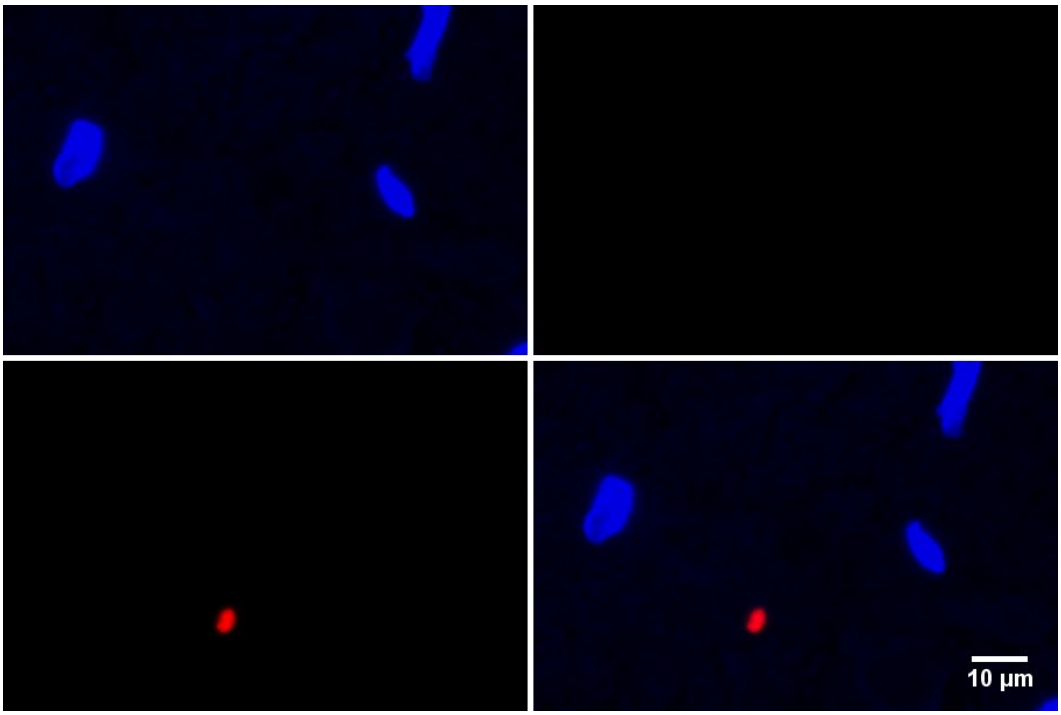

Figure 13 Widefield microscopy image of the brain parenchyma of a mouse suffering from aEAE after injection of nanoparticle modified tdTomato transfected TCR-MOG cells (heterozygote). The parenchymal basement membrane was stained for Laminin (blue). Cells were stained with anti-TCR-Vα3.2 (red) and conjugated to thiol reactive fluorospheres (green).

2.3.5. Identification of a surface marker for transgenic SJL T cells

SJL cells seemed to be superior to 2D2 cells regarding the CNS migration properties and their ability to retain nanoparticles on their surface. However, the maximal cell migration can only be reached if these cells are injected into SJL mice as these cells are designed to induce EAE symptoms in SJL mice targeting myelin proteins of this mouse strain. For this reason, SJL-TCR-PLP11 and SJL-TCR-PLP20 T cells were incubated with anti-TCR-Vß6-PE and analyzed by flow cytometry to determine the specificity of this antibody towards the SJL-TCR-PLP11 and SJL-TCR-PLP20 T cells over SJL-PLP7 cells that lack this transgenic T cell receptor. This way, cells can be stained comparable to the previous experiment for their transgenic T cell receptor to distinguish injected cells from native T cells. Figure 14 shows the specific binding of anti-TCR-Vß6-PE towards both SJL-TCR-PLP11 and SJL-TCR-PLP20 T cells over SJL-PLP7 cells with a saturation of the binding at antibody concentrations of 2 µg/mL.

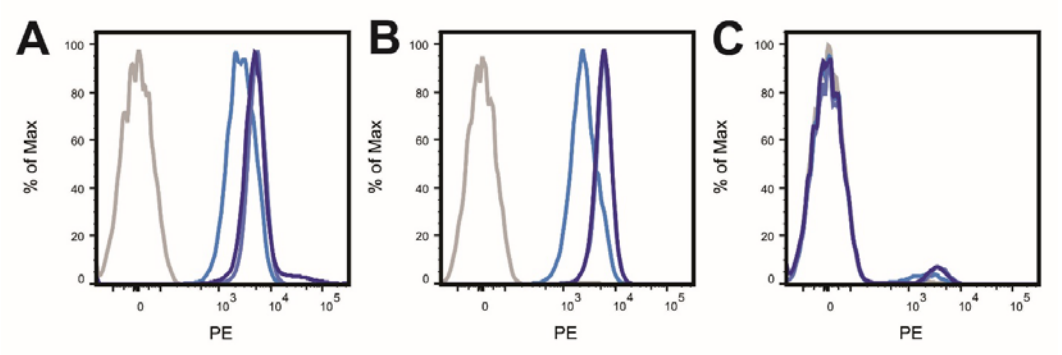

Figure 14 Flow cytometry histogram of (A) SJL-TCR-PLP11 cells (grey) (B) SJL-TCR-PLP20 cells (grey) (C) SJL-PLP7 cells (grey) incubated with 0.4 µg/mL (light blue), 2 µg/mL (blue), 10 µg/mL (dark blue) anti-TCR-Vß6-PE antibody.

2.4. Conclusions

In this chapter, nanoparticle conjugated T cells were injected into C57Bl6 mice via a carotid artery catheter. The *in vivo* migration properties of the un-/modified cells were investigated in brain cryo-sections that were stained using an antibody against laminin, a marker for the endothelial and parenchymal basement membrane. While nanoparticle

conjugated SJL-PLP7 cells seem to be able to cross the BBB in comparable numbers to unmodified cells, these cells had to be stained with a cytosol stain that effectively inhibited nanoparticle conjugation. Modification of this system to a system using intrinsically fluorescent tdTomato expressing T cells, however, lead to a loss of the CNS migration ability for both, nanoparticle modified cells and unmodified control cells. Additionally, intrinsically labeled 2D2 cells are not able to retain their nanoparticle cargo during this migration process. One possibility to bypass these drawbacks could be the use of transgenic SJL-TCR-PLP11/SJL-TCR-PLP20 cells in a SJL mouse. These cells were shown to be able to be stained specifically over native SJL cells by the use of an antibody that is specific for the TCR-Vß chain of the transgenic T cell receptor. Using this visualization technique, a second chemical modification of the cells to achieve a cell body stain or the use of intrinsically labeled 2D2 cells can be bypassed. The proof of concept for this delivery system, however, has still to be validated *in vivo*.

2.5. References

1. Abbott, N.J., *Dynamics of CNS Barriers: Evolution, Differentiation, and Modulation.* Cellular and Molecular Neurobiology, 2005. **25**(1): p. 5-23.
2. Abbott, N.J., L. Ronnback, and E. Hansson, *Astrocyte-endothelial interactions at the blood-brain barrier.* Nat Rev Neurosci, 2006. **7**(1): p. 41-53.
3. Abbott, N.J., et al., *Structure and function of the blood–brain barrier.* Neurobiology of Disease, 2010. **37**(1): p. 13-25.
4. Tietz, S. and B. Engelhardt, *Brain barriers: Crosstalk between complex tight junctions and adherens junctions.* The Journal of Cell Biology, 2015. **209**(4): p. 493-506.
5. Al Ahmad, A., et al., *Astrocytes and pericytes differentially modulate blood-brain barrier characteristics during development and hypoxic insult.* Journal of cerebral blood flow and metabolism : official journal of the International Society of Cerebral Blood Flow and Metabolism, 2011. **31**(2): p. 693-705.
6. Lipinski, C.A., et al., *Experimental and computational approaches to estimate solubility and permeability in drug discovery and development settings1.* Advanced Drug Delivery Reviews, 2001. **46**(1–3): p. 3-26.
7. Pardridge, W.M., *Drug transport across the blood-brain barrier.* Journal of cerebral blood flow and metabolism : official journal of the International Society of Cerebral Blood Flow and Metabolism, 2012. **32**(11): p. 1959-1972.
8. Kreuter, J., *Drug delivery to the central nervous system by polymeric nanoparticles: What do we know?* Advanced Drug Delivery Reviews, 2014. **71**: p. 2-14.

9. Upadhyay, R.K., *Drug Delivery Systems, CNS Protection, and the Blood Brain Barrier.* BioMed Research International, 2014. **2014**: p. 37.
10. Leslie, E.M., R.G. Deeley, and S.P.C. Cole, *Multidrug resistance proteins: role of P-glycoprotein, MRP1, MRP2, and BCRP (ABCG2) in tissue defense.* Toxicology and Applied Pharmacology, 2005. **204**(3): p. 216-237.
11. Engelhardt, B. and L. Sorokin, *The blood–brain and the blood–cerebrospinal fluid barriers: function and dysfunction.* Seminars in Immunopathology, 2009. **31**(4): p. 497-511.
12. Redzic, Z., *Molecular biology of the blood-brain and the blood-cerebrospinal fluid barriers: similarities and differences.* Fluids and barriers of the CNS, 2011. **8**(1): p. 3-3.
13. Liddelow, S.A., *Development of the choroid plexus and blood-CSF barrier.* Frontiers in neuroscience, 2015. **9**: p. 32-32.
14. Spadoni, I., G. Fornasa, and M. Rescigno, *Organ-specific protection mediated by cooperation between vascular and epithelial barriers.* Nature Reviews Immunology, 2017. **17**: p. 761.
15. Engelhardt, B., P. Vajkoczy, and R.O. Weller, *The movers and shapers in immune privilege of the CNS.* Nat Immunol, 2017. **18**(2): p. 123-131.
16. Röhnelt, R.K., et al., *Immunosurveillance modelled in vitro: naive and memory T cells spontaneously migrate across unstimulated microvascular endothelium.* International Immunology, 1997. **9**(3): p. 435-450.
17. Ransohoff, R.M. and B. Engelhardt, *The anatomical and cellular basis of immune surveillance in the central nervous system.* Nat Rev Immunol, 2012. **12**(9): p. 623-635.
18. Engelhardt, B. and R.M. Ransohoff, *Capture, crawl, cross: the T cell code to breach the blood–brain barriers.* Trends in Immunology, 2012. **33**(12): p. 579-589.
19. Lopes Pinheiro, M.A., et al., *Immune cell trafficking across the barriers of the central nervous system in multiple sclerosis and stroke.* Biochimica et Biophysica Acta (BBA) - Molecular Basis of Disease, 2016. **1862**(3): p. 461-471.
20. Lyck, R., et al., *T-cell interaction with ICAM-1/ICAM-2 double-deficient brain endothelium in vitro: the cytoplasmic tail of endothelial ICAM-1 is necessary for transendothelial migration of T cells.* Blood, 2003. **102**(10): p. 3675.
21. Muller, W.A., *Mechanisms of Leukocyte Transendothelial Migration.* Annual Review of Pathology: Mechanisms of Disease, 2011. **6**(1): p. 323-344.
22. Engelhardt, B., et al., *The development of experimental autoimmune encephalomyelitis in the mouse requires alpha4-integrin but not alpha4beta7-integrin.* The Journal of Clinical Investigation, 1998. **102**(12): p. 2096-2105.

3. Conjugation of polymersomes to T cells

3.1. Introduction

The Blood-Brain-Barrier (BBB) represents a major obstacle in drug delivery to the brain. Tight junctions between the endothelial cells physically block the diffusion of drug molecules across the brain endothelium and by active transport mechanisms from the brain to the blood (ABC-transporters) [1-4]. Therefore, delivery of therapeutic drugs across the BBB is extremely challenging. To overcome the barrier properties of the brain endothelium, the potential of nanoparticle formulations and biohybrid- nanoparticle materials is currently under investigation [5-8].

Despite tremendous amounts of research on the topic, most nanoparticle formulations acting in the brain, which may show significant therapeutic effects, suffer from a poor bio-distribution around the whole body or are not able to enter the brain in significant amounts [9-14]. For this reason, nanoparticles have been conjugated to circulatory cells like Macrophages, Neutrophils and Lymphocytes exploiting their natural migratory properties to the brain [15-21]. Macrophages, however, cannot be transferred between individuals without toxic effects. As a major drawback, they have to be isolated, modified and reinjected individually for each patient, which takes a lot of effort (money) and time (limiting their use for end-stage cancer patients) [22]. Currently, Neutrophils and Lymphocytes ($CD8^+$) can be cultured *ex vivo* and transferred between patients, however their trafficking relies on inflammatory conditions of the brain or the BBB [20, 23]. In contrast to previously studied biohybrid-nanoparticle materials, we conjugate nanoparticles to a special subset of Lymphocytes ($CD4^+$ T_{EM} cells), which has been shown to enter the brain parenchyma in an antigen independent manner by diapedesis across the brain endothelium (BBB) and the choroid plexus epithelium (BCSFB) [2, 24, 25]. Another major advantage of using $CD4^+$ T_{EM} cells is that this cell type can be isolated from one donor, restimulated *in vitro* and kept in culture for a prolonged time and finally transferred to a second recipient without major implications. Unlike most examples in literature that utilize micelles, liposomes, nanogels or solid-core nanoparticles for cell conjugation, this study focuses on the cell surface immobilization of polymersomes, bilayered vesicles formed by the use of amphiphilic block copolymers

that can efficiently encapsulate hydrophilic and hydrophobic drugs. The polymer that is used for the self-assembly to polymersomes is PEG-b-PLA, due to its biocompatible and biodegradable polymer blocks [26-28].

3.2. Experimental Section

3.2.1. Materials

All chemicals were used as received unless described otherwise. The polymers Methoxy poly(ethylene glycol)$_{2000}$-b-poly(D,L-lactide)6000 (mPEG$_{2000}$PLA$_{6000}$), amino poly(ethylene glycol)$_{2000}$-b-poly(D,L-lactide)$_{6000}$ (H2N-PEG$_{2000}$PLA$_{6000}$) and methoxy poly(ethylene glycol)$_{1000}$ (mPEG-biton$_{1000}$) were purchased from APM (Montreal, Canada) and stored at 4°C until use. AlexaFluor488 carboxylic acid triethylammonium salt, AlexaFluor488 NHS-ester, (6-((6-(Biotinoyl)amino)hexanoyl)amino)hexanoic acid, sulfosuccinimidyl ester, sodium salt) (biotin-xx-sSE), bis(sulfosuccinimidyl)suberate (BS3), 1-Biotinamido-4-[4'-(maleimidomethyl)cyclohexanecarboxamido]butane (BMCC-biotin), PBS (pH=7.4, tablets for 500 mL) Maleimide-AlexaFluor488, NeutrAvidin, NeutrAvidin-DyLight650, sulfosuccinimidyl (4-iodoacetyl)aminobenzoate (Sulfo-SIAB) and sulfosuccinimidyl 4-(N-maleimidomethyl)cyclohexane-1-carboxylate (Sulfo-SMCC) were purchased from Fisher Scientific. Protein A was purchased from BioVision, Lausen, Switzerland. Recombinant DNER-Fc and ICAM1-Fc chimera protein was purchased from R&D Systems, Abington, U.K.. HPLC-grade chloroform was purchased from Fluka. Nucleopore track-etched polycarbonate membranes (0.2/0.4 µm, 19 mm) were purchased from Sigma Aldrich.

3.2.2. Methods

Absorbance and fluorescence intensity measurements were performed with a Tecan Infinite Pro 200 plate reader. Particle size and zeta potential measurements were performed using a Malvern Zetasizer Nano SZ analyzer by diluting 20 µL of the nanoparticle dispersions in 1 mL, 10 mM NaCl solution or PBS. The measurements were performed using a single scattering angle of 173° at 25 °C. Flow cytometry measurements were performed in FACS buffer (1 mM NaN_3 in DPBS supplemented with 2%FBS) on a Beckman Coulter Gallios instrument equipped with 3 lasers (405 nm, 488 nm, 640 nm) and 10 detectors (450/50, 550/40, 525/40, 575/25, 620/20, 695/30, 755LP, 660/20,

725/20, 755LP) and analyzed with FlowJo (V10.6.1) if not stated otherwise. Confocal microscopy images were taken on an inverted Zeiss LSM700 equipped with a Plan-Apochromat 63x/1.40 DIC oil objective and reconstructed and analyzed with Imaris.

3.2.3. Procedures

Polymersome preparation: Polymersome preparations composed of blends of amino functionalized and methoxy functionalized polymer (mol/mol: 9/1) were formed using the thin-film hydration method as previously reported [1]. In brief, 1 mg H_2N-PEG_2PLA_6 and 9 mg $mPEG_2PLA_6$ were dissolved in chloroform (1 mL). The chloroform was subsequently removed by rotary evaporation to generate a polymer thin film at the wall of a round-bottom flask (5 mL). The resulting thin-film was dried overnight *in vacuo* at room temperature (RT) and hydrated with PBS (1 mL) or an AlexaFluor488 carboxylic acid solution in PBS (1 mL, 0.2 mg/mL) for 6 h at RT. The polymersome suspension was stepwise extruded through two stacked 400 nm and two stacked 200 nm polycarbonate membranes (21-41 passes) using the handhold Avantilipids mini-extruder with a heating block at 65°C. Unencapsulated AlexaFluor488 carboxylic acid was removed using commercially available zeba-spin columns with a MWCO of 7kDA (3x).

Determination of polymersome concentration: Diluted polymersome suspension (V/V, 1:1 in PBS, 100 µL in total) was inserted into wells of a black 96-well plate. Next, 100 µL of AlexaFluor488 carboxylic acid calibration solutions containing 20 to 0.01 µg/mL of dye in PBS were introduced to further wells. The fluorescence intensities of the solutions were recorded at λem = 515 nm when excited at λex = 488 nm and the dye concentration inside of the polymersome suspension (c_i) was determined using the calibration of free dye molecules (0.01-20,000 µg/mL). The number of polymersomes per mL was calculated using the following equation:

$$\frac{\mathrm{n(Polymersome)}}{\mathrm{mL}} = \frac{c_f}{c_i * V_p}$$

Where c_f is the measured concentration of AlexaFluor488 carboxylic acid by fluorescence measurements, c_i is the incorporated concentration of AlexaFluor488 carboxylic acid into the aqueous lumen of the polymersomes (0.2 mg/mL) and V_P is the volume of a single polymersome calculated based on the hydrodynamic diameter.

Surface modification of the polymersomes:

NHS functionalized polymersomes: 100 µL polymer suspension was reacted with **BS3** (10 eq., 3.6 µL, 10 mg/mL in PBS) for 30 min at RT to yield amine reactive polymersomes. After incubation, unreacted linker molecules were removed using commercially available zeba-spin columns with a MWCO of 7 kDA (2x).

4-Iodoacetyl: 100 µL polymer suspension was reacted with **sulfo-SIAB** (10 eq., 6.3 µL, 5 mg/mL in PBS) for 30 min at RT to yield thiol reactive polymersomes. After incubation, unreacted liker molecules were removed using commercially available zeba-spin columns with a MWCO of 7 kDA (2x).

Maleimide functionalized polymersomes: 100 µL polymer suspension was reacted with **sulfo-SMCC** (10 eq., 5.5 µL, 5 mg/mL in PBS) for 30 min at RT to yield thiol reactive polymersomes. After incubation, unreacted liker molecules were removed using commercially available zeba-spin columns with a MWCO of 7 kDA (2x).

Biotinylated polymersomes: 100 µL polymer suspension was reacted with **biotin-xx-sSE** (10 eq., 8.4 µL, 5 mg/mL in PBS) for 30 min at RT to yield biotinylated polymersomes. After incubation, unreacted liker molecules were removed using commercially available zeba-spin columns with a MWCO of 7 kDA (2x).

NeutrAvidin coated polymersomes: 100 µL biotinylated polymersome suspension was reacted with NeutrAvidin (10 eq., 100 µL, 4 mg/mL in PBS) for 1 h at RT to yield NeutrAvidin coated polymersomes. After incubation, unreacted NeutrAvidin was removed using commercially available micro-spin S-400HR columns (1x).

Probing of the surface reactivity of maleimide functionalized polymersomes: 500 µL of an unfluorescent polymer suspension (100% mol) was reacted with **sulfo-SMCC** (10 eq., 27.5 µL, 5 mg/mL in PBS) for 30 min at RT to yield thiol reactive polymersomes. After incubation, unreacted liker molecules were removed using commercially available zeba-spin columns with a MWCO of 7 kDA (2x). The surface reactivity of the polymersomes was probed using NaOH (0.1 M) deprotected SAMSA-fluorescein for 1 h at RT. Unreacted SAMSA-fluorescein was removed using commercially available zeba-spin columns with a MWCO of 7 kDA (2x) and the number of SAMSA-fluorescein tagged polymers was determined using fluorescence measurements on a fluorescein calibration.

Cell lines and cell cultures:

Jurkat cells (line E6-1, ATCC) were cultured in RPMI 1640 glutamax medium (Gibco) supplemented with 10% fetal bovine serum (FBS) (Gibco), 1% penicillin/streptomycin (Gibco), 1% Na-pyruvate (Gibco) and 0.1% HEPES-buffer at 37°C and 5%CO_2.

Encephalitogenic CD4+ effector/memory proteolipid protein (PLP) peptide aa139-153 specific T cells (line SJL/PLP7, TKI, Berne) were cultured in RPMI 1640 glutamax medium (Gibco) supplemented with 10% fetal bovine serum (FBS) (Gibco), 1% penicillin/streptomycin (Gibco), 1% non-essential amino acids (Gibco), 1% Na-pyruvate (Gibco), 0.4% ß-mercaptoethanol (Gibco) and 1% IL-2 supernatant (self-made) at 37°C and 5%CO_2. Cells were typically used for modification and in functional assays at day 3-4 after restimulation.

Cell surface modification:

Biotinylation of T cells: Biotinylation of T cells was performed using biotin-XX-sSE adapted from a previously reported protocol for the surface biotinylation of hMSCs [2]. In brief, cells were washed 2 times with DPBS to remove the RPMI-growth medium and resuspended in DPBS at a cell concentration of 25 x10^6 cells per mL. Then, the cell suspension was cooled on ice and Biotin-XX-SE (5 mg/mL, 200 µL per 25 x10^6 cells) was added for 30 min. Biotinylated T cells were washed 2 times with DPBS to remove unreacted linker molecules and directly used for further cell surface modifications.

NeutrAvidin coating of biotinylated T cells: NeutrAvidin coating of biotinylated T cells was performed according to a previously reported protocol for the probing of biotin groups on hMSCs Alexa488 Streptavidin [2]. In brief, biotinylated T cells were resuspended in 1mL DPBS at a cell concentration of 60 x10^6 cells per mL. Next, 1 mL of NeutrAvidin in DPBS (0.5 mg/mL) was added and cells were incubated for 30 min at room temperature. NeutrAvidin coated cells were washed 2 times with DPBS to remove unreacted NeutrAvidin and directly used for further cell surface modifications.

Cell surface modification with NHS functionalized polymersomes: Cells were washed 2 times in 10 mL DPBS to remove amine containing proteins from the cell suspension and resuspended in DPBS at a concentration of 30 x10^6 cells per mL. An equal volume of NHS functionalized polymersomes in PBS (3 x10^{11} NPs/mL) was added to the cell suspension and incubated at 37°C with gentle mixing every 10 min. After 30 min, 1 mM glycine in PBS (20 µL) was added to the reaction mixture and incubated at 37°C for 10 min to quench the reaction. The suspension was washed 3 times in 10 mL DPBS to remove unbound particles from the cells. Polymersomes were incubated with unmodified

cells as a control for unspecific binding. The particle-cell conjugates were resuspended in NaN_3 (1 mM) and FBS (2%) supplemented DPBS at a cell concentration of 1 $x10^6$ cells/mL and analyzed by flow cytometry.

Cell surface modification with 4-Iodoacetyl/ maleimide functionalized polymersomes: Cells were washed 2 times in 10 mL DPBS to remove thiol containing proteins from the cell suspension and resuspended in DPBS at a concentration of 30 $x10^6$ cells per mL. An equal volume of 4-Iodoacetyl/ maleimide functionalized polymersomes in PBS (3 $x10^{11}$ NPs/mL) was added to the cell suspension and incubated at 37°C with gentle mixing every 10min. After 30 min, 1mM *N*-acetylcysteine in PBS (20 µL) was added to the reaction mixture and incubated at 37°C for 10 min to quench the reaction. The suspension was washed 3 times in 10 mL DPBS to remove unbound particles from the cells. Polymersomes were incubated with unmodified cells as a control for unspecific binding. The particle-cell conjugates were resuspended in NaN_3 (1 mM) and FBS (2%) supplemented DPBS at a cell concentration of 1 $x10^6$ cells/mL and analyzed by flow cytometry.

Cell surface modification of biotinylated cells with NeutrAvidin coated polymersomes: T cells were washed 2 times in 10 mL DPBS and resuspended in DPBS at a concentration of 30 $x10^6$ cells per mL. An equal volume of NeutrAvidin coated polymersomes in PBS with (0.3-15 $x10^{11}$ NPs/mL) was added to the cell suspension and incubated at 37°C with gentle mixing every 10 min. After 30 min, 1 mM biotin-PEG1000 in PBS (20 µL) was added to the reaction mixture and incubated at 37°C for 10 min to quench the reaction. The suspension was washed 3 times in 10 mL DPBS to remove unbound particles from the cells. Polymersomes were incubated with unmodified cells as a control for unspecific binding. The particle-cell conjugates were resuspended in NaN_3 (1 mM) and FBS (2%) supplemented DPBS at a cell concentration of 1 $x10^6$ cells/mL and analyzed by flow cytometry.

Viability assay: Viability assays were performed using AnnexinV – Alexa647 as indicator for apoptosis and DAPI as indicator for necrosis. Briefly, (un-)modified cells were washed once with DPBS (10mL) and 0.3 $x10^6$ cells were resuspended in Annexin binding buffer (300 µL) containing DAPI (1 µg/mL). AnnexinV-Alexa647 conjugate (15 µL) was added and the suspension was kept for 15 min in the dark. Subsequently, 500 µL Annexin binding buffer was added directly followed by analysis of the cells by flow cytometry. For the positive control, 1 $x10^6$ cells were incubated with 1 µM Staurosporin for 24 h to induce apoptosis. Freshly biotinylated and non-biotinylated cells

were used as a negative control. All controls were kept in full cell culture medium/DPBS at 37°C until analysis with the actual sample. Staurosporin treated cells were used to gate the cell populations as described in SI Figure8-9. Viable cells (Q4), apoptotic cells (Q3) and necrotic cells (Q1,Q2)

Preparation of ICAM-1/DNER coated glass slides: In brief, standard 12 well diagnostic slides (ER-202W-CE24, ThermoFisher Scientific) were coated with protein A (20 mg/mL in PBS, pH 9) for 1 h at 37°C. The protein A incubation was followed by 3 PBS washes and subsequent blocking with 1.5% BSA in PBS at 4°C overnight. Wells were washed once with PBS (pH 7.4) and the immobilized protein A was exposed to recombinant purified ICAM-1-FC chimera or DNER-FC chimera for 2 h at 37°C. Finally, wells were blocked with 1.5% BSA in PBS for 30 min at RT and washed once with PBS before use of the slides.

Binding assay: For the binding assay, T cells were collected at 10 $x10^6$ cells/mL in migration buffer (DMEM, 25 mM HEPES, 5% FBS, 2% L-glutamine) and 0.1 $x10^6$ cells were added to each well, followed by incubation of the slide for 30 min at RT on a shaking platform. After incubation, the slides were washed twice by dipping into PBS and fixed for 2h in 2.5% v/v glutaraldehyde in PBS. The number of adherent cells was evaluated by counting the number of bound cells per field of view using a 20x objective mounted on an Olympus CKX41 inverted microscope equipped with a 10 mm x 10 mm/ 10 divisions counting reticle. The experiment was performed in triplicate and wells were counted on 3 different positions.

Preparation of slides for confocal microscopy: Before particle-cell conjugation, cells were washed in DPBS and resuspended at a cell concentration of 20 $x10^6$ cells/10 mL. The cells were incubated with CellTraceViolett (5 mM in DMSO, 20 µL) at 37°C for 20 min. The suspension was filled up to 45 mL with RPMI-growth medium, washed and resuspended in RPMI-growth medium at a cell concentration of 20 $x10^6$ cells/10 mL. After incubation for 10min at 37°C, cells were washed 2 times in 10mL DPBS and used for cell surface conjugation. After conjugation, 1 $x10^6$ cells were incubated with WGA-Texas Red (1 mM, 50 µL) in 1mL DPBS for 30min at RT and spinned on Poly(L-Lysine) coated glass cover-slips for microscopy. After 2 washes in 1mL DPBS cells were fixed in PFA-solution (4% in DPBS, 1 mL) for 10 min and washed in 1 mL DPBS. Finally, the fixed particle-cell conjugates were mounted on ProLong Diamond mounting medium and the microscopy slides were kept at 4°C until analysis by confocal microscopy. Nanoparticles were counted automatically in Imaris by recognition of green fluorescent

spheres with minimal dimensions of 150 nm x 150 nm x 250 nm in the deconvoluted image sets.

3.3. Results and Discussion

3.3.1. Preparation and modification of polymersomes

Polymersomes were prepared using a thin-film hydration method. Therefore, the amphiphilic block copolymer PEG_{2000}-PLA_{6000} with a hydrophilic weight ratio of f_{eo}=0.25 was dissolved in chloroform and subsequently dried onto the glass wall of a round bottom flask. Blends of amino functionalized and methoxy functionalized polymers were used to introduce reactive groups on the surface of the final polymersome enabling the surface modification of the final vesicles with NHS esters (Scheme 1).

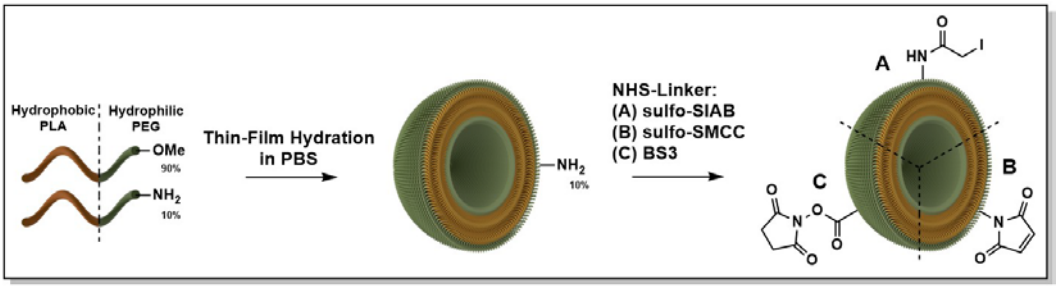

Scheme 1 Preparation of NH2 functionalized polymersomes from a blend of NH2-/mPEG-PLA and further functionalization with (A) sulfo-SIAB to 4-Iodoacetate functionalized polymersomes, (B) sulfo-SMCC to maleimide functionalized polymersomes and (A) BS3 to NHS functionalized polymersomes.

The polymer thin film was rehydrated for 6h with an aqueous medium, either PBS or AlexaFluor488 in PBS, to yield un-/fluorescent polymersomes. AlexaFluor488 was chosen as a fluorescent dye for the labeling of the polymersomes as it represents a triple anion that can be encapsulated into the lumen of the polymersomes with minimal leaking over the hydrophobic membrane of the vesicles. Next, polymersomes are extruded through 2 stacked polycarbonate membranes to size the particles down while decreasing the width of the size distribution of the polymersomes resulting into 200 nm vesicles with a relative narrow size distribution as shown in Figure 1B. Finally, polymersomes were separated from unencapsulated dye molecules by size exclusion chromatography using Zeba-Spin columns. This further enables the determination of the final polymersome

concentration as the dye concentration inside the polymersomes is fixed at the hydration concentration of the dye. Figure 1A represents a cryo-TEM image of the final polymersomes demonstrating the typical ring structures of the vesicles which is a 2 dimensional down-projection of their hollow spherical morphology.

The zeta potential of the particles was increasing with higher mol concentrations of amino functionalized polymer in the polymer blend indicating an increasing amount of positively charged amine groups on the final vesicle surface (SI Figure 1). Polymersome suspensions were investigated further for their stability in full cell culture medium at 37°C. While vesicle size and PDI did not alter over the time course of 5 d, a dye leakage of 25% within 2 days was observed (SI Figure 2-3). This indicates the formation of smaller nanopores in the membrane of the polymersomes as a sign of premature degradation without major integrity issues.

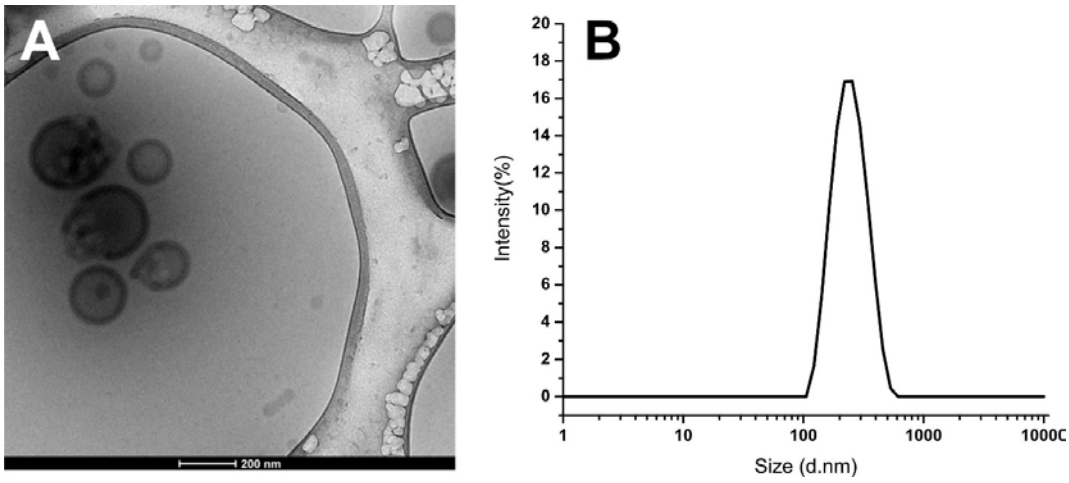

Figure 1 (A) Representative Cryo-TEM images of polymersomes in PBS ($mPEG_{5k}PLA_{15k}$) showing the hollow spherical morphology of the particles. **(B)** Representative size distribution of polymersomes ($mPEG_{5k}PLA_{15k}$) determined by Dynamic Light Scattering. (Average z-size= 230 nm, PDI= 0.081, zeta-potential=-5.22±4.52 mV)

3.3.2. Conjugation of polymersomes to Jurkat cells

The efficiency of different surface chemistries to immobilize polymersomes on the surface of T cells was investigated using immortalized Jurkat cells. To this end, cells were incubated with NHS, 4-iodoacetyl and maleimide functionalized polymersomes in order to covalently conjugate the vesicles to amine or thiol groups on the cell surface. The

reactivity of maleimide functionalized unfluorescent polymersomes towards thiols was verified as a representative example for this surface modification using the fluorescent probe SAMSA-fluorescein (SI-Figure 4). Staining of the cells with a corresponding amino or thiol reactive dye before and after the conjugation enabled monitoring of the consumption of these groups during the conjugation process (SI-Figure 5-8). Interestingly, however, polymersomes could not be immobilized on the surface of Jurkat cells using these direct covalent conjugation strategies indicated by the low increase in nanoparticle associated fluorescence and the low decrease in the fluorescence of the corresponding negative stain. To overcome this issue, polymersomes were conjugated to the Jurkat cells using a sandwich like NeutrAvidin-biotin conjugation approach (Scheme 2) as NeutrAvidin biotin conjugation chemistry represents a highly reliable and thoroughly investigated chemistry approach for the immobilization of micelles and solid core nanoparticles to Stem Cells and human embryonic kidney cells [2-4].

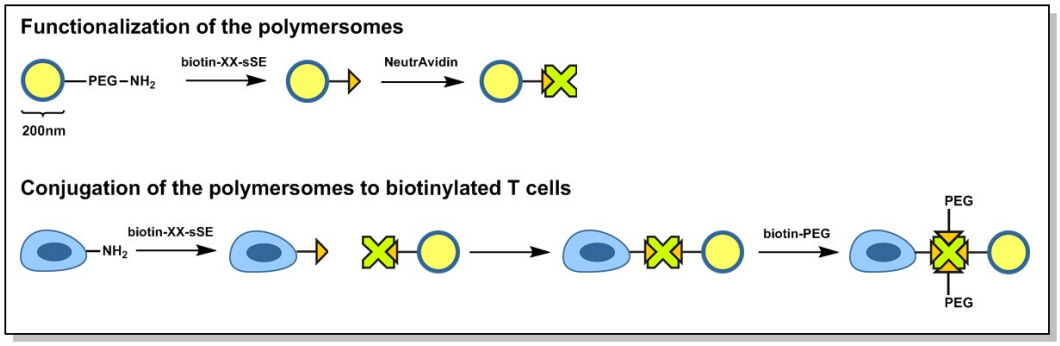

Scheme 2 Polymersome surface modification with biotin-XX-sSE and NeutrAvidin, followed by conjugation to surface modified T cells and quenching of the residual reactive binding sites with mPEG1000-biotin.

In our particular approach, however, NeutrAvidin not only acts as a conjugating protein, but also gives a bio-fouling surface coating to the polymersomes. This is especially important, as we anticipated that the dense PEG brush on the surface of the covalently conjugating polymersomes inhibited their surface bio-fouling properties drastically. These, however, are needed to provide a contact between nanoparticle and cell that is lasting long enough for the covalent reaction to happen. To confirm this hypothesis, NeutrAvidin was immobilized first on the surface of biotinylated polymersomes followed by incubation of these polymersomes with biotinylated cells. In a second experiment, biotinylated cells were incubated first with NeutrAvidin and then with biotinylated

polymersomes (Figure 3). Despite using the same conjugation strategy and conjugation conditions, only the incubation of NeutrAvidin coated polymersomes with biotinylated cells resulted in a significant increase of the polymersome associated fluorescence of cells. Negative staining experiments with NeutrAvidin Dyelight647 visualizing biotin groups of the cell surface before and after polymersome conjugation also confirmed the consumption of free biotin groups during this reaction as can be seen by the drop in NeutrAvidin Dyelight647 fluorescence after the polymersome conjugation by 96.11% (Figure 4). To avoid aggregation of the polymersome cell conjugates and to prevent possible immunogenic effects in later studies, unreacted binding sites of the NeutrAvidin were blocked by incubation of the conjugates with mPEG-biotin$_{1000}$ for all cases.

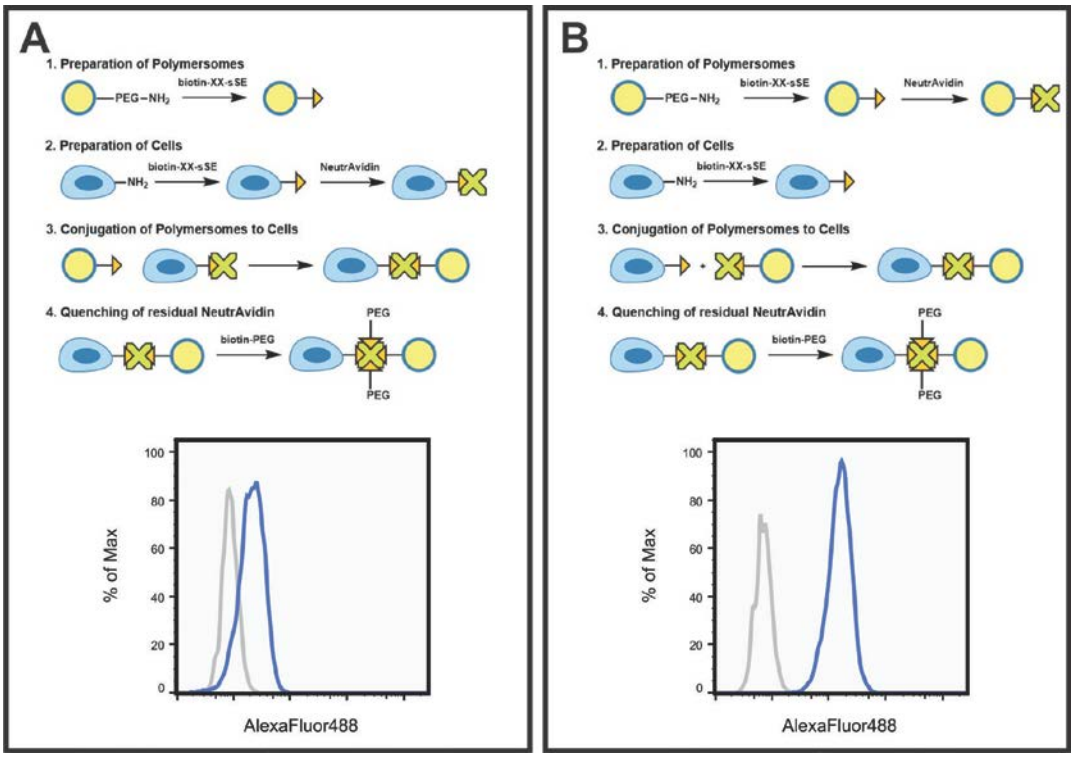

Figure 3 Schematic representation of the preparation and conjugation of **(A)** biotinylated polymersomes to NeutrAvidin coated Jurkat cells and **(B)** NeutrAvidin coated polymersomes to biotinylated Jurkat cells and corresponding histogram representing the AlexaFluor488 fluorescence of unmodified Jurkat cells (grey) and Jurkat cells incubated with an excess of 10,000 polymersomes per cell (blue).

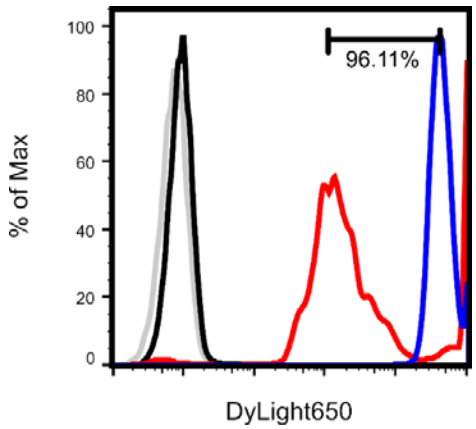

Figure 4 Histogram representing the fluorescence of a NeutrAvidin conjugated probe (NeutrAvidin-DyLight650) of unmodified Jurkat cells (grey), biotinylated Jurkat cells incubated with NeutrAvidin coated polymersomes in black, biotinylated Jurkat cells incubated with NeutrAvidin-DyLight650 (blue) and biotinylated Jurkat cells incubated with NeutrAvidin coated polymersomes and NeutrAvidin-DyLight650 (red). The shift of the geometric mean of the red and the blue curve visualizes the relative consumption of reactive groups during the conjugation process (96.11%).

The possibility to tune the amount of polymersomes on the surface of Jurkat cells using NeutrAvidin biotin chemistry was demonstrated by incubation of cells with different excesses of polymersomes. Increasing the number of polymersomes during the incubation with the cells resulted in higher amounts of nanoparticles on the cell surface as demonstrated by the subsequent increase of the nanoparticle associated florescence in the FACS analysis of the final conjugates (Figure 5). The exact amount of polymersomes on the surface of Jurkat cells was investigated using confocal microscopy imaging. Therefore, the cell body was stained in cyan using CellTraceViolett, the cell membrane was stained in red using WGA-TexasRed and particles were imaged in green as a result of AlexaFluor488 fluorescence. To count the nanoparticles on the cell surface, single cell z-stacks were loaded into Imaris and analyzed for green fluorescent ellipsoids with a minimal dimension of 150 nm x 150 nm x 250 nm (width x lenght x hight). This analysis revealed that the particle immobilization could be tuned between 17-84 particles per cell (n=8) (Figure6-7).

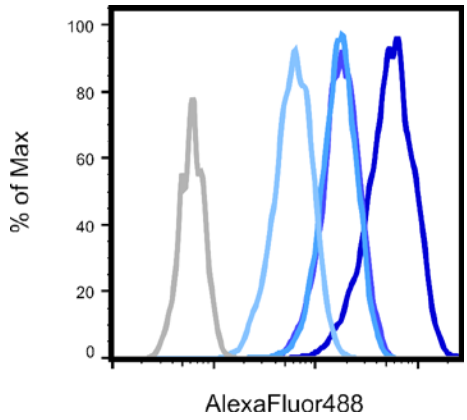

Figure 5 Histogram representing the polymersome fluorescence of unmodified Jurkat cells (grey) and biotinylated Jurkat cells incubated with increasing excesses (1,000-50,000 polymersomes per cell) of NeutrAvidin coated polymersomes (light-dark blue).

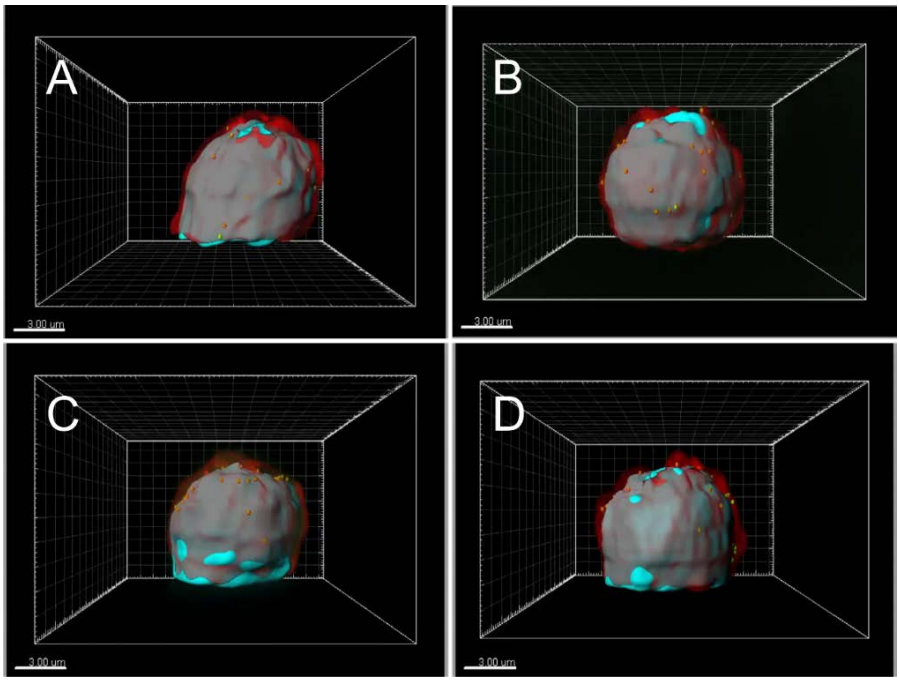

Figure 6 Representative 3D reconstructions of confocal images of biotinylated Jurkat cells incubated with an excesses of **(A)** 1.000, **(B)** 5.000, **(C)** 10.000 and **(D)** 50.000 NeutrAvidin coated polymersomes per cell. Whole cell body staining was assessed using CellTraceViolett (cyan) and membrane staining using WGA-TexasRed (red). Polymersome fluorescence is associated to AlexaFluor488 encapsulated into the aqueous lumen of the polymersomes (green).

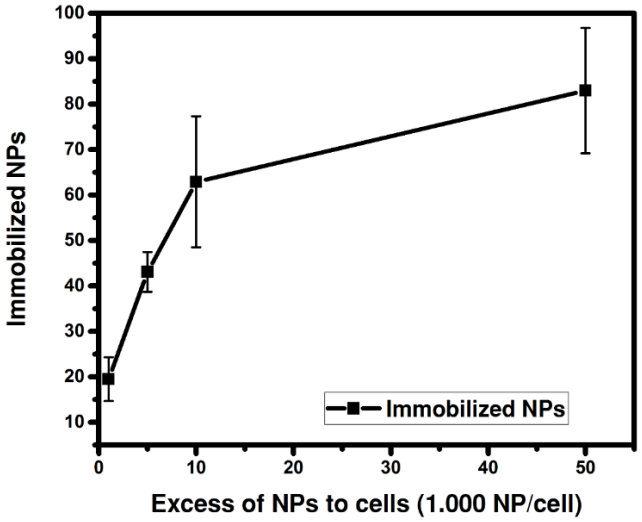

Figure 7 Count of surface immobilized polymersomes on Jurkat cells (y-axis) as a function of particle to cell excess during cell conjugation (x-axis). Polymersome counts are performed automatically based on 3D-reconstructions of confocal images (n=8).

In contrast, incubation of biotinylated polymersomes with biotinylated cells or NeutrAvidin coated polymersomes with unmodified control cells results in no significant increase of nanoparticle associated fluorescence compared to the control suggesting very low unspecific binding effects (Figure 8).

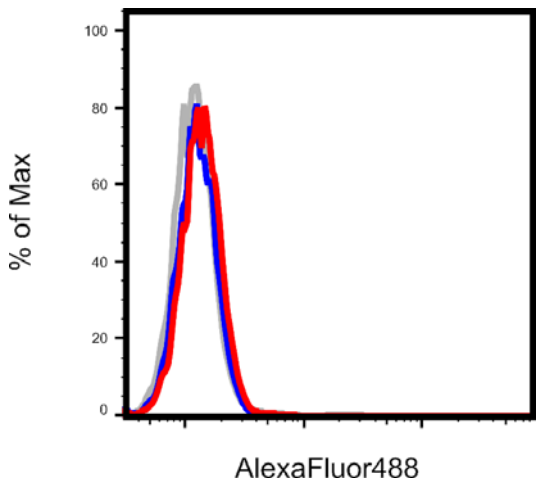

Figure 8 Histogram representing polymersome fluorescence of unmodified Jurkat cells (grey), biotinylated Jurkat cells incubated with biotinylated polymersomes (blue) and unmodified Jurkat cells incubated with NeutrAvidin coated polymersomes (red).

To investigate the impact of polymersome conjugation on cellular key functions of the Jurkat cells, a proliferation and a viability assay were performed. Cell proliferation was assessed using the cytosol dye CellTrace Violet (CTV). As cells proliferate, the initial CTV associated fluorescence decreases over time as a result of dye dilution over cell division. For unmodified Jurkat cells, this decrease is typically 2-fold over 24 h as these cells have a proliferation cycle of 24 h. Figure 9B shows this fluorescent decrease for unmodified Jurkat cells (black and grey) and for polymersome conjugated cells (dark and light blue) as measured by flow cytometry. Fluorescence intensities perfectly overlapped for both time points indicating that polymersome conjugation has little impact on cell proliferation. Furthermore, Figure 9A shows a comparable decrease of nanoparticle associated fluorescence indicating that this conjugation is stable over the investigated timeframe and that the decrease in surface immobilized polymersomes is mainly due to cell division.

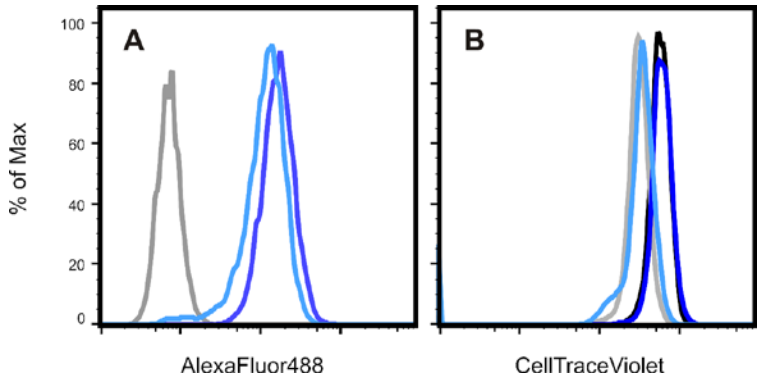

Figure 9 Histogram representing **(A)** polymersome fluorescence and **(B)** the fluorescence of a proliferation marker (CellTraceViolet) of unmodified Jurkat cells at t=0h (black) and t=24h (grey) and biotinylated Jurkat cells incubated with NeutrAvidin coated polymersomes at t=0h (dark blue) and t=24h (light blue).

Cell viability was assessed in an AnnexinV-DAPI assay. AnnexinV binds to phosphatidyl serine, a lipid that is only translocated to the exterior cell membrane under early apoptotic conditions. DAPI is cell membrane impermeable and is only fluorescent if it intercalates in DNA therefore it is used as an indicator for necrosis. No significant difference in cell viability was observed for cells incubated with an excess of up to 5,000 polymersomes per cell (Figure 10). However, early apoptosis was induced for higher amounts of polymersomes as shown in the scatter plots of SI Figure 9.

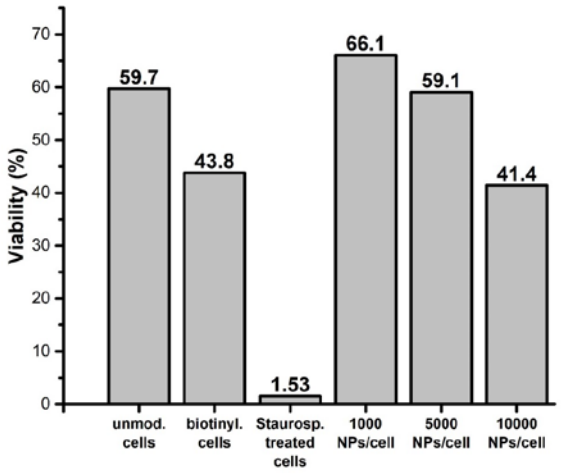

Figure 10 Bar plot of the viability of unmodified Jurkat cells, biotinylated Jurkat cells, Jurkat cells incubated with Staurosporin and Jurkat cells incubated with 1,000/5,000/10,000 polymersomes per cell as determined in a AnnexinV/DAPI assay.

3.3.3. Conjugation of polymersomes to primary T cells (SJL-PLP7)

To evaluate the impact of polymersome T cell conjugation on T cell function, polymersomes were conjugated to encephalitogeneic SJL-PLP7 cells. This cell line plays a major role in the immune-surveillance of the brain. SJL-PLP7 T cells are known to cross the Blood Brain Barrier in a 3 step mechanism. First, they adhere to the brain endothelium by ICAM-1/LFA-1 interaction. Next, they start to crawl against the blood flow until they undergo trans- or paracellular diapedesis through the brain endothelium to reside in the perivascular space. Here they sample for antigen presenting cells. In case of a disease, the SJL-PLP7 cells get reactivated, migrate to the brain parenchyma and release pro-inflammatory cytokines recruiting a variety of other T cells to the brain.[5] This special T cell subset is of particular interest as polymersome decorated SJL-PLP7 T cells could be used to efficiently delivery drugs across the BBB to the brain parenchyma. (Figure 11)

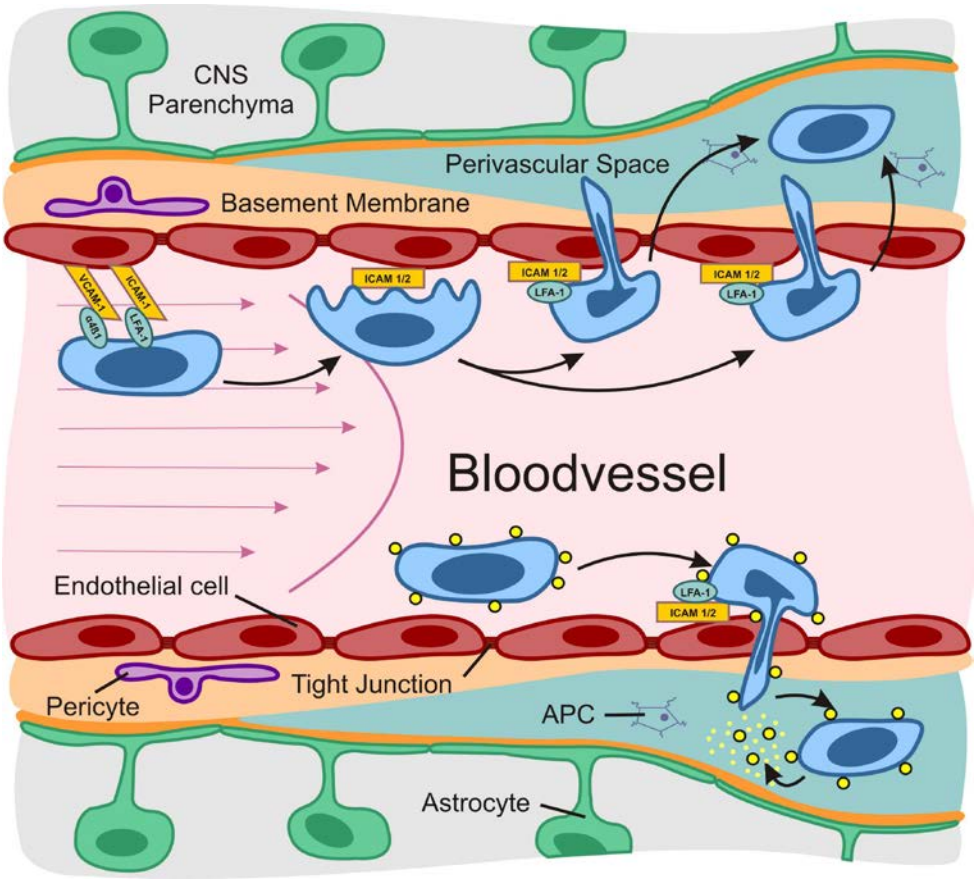

Figure 11 Migration of CD4+ T cells at the brain endothelium. T cells arrest at the endothelium as result of integrin recognition of ICAM-1 and VCAM-1. After polarization T cells crawl against the blood flow and undergo trans- or paracellular diapedesis to sample the perivascular space for antigen presenting cells (APCs). Drug loaded nanoparticles can be immobilized on the surface of these T cells in a cellular backpack approach to be carried across the BBB. Active or passive triggering release mechanisms can be used to release the NP cargo in the perivascular space or the CNS parenchyma.

The previously optimized conditions for polymersome T-cell conjugation were transferred to primary T cells (SJL-PLP7). Analysis of the conjugates by flow cytometry showed comparable fluorescence intensity shifts as observed before with Jurkat cells as shown in Figure 12. As apoptosis of the conjugates was expected to increase with increasing amounts of immobilized polymersomes, a viability assay was performed directly post conjugation and 24 h after conjugation. Even though polymersome conjugation also increases apoptosis of primary T cells like it was the case for Jurkat cells (SI Figure 10), viability was almost fully restored after incubation of the conjugates at 37°C in full cell culture medium for 24 h (Figure 13).

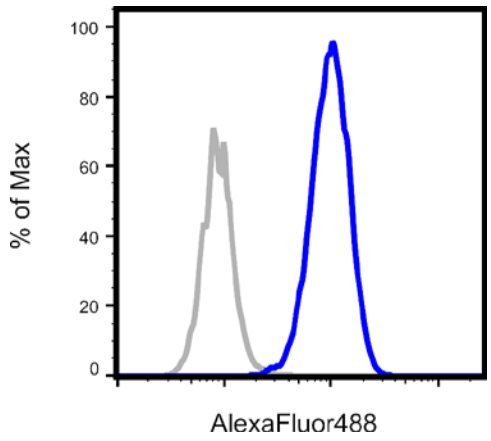

Figure 12 Histogram representing polymersome fluorescence of unmodified SJL/PLP7 cells (grey) and biotinylated SJL/PLP7 cells incubated with NeutrAvidin coated polymersomes (blue).

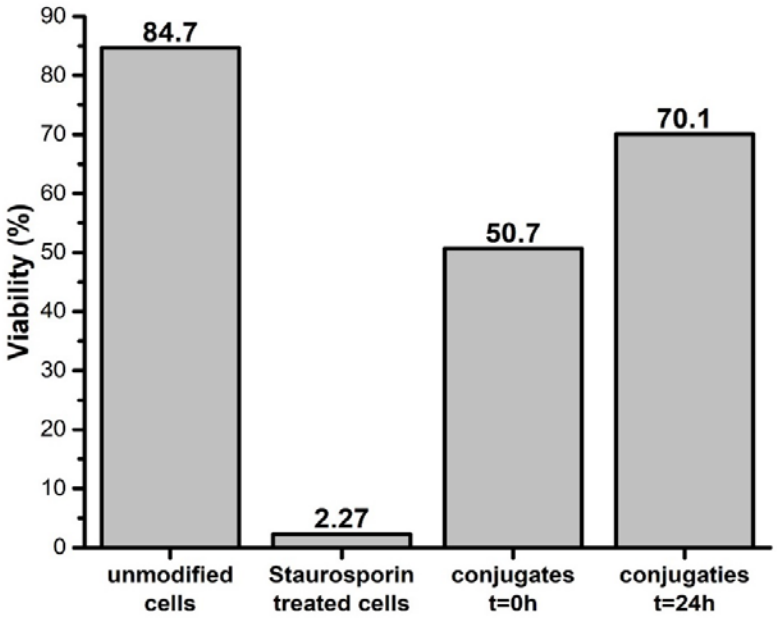

Figure 13 Bar plot of the viability of unmodified SJL-PLP7 cells, SJL-PLP7 cells incubated with Staurosporin and SJL-PLP7 cells incubated with 10,000 polymersomes per cell after incubation for 0 h/24 h in full cell culture medium as determined in a AnnexinV/DAPI assay.

The ability of the polymersome T-cell conjugates to bind to brain endothelium via LFA-1/ICAM-1 interaction was assessed qualitatively in an ICAM-binding assay. In this case, un-/modified T cells were incubated on a glass slide coated with protein A and ICAM/DNER-FC antibody chimeras. The combination of protein A and the ICAM- or

DNER chimera coating hereby ensures the correct directional immobilization of the proteins to enable T-cell binding to the modified glass substrate. The binding of the polymersome T cell conjugates was shown to be specific to ICAM-1 over the control protein DNER and showed no significant difference in ICAM binding compared to unmodified control cells as shown in Figure 14.

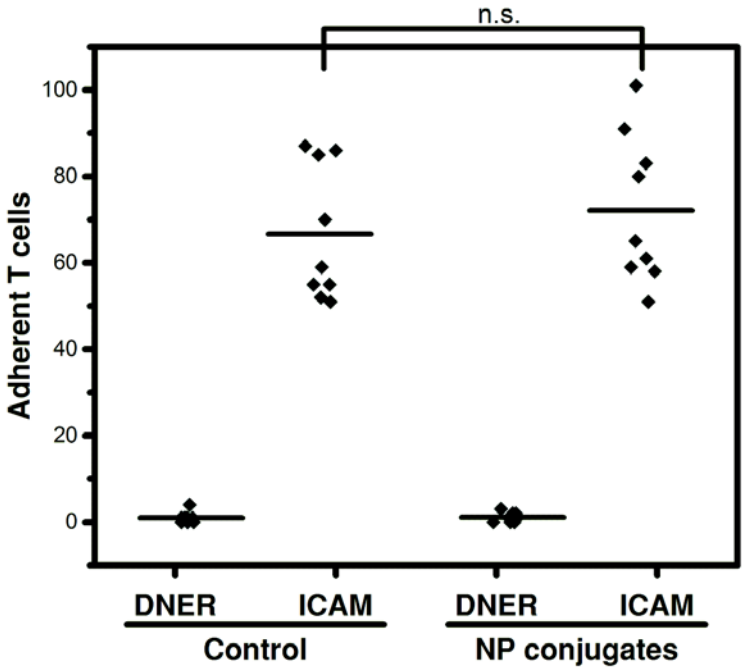

Figure 14 T-cell binding to ICAM-1. Cell count of a binding assay on ICAM-1 and DNER coated wells for unmodified control cells and polymersome T-cell conjugates performed at RT for 30 min under moderate shear conditions. Each dot represents one cell count from the diagonal of a 10 mm x 10 mm / 10 divisions counting reticle using a 20x objective. Each well was counted at 3 different positions. The horizontal bar represents the mean over all counts. The P-value was determined by a *t-test* (ns: P>0.05).

3.4. Conclusions

The immobilization of polymersomes on the surface of T cells was shown to be drastically influenced by the surface anti-fouling properties of the nanoparticles. While the dense PEG brush on the surface of the polymersomes prevented the covalent conjugation approaches based on maleimide-thiol, iodoacetamide-thiol and NHS-amine

chemistry. However, polymersomes were coated with NeutrAvidin to overcome this drawback as NeutrAvidin alters their surface properties. Furthermore, the immobilization of NeutrAvidin coated polymersomes to biotinylated T cells was shown to be tunable regarding the surface concentration of immobilized nanoparticles using flow cytometry and confocal microscopy imaging techniques. Moreover, immobilization of relatively high surface concentrations of polymersomes did not inhibit cellular key functions like proliferation and cell viability. Lastly, a first *in vitro* assay was used to determine the binding of polymersome T-cell conjugates to the endothelial inflammation marker ICAM-1, that mediates the extravasation of T cells on the level of the brain endothelium. Polymersome conjugation was shown to have no significant impact on this binding behavior. Together these results emphasize the high potential for polymersome T cell conjugates as a universal carrier system to cross the BBB.

3.5. References

1. Tietz, S. and B. Engelhardt, *Brain barriers: Crosstalk between complex tight junctions and adherens junctions.* The Journal of Cell Biology, 2015. **209**(4): p. 493-506.
2. Ransohoff, R.M. and B. Engelhardt, *The anatomical and cellular basis of immune surveillance in the central nervous system.* Nat Rev Immunol, 2012. **12**(9): p. 623-635.
3. Engelhardt, B., P. Vajkoczy, and R.O. Weller, *The movers and shapers in immune privilege of the CNS.* Nat Immunol, 2017. **18**(2): p. 123-131.
4. Abbott, N.J., et al., *Structure and function of the blood–brain barrier.* Neurobiology of Disease, 2010. **37**(1): p. 13-25.
5. Zhang, T.-T., et al., *Strategies for transporting nanoparticles across the blood-brain barrier.* Biomaterials Science, 2016. **4**(2): p. 219-229.
6. Upadhyay, R.K., *Drug Delivery Systems, CNS Protection, and the Blood Brain Barrier.* BioMed Research International, 2014. **2014**: p. 37.
7. Charabati, M., et al., *Overcoming the Brain Barriers: From Immune Cells to Nanoparticles.* Trends in Pharmacological Sciences, 2020. **41**(1): p. 42-54.
8. Banskota, S., P. Yousefpour, and A. Chilkoti, *Cell-Based Biohybrid Drug Delivery Systems: The Best of the Synthetic and Natural Worlds.* Macromolecular Bioscience, 2017. **17**(1): p. 1600361.
9. Barua, S. and S. Mitragotri, *Challenges associated with Penetration of Nanoparticles across Cell and Tissue Barriers: A Review of Current Status and Future Prospects.* Nano today, 2014. **9**(2): p. 223-243.
10. Nowak, M., M.E. Helgeson, and S. Mitragotri, *Delivery of Nanoparticles and Macromolecules across the Blood–Brain Barrier.* Advanced Therapeutics, 2020. **3**(1): p. 1900073.

11. Xie, J., et al., *Nanomaterial-based blood-brain-barrier (BBB) crossing strategies.* Biomaterials, 2019. **224**: p. 119491.
12. Tang, W., et al., *Emerging blood–brain-barrier-crossing nanotechnology for brain cancer theranostics.* Chemical Society Reviews, 2019. **48**(11): p. 2967-3014.
13. Zhou, Y., et al., *Crossing the blood-brain barrier with nanoparticles.* Journal of Controlled Release, 2018. **270**: p. 290-303.
14. Kreuter, J., *Nanoparticulate systems for brain delivery of drugs.* Advanced Drug Delivery Reviews, 2001. **47**(1): p. 65-81.
15. Anselmo, A.C. and S. Mitragotri, *Cell-Mediated Delivery of Nanoparticles: Taking Advantage of Circulatory Cells to Target Nanoparticles.* Journal of controlled release : official journal of the Controlled Release Society, 2014. **0**: p. 531-541.
16. Tang, L., et al., *Enhancing T cell therapy through TCR-signaling-responsive nanoparticle drug delivery.* Nature Biotechnology, 2018.
17. Xie, Y.-Q., et al., *Redox-responsive interleukin-2 nanogel specifically and safely promotes the proliferation and memory precursor differentiation of tumor-reactive T-cells.* Biomaterials Science, 2019. **7**(4): p. 1345-1357.
18. Wayne, E.C., et al., *TRAIL-coated leukocytes that prevent the bloodborne metastasis of prostate cancer.* Journal of Controlled Release, 2016. **223**: p. 215-223.
19. Wayteck, L., et al., *Hitchhiking nanoparticles: Reversible coupling of lipid-based nanoparticles to cytotoxic T lymphocytes.* Biomaterials, 2016. **77**: p. 243-254.
20. Stephan, M.T., et al., *Therapeutic cell engineering with surface-conjugated synthetic nanoparticles.* Nat Med, 2010. **16**(9): p. 1035-1041.
21. Stephan, M.T., et al., *Synapse-directed delivery of immunomodulators using T-cell-conjugated nanoparticles.* Biomaterials, 2012. **33**(23): p. 5776-5787.
22. Choi, M.-R., et al., *Delivery of nanoparticles to brain metastases of breast cancer using a cellular Trojan horse.* Cancer Nanotechnology, 2012. **3**(1-6): p. 47-54.
23. Xue, J., et al., *Neutrophil-mediated anticancer drug delivery for suppression of postoperative malignant glioma recurrence.* Nat Nano, 2017. **12**(7): p. 692-700.
24. Engelhardt, B. and R.M. Ransohoff, *Capture, crawl, cross: the T cell code to breach the blood–brain barriers.* Trends in Immunology, 2012. **33**(12): p. 579-589.
25. Lyck, R. and B. Engelhardt, *Going Against the Tide – How Encephalitogenic T Cells Breach the Blood-Brain Barrier.* Journal of Vascular Research, 2012. **49**(6): p. 497-509.
26. Ahmed, F. and D.E. Discher, *Self-porating polymersomes of PEG–PLA and PEG–PCL: hydrolysis-triggered controlled release vesicles.* Journal of Controlled Release, 2004. **96**(1): p. 37-53.
27. Discher, D.E. and F. Ahmed, *POLYMERSOMES.* Annual Review of Biomedical Engineering, 2006. **8**(1): p. 323-341.
28. Alibolandi, M., et al., *Synthesis and self-assembly of biodegradable polyethylene glycol-poly (lactic acid) diblock copolymers as polymersomes for preparation of sustained release system of doxorubicin.* International Journal of Pharmaceutical Investigation, 2015. **5**(3): p. 134-141.
29. Cheng, H., et al., *Nanoparticulate Cellular Patches for Cell-Mediated Tumoritropic Delivery.* ACS Nano, 2010. **4**(2): p. 625-631.
30. Krishnamachari, Y., M.E. Pearce, and A.K. Salem, *Self-Assembly of Cell–Microparticle Hybrids.* Advanced Materials, 2008. **20**(5): p. 989-993.

31. Mooney, R., et al., *Conjugation of pH-responsive nanoparticles to neural stem cells improves intratumoral therapy.* Journal of controlled release : official journal of the Controlled Release Society, 2014. **191**: p. 82-89.

3.6. Supporting Information

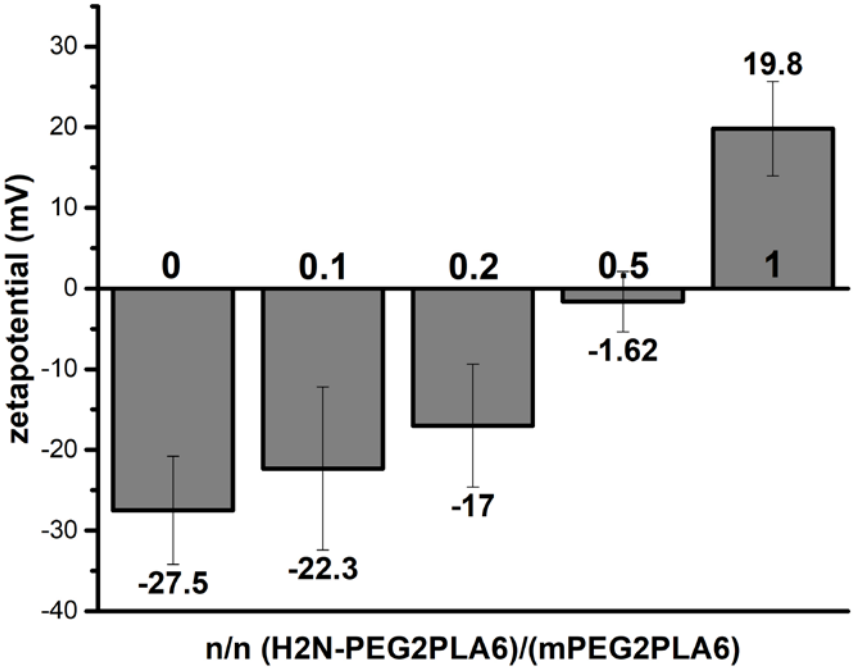

SI Figure 1 Bar plot representing the zeta potential of polymersomes prepared by thin film hydration of thin films containing different blends (n/n) of mPEG-PLA and NH2-PEG-PLA.

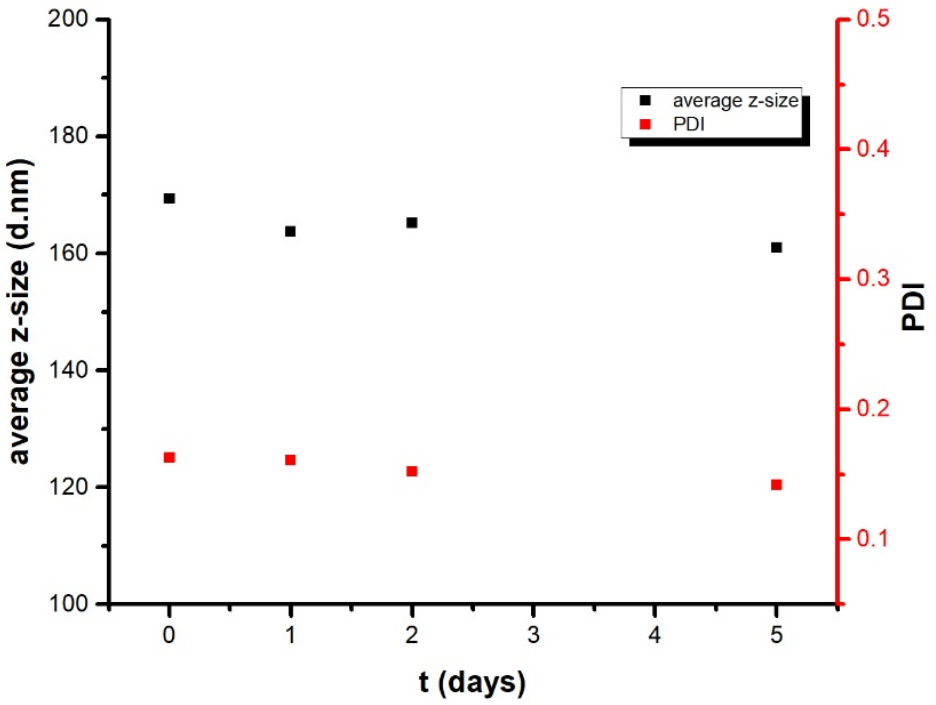

SI Figure 2 Average z-size and PDI of PEG-PLA polymersomes after incubation in full cell culture medium at 37°C.

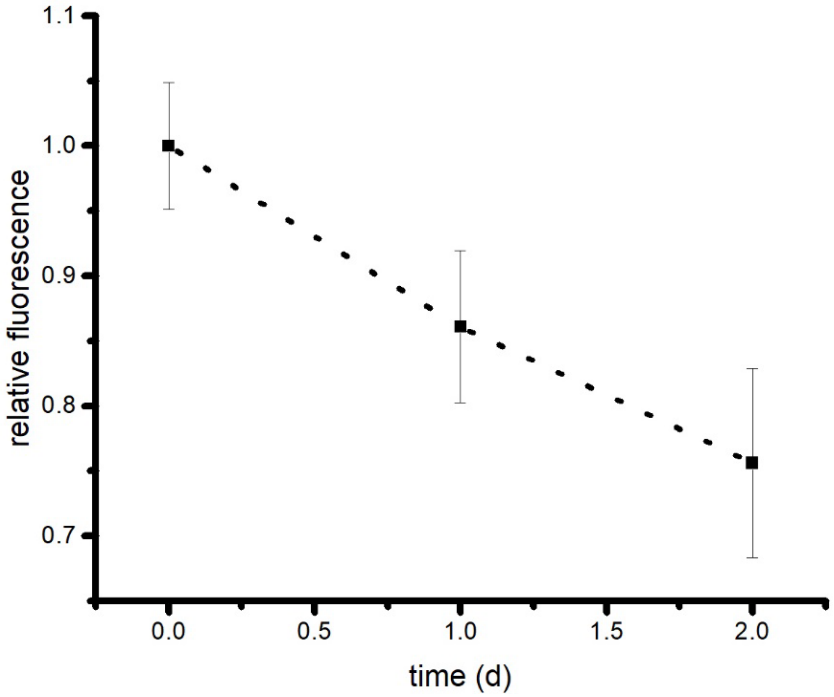

SI Figure 3 Relative fluorescence of polymersomes encapsulating AlexaFluor488 after incubation in full cell culture medium at 37°C.

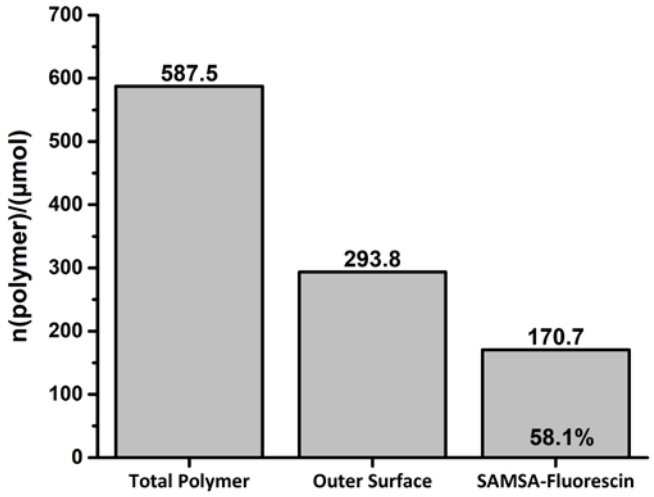

SI Figure 4 Total number (theoretical) of polymers in a maleimide modified polymersome suspension, number of polymers on the outer surface of these polymersomes and number of fluorescein groups measured on the surface of the polymersomes after reaction with SAMSA-fluorescein. The labeling efficiency was 58.1%.

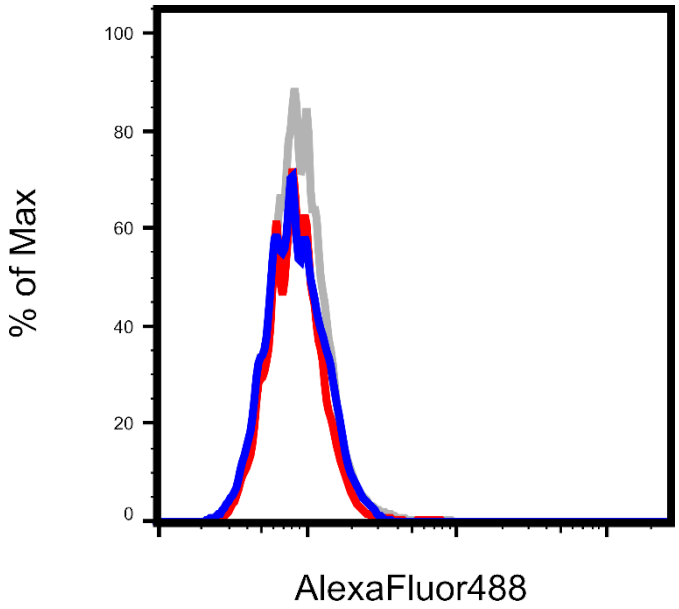

SI Figure 5 Histogram representing polymersome fluorescence of unmodified Jurkat cells (grey), Jurkat cells incubated with iodoacetyl modified polymersomes (red) and Jurkat cells incubated with maleimide modified polymersomes (blue).

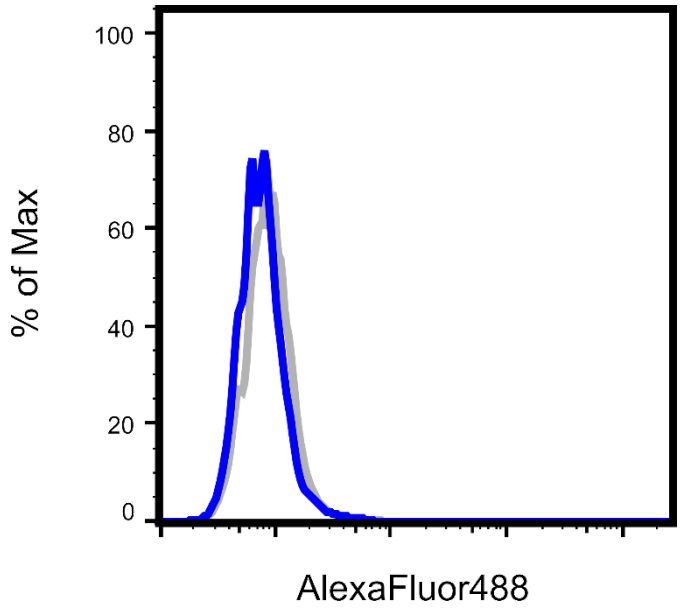

SI Figure 6 Histogram representing polymersome fluorescence of unmodified Jurkat cells (grey) and Jurkat cells incubated with NHS-ester modified polymersomes (blue).

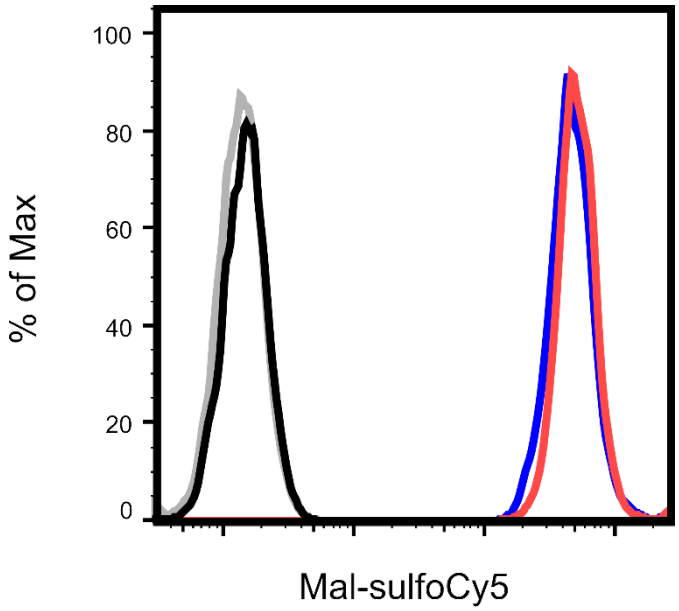

SI Figure 7 Histograms representing the fluorescence a thiol reactive probe (maleimide-sulfo-cy5) of unmodified Jurkat cells (grey), Jurkat cells incubated with maleimide modified polymersomes (black), Jurkat cells incubated with maleimide-sulfo-Cy5 (blue) and Jurkat cells incubated with maleimide-sulfo-Cy5 and maleimide modified polymersomes (red). The shift of the red to the blue curve visualizes the relative consumption of reactive groups during the conjugation process (0%).

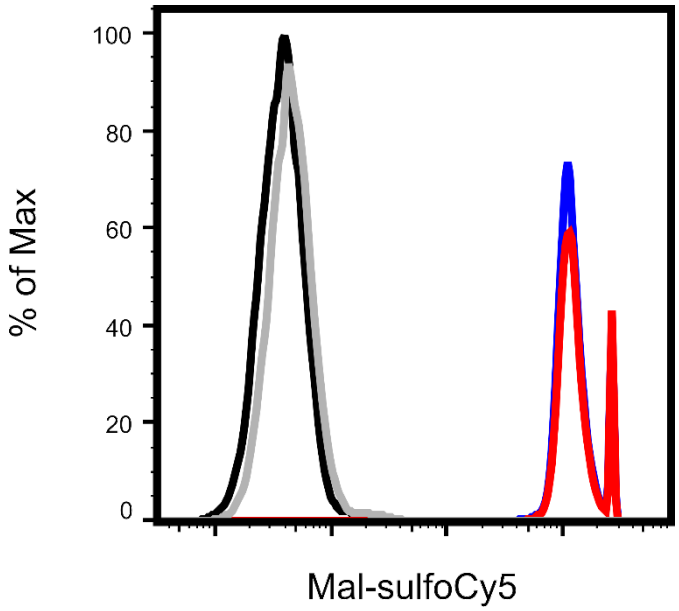

SI Figure 8 Histograms representing the fluorescence a thiol reactive probe (maleimide-sulfo-cy5) of unmodified Jurkat cells (grey), Jurkat cells incubated with iodoacetyl modified polymersomes (black), Jurkat cells incubated with maleimide-sulfo-Cy5 (blue) and Jurkat cells incubated with maleimide-sulfo-Cy5 and iodoacetyl modified polymersomes (red). The shift of the geometric mean of the red and the blue curve visualizes the relative consumption of reactive groups during the conjugation process (0%).

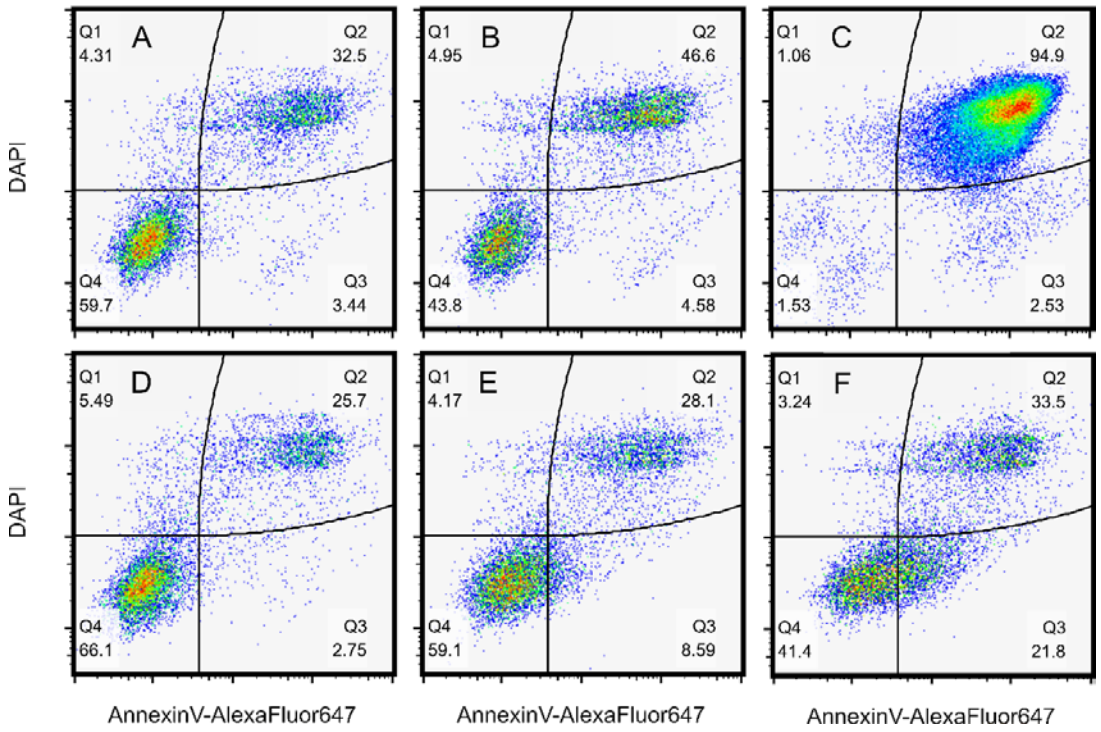

SI Figure 9 Viability assay of **(A)** unmodified Jurkat cells, **(B)** biotinylated Jurkat cells (C) Jurkat cells incubated with Staurosporin (24 h) to induce apoptosis and necrosis for the positive control and biotinylated Jurkat cells incubated with an excess of **(D)** 1000 NPs/cell, **(E)** 5000 NPs/cell and **(F)** 10000 NPs/cell NeutrAvidin coated polymersomes. DAPI fluorescence is associated to cell necrosis, Alexa647 fluorescence to cell apoptosis.

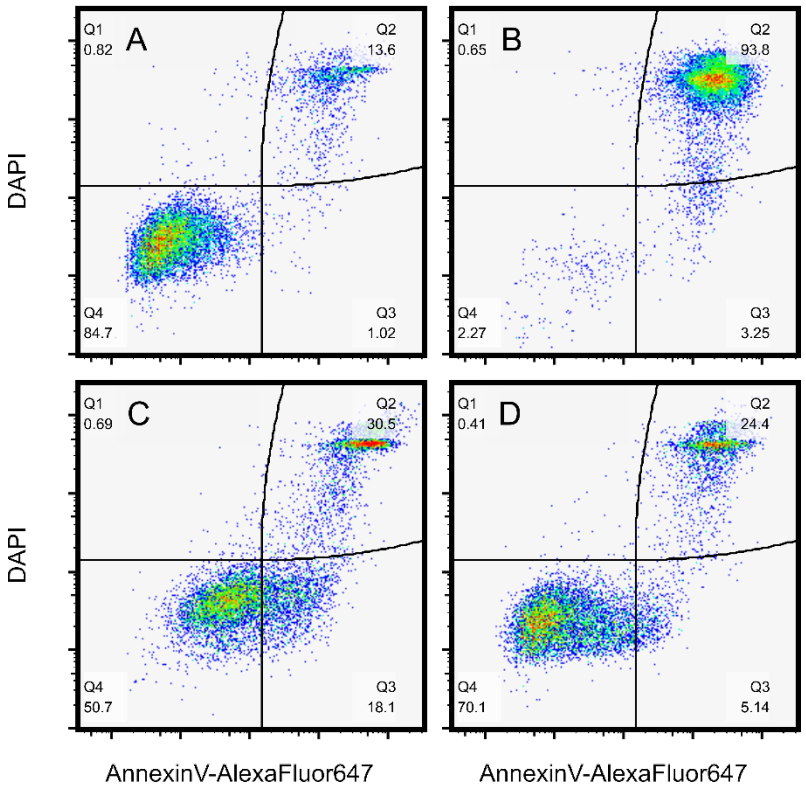

SI Figure 10 Viability assay of **(A)** unmodified SJL-PLP7 cells **(B)**, SJL-PLP7 cells incubated with Staurosporin (24 h) to induce apoptosis and necrosis for the positive control and biotinylated SJL-PLP7 cells incubated with NeutrAvidin coated polymersomes at **(C)** t=0h and **(D)** t=24h. DAPI fluorescence is associated to cell necrosis, Alexa647 fluorescence to cell apoptosis.

4. Identification of cell surface proteins capable of covalent and non-covalent anchoring of nanoparticles

4.1. Introduction

As elucidated in Chapter 2 and Chapter 3, nanoparticles, in particular polymersomes, conjugated to the surface of CD4+ T_{EM} cells provide a promising tool for the antigen independent delivery of drugs across the Blood Brain Barrier. The conjugation of polymersomes to Jurkat cells and SJL-PLP7 cells, however, was shown to be restricted to the use of NeutrAvidin-biotin based conjugation strategies, due to the anti-biofouling properties of the polymersome surface. As a result, cells were biotinylated on amine groups on the cell surface enabling the NeutrAvidin-biotin mediated conjugation of the polymersomes. Chapter 4 explores additional NeutrAvidin-biotin based conjugation strategies to T cells comparing them in regard to the amount of surface immobilized polymersomes as well as their impact on cellular key functions. Indeed, conjugation of micro- and nanoparticles to cell surfaces using biotin/avidin based strategies is not a new concept and has been investigated in various previous studies using different cell biotinylation approaches. However, these concepts were never compared to each other or applied to polymersome cell conjugation.

Generally, cells can be biotinylated on surface proteins typically utilizing amine reactive chemistries. As an example, Cheng et al. utilized sulfo-NHS-LC-biotin, an NHS-biotin linker, to biotinylate both, mesenchymal Stem Cells (MSCs) and HUVECs enabling the cell surface modification with NeutrAvidin coated polystyrene nanoparticles [1]. Similarly, sulfo-NHS-LC-biotin was utilized in a most recent study to biotinylate MSCs, enabling the conjugation of 400nm biotinylated chitosan nanoparticles to the cell surface by simultaneous co-incubation of the biotinylated cells with the biotinylated nanoparticles and streptavidin [2].

Another approach to modify cell surfaces with biotin enabling avidin based conjugation to nanoparticles is based on lipid insertion techniques [3]. As a recent example, lung cancer cells were biotinylated by incubation with Cholesterol-PEG-biotin followed by the cell surface immobilization of 7nm avidin modified quantum dots [4].

Lastly, cells can be biotinylated via sialic acid sugar residues present on glycoproteins of the membrane followed by nanoparticle conjugation. Modification of the sialic acid can generally be performed in two different ways. First, by direct chemical modification of the sialic acid, for example by oxidation and further modification [5], or secondly by incubation of the cells with modified sugars that are incorporated into the sialic acid via the cell metabolism opening the possibility to orthogonal bio-conjugation strategies [6]. Recently, a covalent sialic acid modification was reported by Yang et al.. In this study, the researchers used streptavidin to conjugate biotin-PGMA modified SiO_2 nanoparticles to Hela cells that were biotinylated via a 2-step process [7]. First, alcohol groups of the sialic acid groups on the cell surface were oxidated to aldehydes with sodium periodate. This oxidation enabled the bio-orthogonal modification of the sialic acid groups with biotin-hydrazide in a second step. As metabolic engineering of sialic acid already opens the possibility for further bio-orthogonal conjugation, this method is not commonly explored further regarding biotin/Avidin mediated nanoparticle cell conjugation but rather commonly regarding direct click chemistry mediated nanoparticle cell conjugation. One early example is the conjugation of 10nm DBCO modified quantum dots to azide groups of CHO cells that have been incubated with ManNAz [8].

4.2. Experimental Section

4.2.1. Materials

All chemicals were used as received unless described otherwise. The polymers Methoxy poly(ethylene glycol)$_{2000}$-b-poly(D,L-lactide)6000 ($mPEG_{2000}PLA_{6000}$), amino poly(ethylene glycol)$_{2000}$-b-poly(D,L-lactide)$_{6000}$ ($H2N\text{-}PEG_{2000}PLA_{6000}$) and methoxy poly(ethylene glycol)$_{1000}$ ($mPEG\text{-}biton_{1000}$) were purchased from APM (Montreal, Canada). AlexaFluor488 carboxylic acid triethylammonium salt, AlexaFluor488 NHS-ester, AlexaFluor488 C_5 maleimide, AnnexinV – AlexaFluor647, 1-Biotinamido-4-[4'-(maleimidomethyl)cyclohexanecarboxamido]butane (Biotin-BMCC), (6-((6-(Biotinoyl)amino)hexanoyl)amino)hexanoic acid, sulfosuccinimidyl ester, sodium salt) (biotin-xx-sSE), 4',6-diamidino-2-phenylindole (DAPI), tetraacylated N-azidoacetylmannosamine (ManNAz), Neutravidin, NeutrAvidin-DyeLight650, PBS (pH=7.4, tablets for 500 mL), Staurosporin and wheat germ agglutinin, Texas Red-X conjugate (WGA-TexasRed) were purchased from FischerScientific. 1,2-distearoyl-sn-

glycero-3-phosphoethanolamine-N-[biotinyl(polyethylene glycol)-2000] (DSPE-PEG_{2000}-biotin) was purchased from LubioScience. Protein A was purchased from BioVision, Lausen, Switzerland and stored at 0°C (20 mg/mL stock solution in PBS, pH 9). Recombinant DNER-Fc and ICAM1-Fc chimera protein was purchased from R&D Systems, Abington, U.K and stored at 0°C (1 mg/mL in DPBS). HPLC-grade Chloroform was purchased from Fluka. Dibenzocyclooctyne-PEG4-biotin conjugate (DBCO-PEG4-biotin) and Poly(L-Lysin) (84 kDA, 0.01%) was purchased from SigmaAldrich.

4.2.2. Methods

Absorbance and fluorescence intensity measurements were performed with a Tecan Infinite Pro 200 plate reader. Size, size distribution and zeta-potential of nanoparticles were determined using a zetasizer (NANO-ZS, Malvern, UK) at a scattering angle of 173° using back-scattering detection. Briefly, 20 µL of polymersome suspension (10 mg/mL) was diluted in 980 µL PBS at pH=7.4 for measurement of the size distribution or in 980 µL NaCl solution (1mM) at pH=7.4 for measurement of the ζ-potential. All measurements were carried out at 25°C. The final vesicle suspensions were stored at 4°C to prevent degradation and were used within 7 days after preparation. Cell conjugation experiments were performed in clear u-shaped 96well-plates with a cell repellent surface purchased from Greiner Bio-One GmbH. Flow cytometry measurements were performed in FACS buffer (1 mM NaN_3 in DPBS supplemented with 2%FBS) on a Beckman Coulter Gallios instrument equipped with 3 lasers (405 nm, 488 nm, 640 nm) and 10 detectors (450/50, 550/40, 525/40, 575/25, 620/20, 695/30, 755LP, 660/20, 725/20, 755LP) and analyzed with FlowJo (V10.6.1) if not stated otherwise. Confocal microscopy images were taken on an inverted Zeiss LSM700 equipped with a Plan-Apochromat 63x/1.40 DIC oil objective and reconstructed and analyzed with Imaris.

4.2.3. Procedures

Polymersome preparation: Polymersome suspensions composed of blends of amino functionalized and methoxy functionalized polymer (mol/mol: 9/1) were formed using the thin-film rehydration method. In brief, 1 mg H2N-PEG_2PLA_6 and 9mg mPEG_2PLA_6 were dissolved in chloroform (1 mL). The chloroform was subsequently removed by rotary evaporation to generate a polymer thin film at the wall of a round-bottom flask (5 mL). The resulted thin-film was dried overnight *in vacuo* at RT and hydrated with an

AlexaFluor488 solution in PBS (1 mL, 0.2 mg/mL, pH= 7.4) for 6 h at RT. The polymersome suspension was extruded through two stacked 200 nm polycarbonate membranes (21x-31x passes) using the handhold Avantilipids mini-extruder with a heating block at 65°C. Unencapsulated Alexa488 was removed using commercially available zeba-spin columns with a MWCO of 7 kDA (3x).

Determination of polymersome concentration: Diluted polymersome suspension (V/V, 1:1 in PBS, 100 µL in total) was inserted into wells of a black 96-well plate. Next, 100 µL of AlexaFluor488 carboxylic acid calibration solutions containing 0.01 to 20 µg/mL of dye in PBS were introduced to further wells. The fluorescence intensities of the solutions were recorded at λ_{em} = 515 nm when excited at λ_{ex} = 488 nm and the dye concentration inside of the polymersome suspension ($\mathbf{c_i}$) was determined using the calibration of free dye molecules (0.01-20,000 µg/mL). The number of polymersomes per mL was calculated using the following equation:

$$\frac{\mathrm{n(Polymersome)}}{\mathrm{mL}} = \frac{c_f}{c_i * V_p}$$

Whereas c_f is the measured concentration of AlexaFluor488 by the fluorescence measurement, c_i is the incorporated concentration of Alexa488 into the polymersomes (0.2 mg/mL) and V_P is the volume of a single polymersome. To obtain the volume of a single polymersome, the average hydrodynamic size of the polymersomes was used as the diameter.

Biotinylation of Polymersomes: 100 µL polymersome suspension was reacted with biotin-XX-sSE (10 eq., 5 mg/mL, 8.4 µL) for 30 min at RT to obtain biotinylated polymersomes. The reaction mixture was purified using commercially available zeba-spin columns with a MWCO of 7 kDA.

NeutrAvidin coating of polymersomes: 100 µL biotinylated polymersome suspension was reacted with Neutravidin in PBS (1 eq., 4 mg/mL, 100 µL) ,for 1 h at RT. The excess of protein was removed using microspin S-400HR spin columns. Surface modified polymersomes were used for cell conjugation directly after the preparation to avoid a loss of reactivity.

Cell lines and cell cultures

Jurkat cells (line E6-1, ATCC) were cultured in RPMI 1640 glutamax medium (Gibco) supplemented with 10% fetal bovine serum (FBS) (Gibco), 1% penicillin/streptomycin

(Gibco), 1% Na-pyruvate (Gibco) and 0.1% HEPES-buffer at 37°C and 5%CO_2. *Encephalitogenic CD4+ effector/memory proteolipid protein (PLP) peptide aa139-153 specific T cells (line SJL/PLP7, TKI Bern)* were cultured in RPMI 1640 glutamax medium (Gibco) supplemented with 10% fetal bovine serum (FBS) (Gibco), 1% penicillin/streptomycin (Gibco), 1% non-essential amino acid (Gibco), 1% Na-pyruvate (Gibco), 0.4% β-mercaptoethanol (Gibco) and 1% IL-2 supernatant (self-made) at 37°C and 5%CO_2. Cells were typically used for modification and in functional assays at day 3 after restimulation.

Cell surface modification

Biotinylation of T cells

Biotinylation with Biotin-XX-sSE: Biotinylation of T cells on amine groups was performed using biotin-XX-sSE adapted from a previously reported protocol for the surface biotinylation of hMSCs [1]. In brief, cells were washed 2 times with DPBS to remove the RPMI-growth medium and resuspended in DPBS at a cell concentration of 25 x10^6 cells per mL. Then, the cell suspension was cooled on ice and Biotin-XX-sSE (5 mg/mL, 200 µL per 25 x10^6 cells) was added for 30 min. Biotinylated T cells were washed 2 times with DPBS to remove unreacted linker molecules and directly used for further cell surface modifications.

Biotinylation with Biotin-BMCC: Biotinylation of T cells on thiol groups was performed using biotin-BMCC. In brief, cells were washed 2 times with DPBS to remove the RPMI-growth medium and resuspended in DPBS at a cell concentration of 25 x10^6 cells per mL. Then, the cell suspension was cooled on ice and Biotin-BMCC (12.5 mg/mL, 250 µL per 25 x10^6 cells) was added for 30 min. Biotinylated T cells were washed 2 times with DPBS to remove unreacted linker molecules and directly used for further cell surface modifications.

Biotinylation with DSPE-PEG_{2000}-biotin: Biotinylated lipids were inserted into T-cell membranes using DSPE-PEG_{2000}-biotin. In brief, DSPE-PEG_{2000}-biotin in $HCCl_3$ (25 mg/mL) was dried in a glass vial and hydrated with DPBS overnight (1 mg/mL) at RT. T cells were washed 2 times with DPBS to remove the RPMI-growth medium and resuspended at a cell concentration of 1 x10^6 cells per mL (20 x10^6/20 mL). Next, T cells were incubated with DSPE-PEG-biotin suspension (50 µL per 1 x10^6 cells) for 1h at 37°C. Biotinylated T cells were washed 2 times with DPBS to remove unreacted linker molecules and directly used for further cell surface modifications.

Biotinylation using ManNAz and DBCO-PEG4-biotin**:** Biotinylation on glycosyl groups of T cells was performed using ManNAz and DBCO-PEG4-biotin. In brief, T cells were cultured for 48-72 h with ManNAz (40µM) supplemented growth medium. After 48-72 h, cells were washed 2 times with DPBS to remove the supplemented RPMI medium and resuspended at a cell concentration of 1 $x10^6$ cells/mL (25 $x10^6$ cells/25 mL) in HBSS. DBCO-PEG-biotin was added to the cell suspension in a final concentration of 10 mM followed by incubation for 1 h at 37°C. Biotinylated T cells were washed 2 times with DPBS to remove unreacted linker molecules and directly used for further cell surface modifications.

Cell surface modification of biotinylated T cells with NeutrAvidin coated polymersomes: T cells were washed 2 times in 10mL DPBS and resuspended in DPBS at a concentration of 30 $x10^6$ cells per mL. An equal volume of NeutrAvidin coated polymersomes in PBS with (0.3-15 $x10^{11}$ NPs/mL) was added to the cell suspension and incubated at 37°C with gentle mixing every 10min. After 30 min, 1 mM biotin-PEG1000 in PBS (20 µL) was added to the reaction mixture and incubated at 37°C for 10 min to quench the reaction. The suspension was washed 3 times in 10mL DPBS to remove unbound particles from the cells. Polymersomes were incubated with unmodified cells as a control for unspecific binding. The particle-cell conjugates were resuspended in NaN_3 (1mM) and FBS (2%) supplemented DPBS at a cell concentration of 1 $x10^6$ cells/mL and analyzed by flow cytometry.

Probing of biotin groups on the cell surface of T cells: Un-/biotinylated T cells were washed 2 times in DPBS and reacted with NeutrAvidin-DyeLight650 conjugate (10 µL stock solution/2 $x10^6$ cells/1 mL) at RT for 20min. DyeLight650 labeled cells were washed 3 times with DPBS and resuspended in NaN_3 (1 mM) and FBS (2%) supplemented DPBS at a cell concentration of 1 $x10^6$ cells/mL and analyzed by flow cytometry. The difference in MFI of the DyeLight650 associated cannel before and after polymersome conjugation was interpreted as the percentage of biotin consumption/blocking as a result of polymersome conjugation.

Viability assay: Viability assays were performed using AnnexinV – Alexa647 as indicator for apoptosis and DAPI as indicator for necrosis. Briefly, (un-)modified cells were washed once with DPBS (10 mL) and 0.3 $x10^6$ cells were resuspended in Annexin binding buffer (300 µL) containing DAPI (1 µg/mL). AnnexinV-Alexa647 conjugate (15 µL) was added and the suspension was kept for 15 min in the dark. Subsequently, 500 µL Annexin binding buffer was added directly followed by analysis of the cells by

flow cytometry. For the positive control, 1 $x10^6$ cells were incubated with 1 µM Staurosporin for 24 h to induce apoptosis. Freshly biotinylated and non-biotinylated cells were used as a negative control. All controls were kept in full cell culture medium/DPBS at 37°C until analysis with the actual sample. Staurosporin treated cells were used to gate the cell populations as followed: Viable cells (Q4), apoptotic cells (Q3) and necrotic cells (Q1,Q2)

Quantification of free amine groups on the surface of T cells: Free amine groups on the surface of T cells were quantified using AlexaFluor488 NHS ester. In brief, un-/biotinylated cells were washed 2 times in DPBS (10 mL) and resuspended in DPBS at a concentration of 3 $x10^6$ cells/mL. Cells were cooled on ice and AlexaFluor488 NHS ester was added (5 mg/mL in DPBS, 10µL) for 20 min. Unreacted dye molecules were removed by 2 subsequent washes in DPBS and 1 wash in FACS buffer. The MESF value of labeled cells was determined using commercially available Quantum Beads (BANGS Lab, Inc.). Therefore, quantum beads in different concentration were analyzed by FACS to obtain a linear fluorescence calibration curve as described in the manufacturer`s instructions. Then samples were measured at the same optical settings. The mean geometric mean of 3 measurements per sample condition was used to determine the MESF value of the corresponding sample.

Quantification of free thiol groups on the surface of T cells: Free amine groups on the surface of T cells were quantified using AlexaFluor488 C_5 maleimide. In brief, un-/biotinylated cells were washed 2 times in DPBS (10 mL) and resuspended in DPBS at a concentration of 3 $x10^6$ cells/mL. Cells were reacted with AlexaFluor488 C_5 maleimide (12.5 mg/mL in DMSO, 5µL) for 20 min at RT. Unreacted dye molecules were removed by 2 subsequent washes in DPBS and 1 wash in FACS buffer. The MESF value of labeled cells was determined using commercially available Quantum Beads (BANGS Lab, Inc.) Therefore, quantum beads in different concentration were analyzed by FACS to obtain a linear fluorescence calibration curve as described in the manufacturer`s instructions. Then samples were measured at the same optical settings. The mean geometric mean of 3 measurements per sample condition was used to determine the MESF value of the corresponding sample.

Quantification of biotinylated lipid and sialic acid groups: Biotinylated lipid and silalic acid groups on the surface of T cells were quantified directly using Streptavidin AlexaFluor488 conjugate. In brief, biotinylated cells were washed 2 times in DPBS (10mL) and resuspended in DPBS at a concentration of 2 $x10^6$ cells/mL. Sreptavidin

AlexaFluor488 (1 mg/mL, 50 µL) was added to 1 mL of cell suspension for 30 min at RT. Unreacted dye molecules were removed by 2 subsequent washes in DPBS and 1 wash in FACS buffer. The MESF value of labeled cells was determined using commercially available Quantum Beads (BANGS Lab, Inc.) Therefore, quantum beads in different concentration were analyzed by FACS to obtain a linear fluorescence calibration curve as described in the manufacturer`s instructions. Then samples were measured at the same optical settings. The mean geometric mean of 3 measurements per sample condition was used to determine the MESF value of the corresponding sample.

Preparation of slides for confocal microscopy: Before particle-cell conjugation, cells were washed in DPBS and resuspended at a cell concentration of 20 $x10^6$ cells/10 mL. The cells were incubated with CellTraceViolett (5 mM in DMSO, 20 µL) at 37°C for 20min. The suspension was filled up to 45 mL with RPMI-growth medium and incubated for 10min at 37°C. Cells were washed 2 times in 10 mL DPBS and used for cell surface conjugation. After conjugation, 0.5 $x10^6$ cells were incubated with WGA-Texas Red (1 mM, 50 µL) in 1mL DPBS for 30 min at RT. Glass cover-slips were coated with poly(L-Lysine) for 10 min at RT and cells were immobilized onto the cover slips by centrifugation at 200 g for 3 min. After 2 washes in 1 mL DPBS cells were fixed in PFA-solution (4% in DPBS, 1 mL) for 10 min and washed again in 1 mL DPBS. Finally, the fixed particle-cell conjugates were mounted on ProLong Diamond mounting medium and the microscopy slides were kept at 4°C until analysis by confocal microscopy. Nanoparticles were counted automatically in Imaris by recognition of green fluorescent spheres with minimal dimensions of 150 nm x 150 nm x 250 nm in the deconvoluted image sets.

Identification of cell surface proteins anchoring the NHS-biotin mediated conjugation of polymersomes to Jurkat cells: First, biotinylation of Jurkat cells on amine groups was performed using biotin-SS-sSE. In brief, cells were washed 2 times with DPBS to remove the RPMI-growth medium and resuspended in DPBS at a cell concentration of 25 $x10^6$ cells per mL. Then, the cell suspension was cooled on ice and Biotin-SS-sSE (5 mg/mL, 200 µL per 25 $x10^6$ cells) was added for 30 min. Biotinylated T cells were washed 2 times with DPBS to remove unreacted linker, resuspended at a cell concentration of 25 $x10^6$ cells per mL and incubated with an equivolume of NeutrAvidin coated fluospheres in MilliQ water at an excess of 250 NPs/ cell. The resulting nanoparticle-cell conjugates were washed 3 times with DPBS and resuspended in lysis buffer (2% CHAPS w/V, 0.8% Pharmalyte V/V, 5 mM Pefablock, 9.5 M urea) at a

concentration of 10 x10^6 cells per mL. The suspension was lysed by 3 subsequent cycles of vortexing and sonication at 40W (30 s each) and pelleted through an equivolume of a 20% sucrose solution at 13.000 g for 15 min. The pellet was washed 3 times in MilliQ water and incubated in 400 µL reduction buffer (10 mM DTT, 50 mM NH_4CO_3, 8 M urea) for 45 min at 60°C under vigorous stirring. Iodoacetamide (440 mM, 20 µL) was added and the suspension was allowed to cool down to RT for 1 h. The nanoparticles were removed by centrifugation at 30.000 g for 5 min and the supernatant containing the CAM-thiopropanoyl tagged surface proteins was loaded on a 10% SDS-gel to purify the proteins from the reagents. The protein bands were cut out, digested with Trypsin and analyzed via LC-MSMS.

4.3. Results and Discussion

4.3.1. Conjugation of polymersomes to Jurkat cells

NeutrAvidin coated polymersomes were synthesized as described in Chapter 3. In brief, polymersomes were formed by thinfilm hydration of a blend of amine functionalized and methoxy functionalized $PEG_{2000}PLA_{6000}$ (mol/mol, 1/9). Amine functionalized polymersomes were sized down by extrusion (200 nm) and functionalized with biotin-XX-sSE prior to incubation with NeutrAvidin. The final polymersome suspension was incubated at an excess of 10,000 polymersomes per cell with Jurkat cells that were biotinylated by different approaches to compare effect on the final surface immobilization of polymersomes (Scheme 1). In detail, cells were biotinylated on amine and thiol groups of proteins by incubation with biotin-XX-sSE and biotin-BMCC, on the cell membrane by insertion of DSPE-PEG-biotin into the lipid bilayer and on sialic acid residues by successive incubation of the cells with ManNAz and DBCO-PEG_4-biotin.

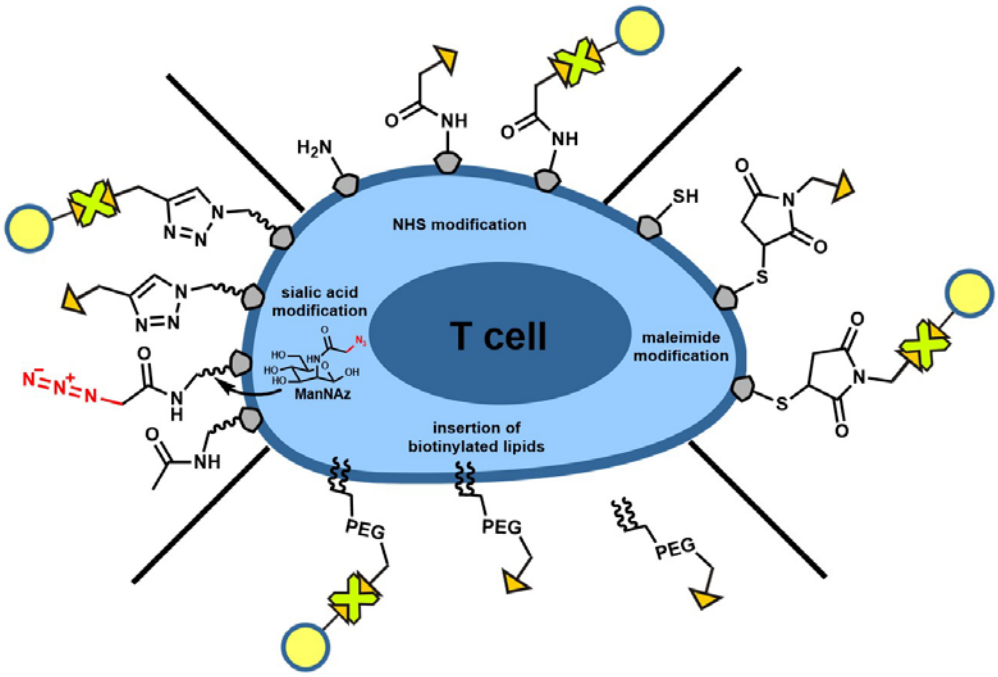

Figure 1 Schematic representation of different biotin/NeutrAvidin mediated cell surface modification strategies with polymersomes. Amine and thiol groups of surface proteins can be biotinylated using NHS and maleimide functionalized biotin linkers. Direct biotinylation of cell membrane lipids can be achieved by lipid insertion of biotinylated lipids. Metabolic modification of sialic acid groups on glycoproteins with manosyl-N-azid enables the biotinylation via biocompatible triazol formation. The final cell surface immobilization with polymersomes is achieved by incubation of NeutrAvidin coated polymersomes with the biotinylated cells.

The total amount of displayed biotin groups on the cell surface was probed using quantitative Flow Cytometry (Figure 2). The number of biotin groups introduced on proteins were determined indirectly by staining of the residual amine and thiol groups with NHS-AlexaFluor488 and Mal-AlexaFluor488, respectively (SI Table 1+2). The number of biotin groups introduced by lipid insertion and modification of sialic acid were determined directly using a StreptAvidin-AlexaFluor488 conjugate (SI Table 3+4).

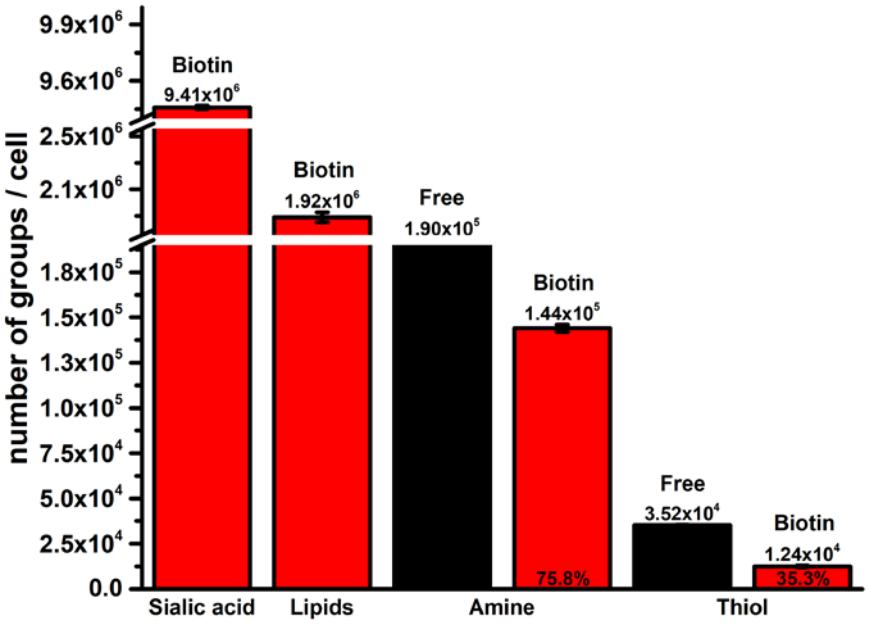

Figure 2 Column plot representing the total number of reactive surface groups (black) and biotinylated surface groups (red) on the surface of ManNAz modified and unmodified Jurkat cells determined by quantitative flow cytometry (n=3).

Under standard conditions, amine groups on the surface of Jurkat cells are about 5 times more abundant then reduced thiol groups. As biotinylation using biotin-XX-sSE proceeds with 75.8% and biotinylation using biotin-BMCC with 35.3%, this results in a 10 times higher count of biotin groups for the biotinylation on amine groups. Again about 10 times higher amounts of biotin groups can be introduced on the surface of Jurkat cells by incubation with DSPE-PEG-biotin, a lipid derivative that is able to insert into the lipid bilayer. It is important to note, that DSPE-PEG-biotin may partially bind to the cell surface by non- specific binding rather than by complete lipid insertion. The highest counts of biotin groups on the cell surface (ca. 9.5 $x10^6$) were reached by modification of the sialic acid groups upon incubation of the Jurkat cells with ManNAz for 72 h followed by reaction with DBCO-PEG4-biotin.

The consumption of biotin groups upon polymersome conjugation was determined by negative staining of the cells before and after conjugation with a NeutrAvidin-DyeLight650 conjugate to stain residual biotin groups on the cell surface (Figure 3+4). With 87-99%, the conversion of biotin groups is consistently high for all cases, except for the conjugation to thiol groups. Polymersome associated fluorescence does not significantly increase for this case either as determined by flow cytometry. While the

conversion and the relative amount of lipid anchored biotin groups is the highest, the polymersome associated fluorescence for this case is insignificantly low. This can be explained in case that DSPE-PEG-biotin is mostly associated to the cell membrane by unspecific binding effects and only minor by proper insertion into the lipid bilayer. These results indicate, that thiol groups and on the surface of T cells and biotinylated lipids that are inserted into the cell membrane of T cells, are not suitable for NeutrAvidin mediated polymersome conjugation. The conversion of biotin groups for biotinylation on amine groups and on sialic acid groups is comparable, also resulting in high polymersome associated fluorescence. Thus, only these two conjugation strategies were investigated by confocal microscopy regarding the absolute number of immobilized polymersomes and polymersome internalization.

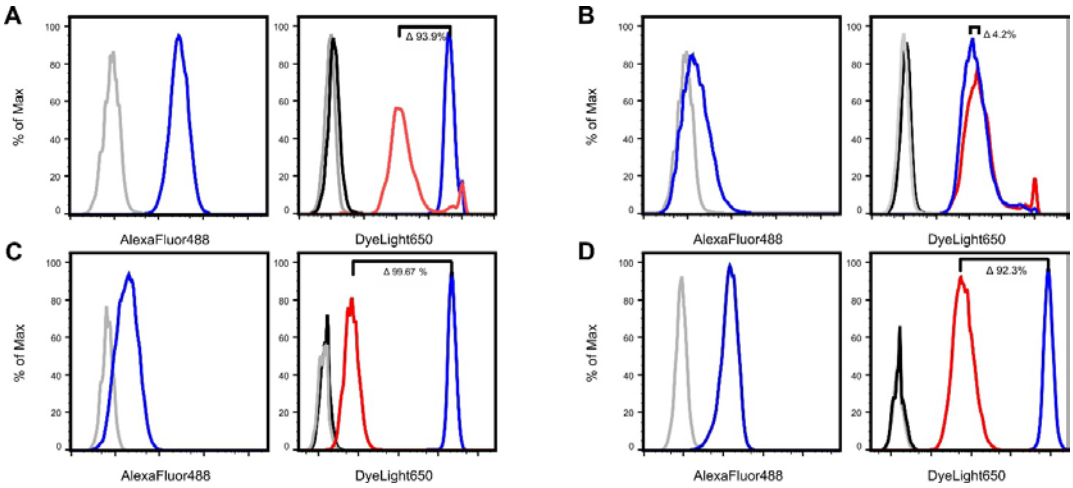

Figure 3 left: Histogramm representing polymersome fluorescence of unmodified Jurkat cells (grey) and biotinylated Jurkat cells incubated with NeutrAvidin coated polymersomes (blue). right: Histogramm representing NeutrAvidinDyeLight650 fluorescence of unmodified Jurkat cells (grey), biotinylated Jurkat cells incubated with NeutrAvidin coated polymersomes (black), unmodified Jurkat cells incubated with NeutrAvidinDyeLight650 (blue) and biotinylated cells incubated with NeutrAvidin coated polymersomes and NeutrAvidinDyeLight650 (red). Jurkat cells were biotinylated on (A) amine groups of surface proteins using biotin-xx-sSE, (B) thiol groups of surface proteins using biotin-BMCC, (C) membrane lipids by insertion of DSPE-PEG-biotin into the lipid bilayer of the cell membrane and (D) sialic acid residues of the glycocalix by subsequent incubation of the Jurkat cells with ManNAz and DBCO-PEG(4)-biotin.

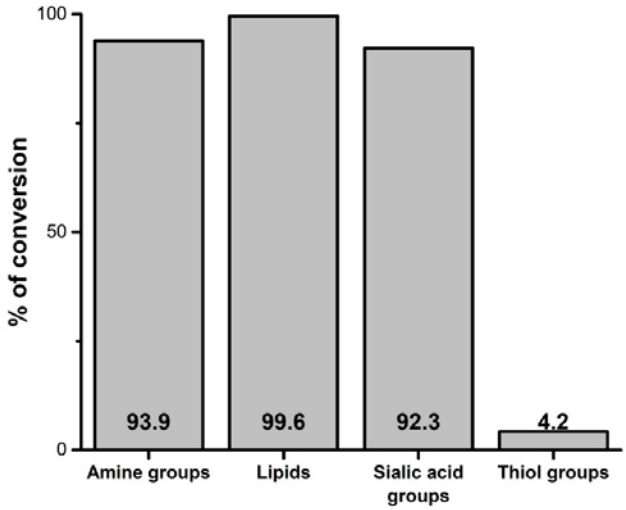

Figure 4 Relative consumption of surface biotin groups of Jurkat cells that were biotinylated at sialic acid groups, lipids, amine groups and thiol groups after incubation with NeutrAvidin coated polymersomes.

4.3.2. Confocal microscopy analysis of amine and sialic acid anchored polymersome Jurkat conjugates

The exact amount of polymersomes on the surface of Jurkat cells was investigated using confocal microscopy imaging. Therefore, the cell body was stained in cyan using CellTrace Violet, the cell membrane was stained in red using WGA-TexasRed and particles were imaged in green as a result of AlexaFluor488 fluorescence. To count the nanoparticles on the cell surface, single cell z-stacks were loaded into Imaris and analyzed for green fluorescent ellipsoids with a minimal dimension of 150nm x 150nm x 250nm (width x lenght x hight). Figure 5 and Figure 6 show 3d reconstructions of representative confocal microscopy images of NHS-biotin and sialic acid modified Jurkat cells incubated with an excess of 10,000 NeutrAvidin coated polymersomes per cell. None of the surface modification strategies resulted in polymersome internalization with a total number of 62.9 ±14.4 and 28.9 ±6.4 (n=8) surface immobilized polymersomes per cell, respectively.

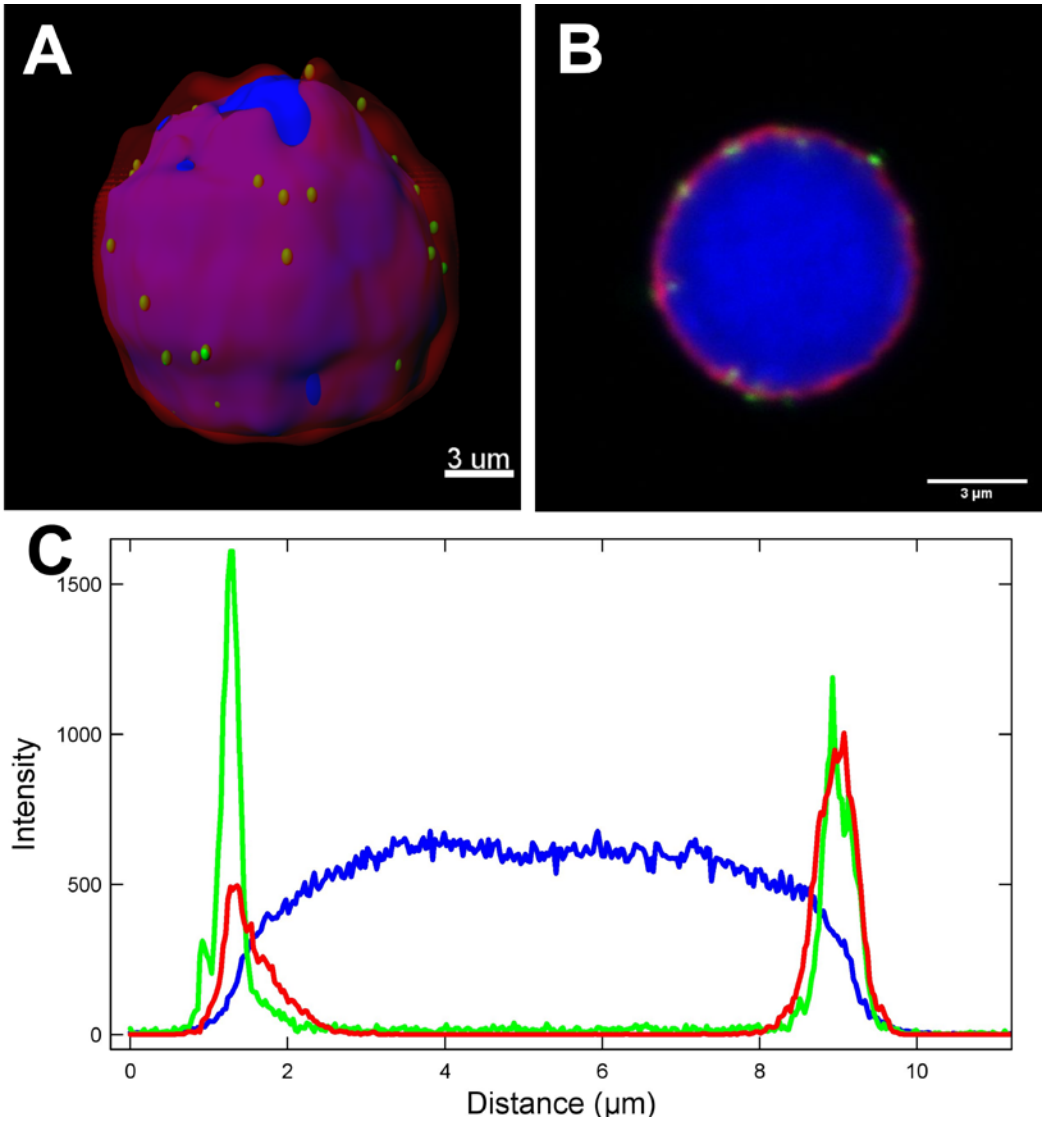

Figure 5 3D reconstruction (A), cross section (B) and intensity profile (C) of representative confocal microscopy images of NHS-biotin modified Jurkat cells incubated with an excess of 10,000 NeutrAvidin coated polymersomes per cell. Whole cell body staining was assessed using CellTrace Violet (blue) and membrane staining using WGA-TexasRed (red). Polymersome fluorescence is associated to AlexaFluor488 encapsulated into the aqueous lumen of the polymersomes (green).

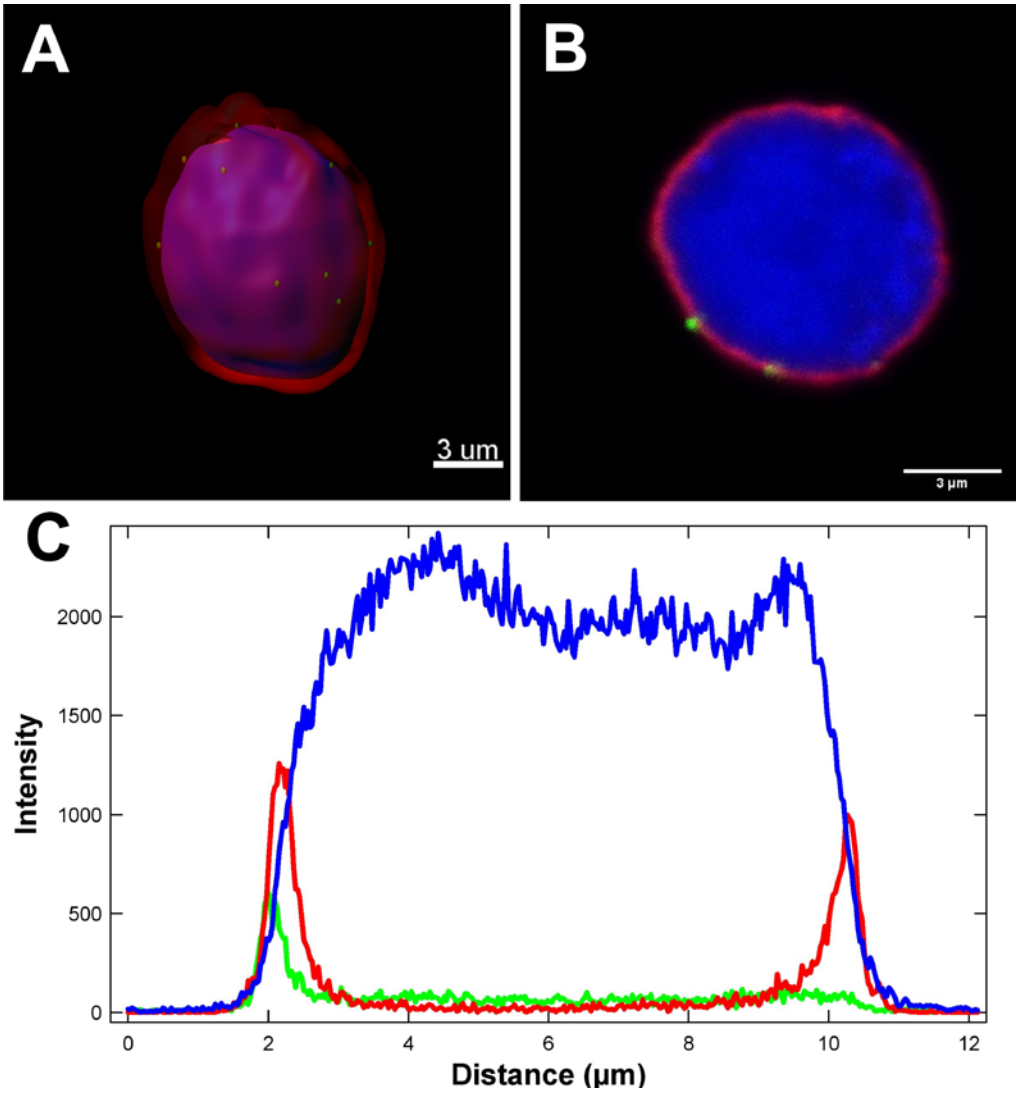

Figure 6 3D reconstruction (A), cross section (B) and of representative intensity profile (C) confocal microscopy images of sialic acid modified Jurkat cells incubated with an excess of 10,000 NeutrAvidin coated polymersomes per cell. Whole cell body staining was assessed using CellTrace Violet (blue) and membrane staining using WGA-TexasRed (red). Polymersome fluorescence is associated to AlexaFluor488 encapsulated into the aqueous lumen of the polymersomes (green).

4.3.3. Key cellular functions of amine and sialic acid anchored polymersome Jurkat conjugates

Immobilization of NeutrAvidin coated polymersomes on the surface of Jurkat cells that were biotinylated by modification of amine groups and modification of the sialic acid groups showed the highest polymersome deposition in the FACS plots. Therefore, these two conjugation strategies were further investigated regarding their cellular key functions. Cell proliferation was assessed using the cytosol dye CellTrace Violet (CTV) as previously described in Chapter 3. Figure 7B and 8B show the fluorescent decrease for unmodified Jurkat cells (black and grey) and NHS and sialic acid modified cells incubated with NeutrAvidin coated polymersomes (dark and light blue). Neither of the two conjugation strategies showed any influence on the cell proliferation behavior compared to unmodified T cells. The decrease of nanoparticle associated fluorescence shown in Figure 7A and 8A is in both cases comparable to the decrease of the CTV associated fluorescence in Figure 7B and 8B. Therefore, this decrease is rather a result of cell division then from polymersome detachment, due to an unstable conjugation.

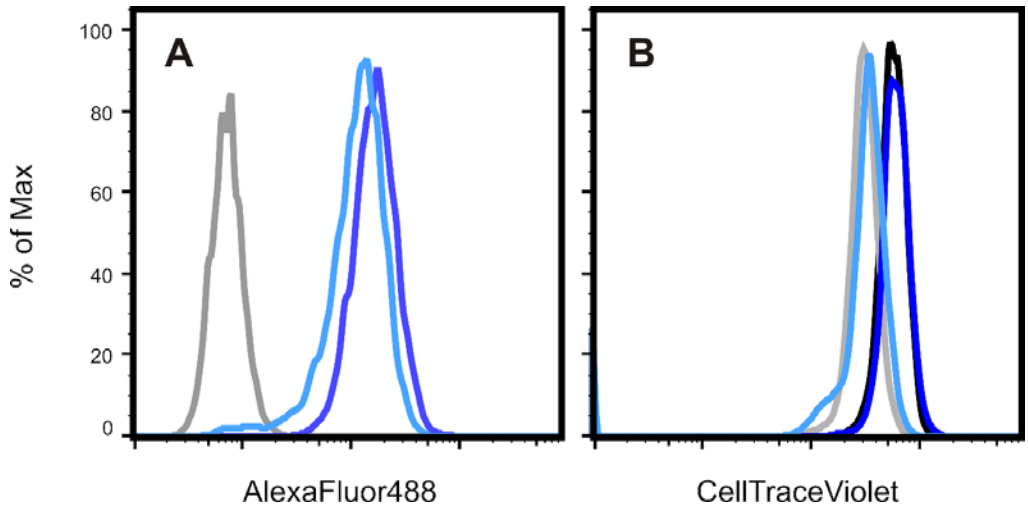

Figure 7 Histogram representing **(A)** polymersome fluorescence and **(B)** the fluorescence of a proliferation marker (CellTraceViolet) of unmodified Jurkat cells at t=0 h (black) and t=24 h (grey) and Jurkat cells incubated with NHS-biotin and NeutrAvidin coated polymersomes at t=0 h (dark blue) and t=24 h (light blue).

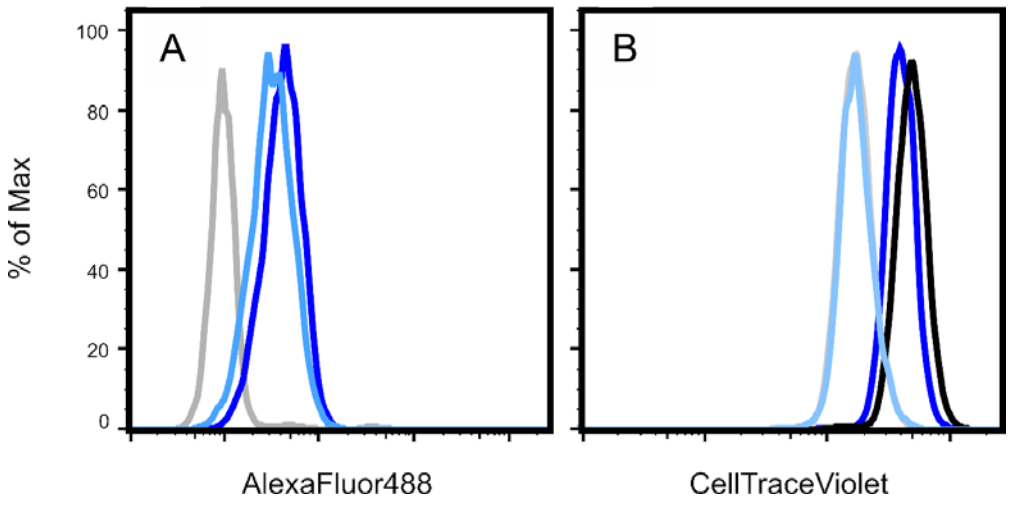

Figure 8 Histogram representing **(A)** polymersome fluorescence and **(B)** the fluorescence of a proliferation marker (CellTraceViolet) of unmodified Jurkat cells at t=0 h (black) and t=24 h (grey) and Jurkat cells incubated with ManNAz/DBCO-PEG4-biotin and NeutrAvidin coated polymersomes at t=0 h (dark blue) and t=24 h (light blue).

The viability of the polymersome cell conjugates was assessed in a DAPI/AnnexinV viability assay as previously described in Chapter 3. Figure 9 shows the decrease of cell viability upon incubation of NHS-biotin cells with an excess of 10,000 polymersomes per cell. This decrease is attributed to an increase in apoptosis, which is still a reversible process, with no difference in cell necrosis (SI Figure 1). Figure 10, in contrast, shows the decrease of cell viability upon incubation of sialic acid modified cells with an excess of 10,000 polymersomes per cell. Here, cells show an induction of apoptosis directly after polymersome conjugation. In the latter case, however, incubation of the polymersome conjugated cells in full cell culture medium for 24 h leads to a slight increase in necrosis and a drastic increase apoptosis (SI Figure 2).

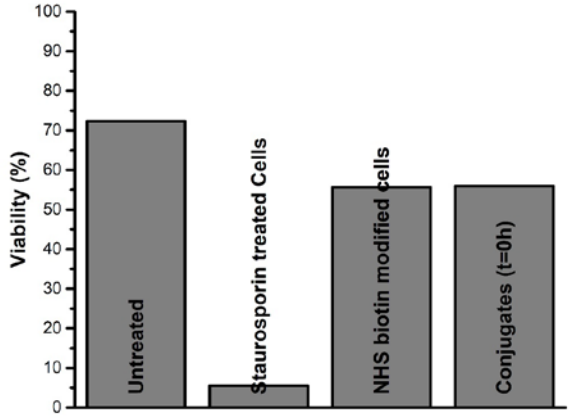

Figure 9 Bar plot representation of the viability of unmodified Jurkat cells, Jurkat cells incubated with Staurosporin, NHS-biotin modified Jurkat cells and NHS-biotin modified Jurkat cells incubated with 10,000 polymersomes per cell as determined in a AnnexinV/DAPI assay.

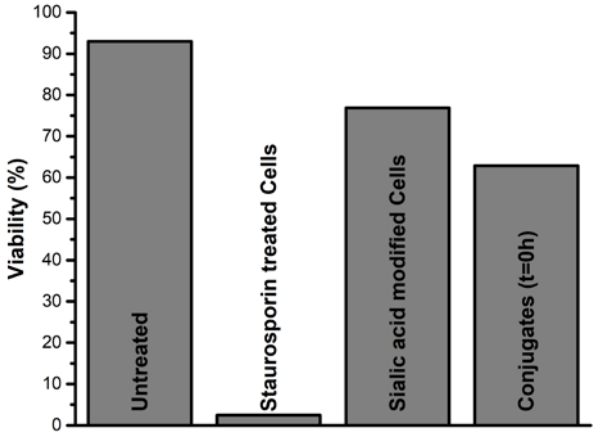

Figure 10 Bar plot representation of the viability of unmodified Jurkat cells, Jurkat cells incubated with Staurosporin, sialic acid modified Jurkat cells and sialic acid modified Jurkat cells incubated with 10,000 polymersomes per cell at t=0 h as determined in a AnnexinV/DAPI assay.

4.3.4. Cellular key functions of amine and sialic acid anchored polymersome SJL/PLP7 conjugates

The impact of polymersome T cell conjugation to amine groups and to sialic acid groups on T cell function was investigated by conjugation of polymersomes to encephalitogeneic SJL-PLP7 cells. SJL-PLP7 T cells play an important key role in the immunosurveillance of the brain by CNS infiltration in a 3-step mechanism. After adherence to the brain endothelium by ICAM-1/LFA-1 interaction, they start to crawl against the blood flow

until they undergo trans- or paracellular diapedesis through the brain endothelium. By sampling the perivascular space for antigen presenting cells, SJL-PLP7 cells can recognize disease related antigens. After recognition of an antigen, these cells get reactivated and migrate further to the brain parenchyma, where they release pro-inflammatory cytokines in order to recruit a variety of other T cells to the brain [9]. SJL-PLP7 are of particular interest as this specific subset of T cells be used to efficiently delivery drugs across the BBB to the brain parenchyma if decorated with polymersomes. (Figure 11)

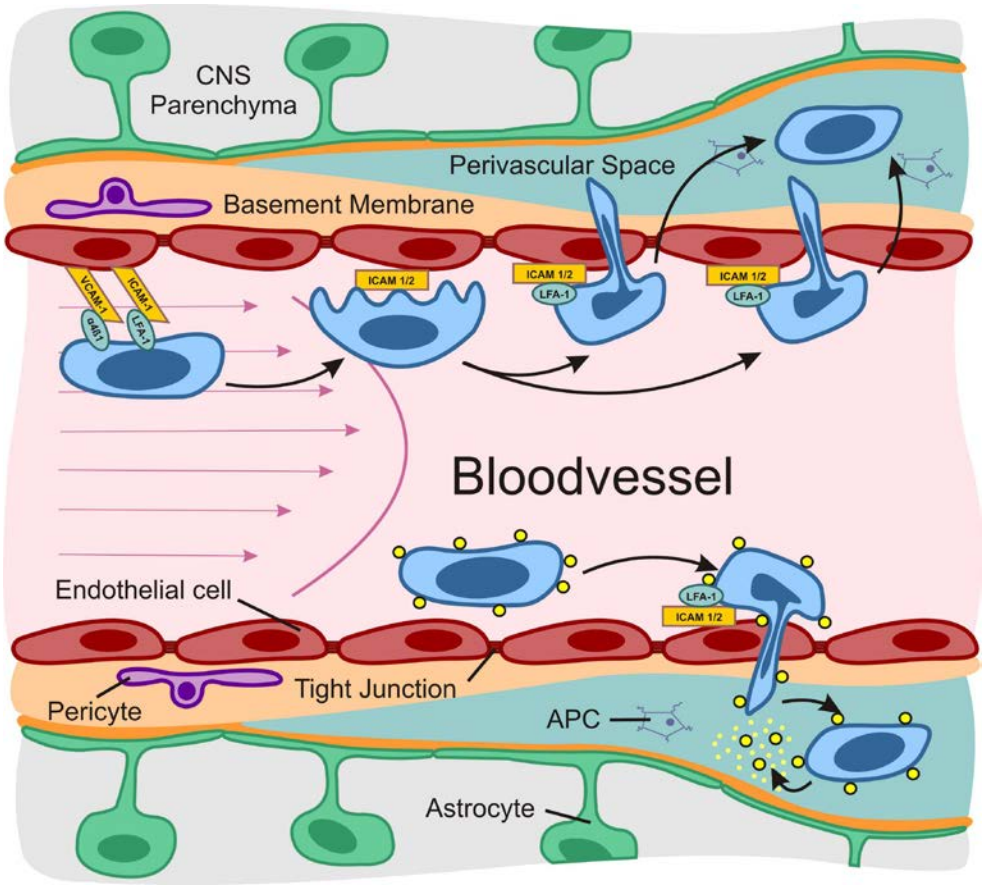

Figure 11 Migration of CD4+ T cells at the brain endothelium. T cells arrest at the endothelium as result of integrin recognition of ICAM-1 and VCAM-1. After polarization T cells crawl against the blood flow and undergo trans- or paracellular diapedesis to sample the perivascular space for antigen presenting cells (APCs). Drug loaded nanoparticles can be immobilized on the surface of these T cells in a cellular backpack approach to be carried across the BBB. Active or passive triggering release mechanisms can be used to release the NP cargo in the perivascular space or the CNS parenchyma.

Jurkat cells represent an immortalized cell line, which lacks most surface markers present on these primary T cells. Therefore, the total count of surface amine and thiol groups is significantly lower than for SJL-PLP7 cells, which expose ca. 1.2 $x10^6$ amine and 0.2 $x10^6$ thiol groups on their surface (Figure 12 + SI Table 5-6). As biotinylation with biotin-XX-sSE proceeds with 21.7% and with biotin-BMCC with 51.5% for SJL-PLP7 cells, this results in a total number of ca. 250,000 amine anchored biotin groups (5 times more than for Jurkat cells) and 100,000 thiol anchored biotin groups (10 times more than for Jurkat cells).

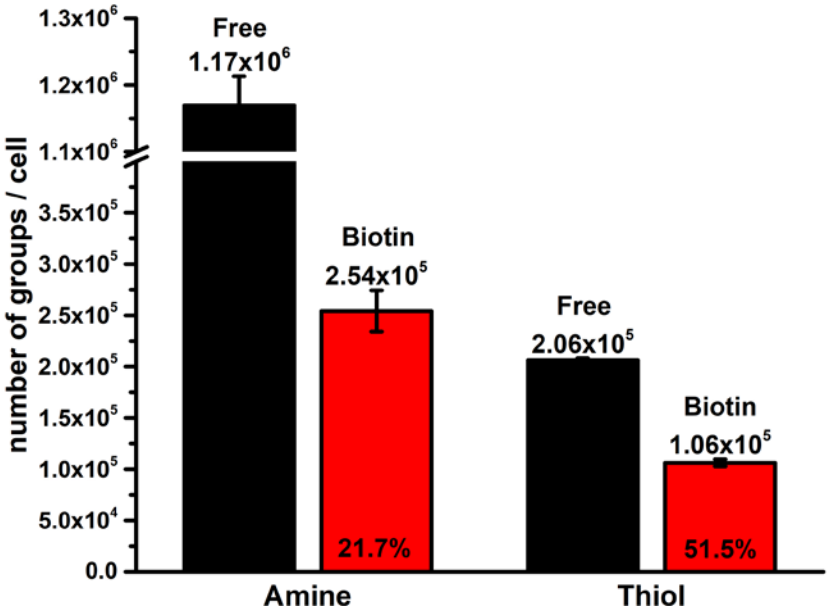

Figure 12 Column plot representing the total number of reactive surface groups (black) and biotinylated surface groups (red) on the surface of SJL-PLP7 cells determined by quantitative flow cytometry (n=3).

While conjugation of polymersomes to Mal-biotin modified SJL-PLP7 cells still did not result into a significant increase in polymersome associated fluorescence, conjugation to NHS-biotin modified SJL-PLP7 cells resulted into an increase in polymersome associated fluorescence comparable to the polymersome conjugation to NHS-biotin modified Jurkat cells before as shown in Figure 13.

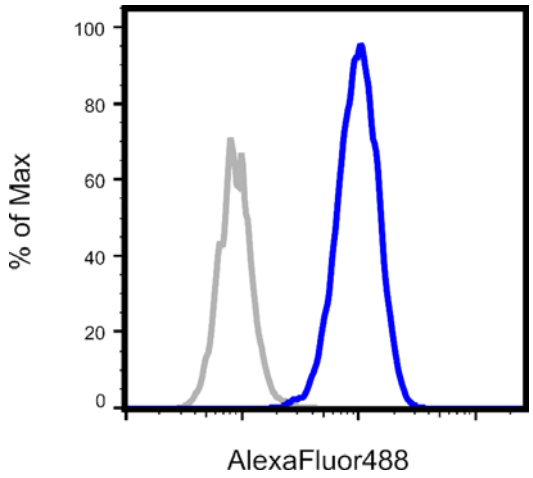

Figure 13 Histogram representing polymersome fluorescence of unmodified SJL/PLP7 cells (grey) and NHS-biotin modified SJL/PLP7 cells incubated with NeutrAvidin coated polymersomes (blue).

As SJL-PLP7 cells lose their encephalitogeneic properties latest 4 days after restimulation, primary T cells could only be incubated with ManNAz for a maximum of 48 h. Consequently, metabolic modification of SJL-PLP7 cells with azide modified sugars results in a lower amount of azide groups on the surface of SJL-PLP7 cells compared to Jurkat cells. Figure 14 shows that this also leads to a significant decrease of polymersome associated fluorescence for biotinylated cells incubated with the same excess of NeutrAvidin coated polymersomes.

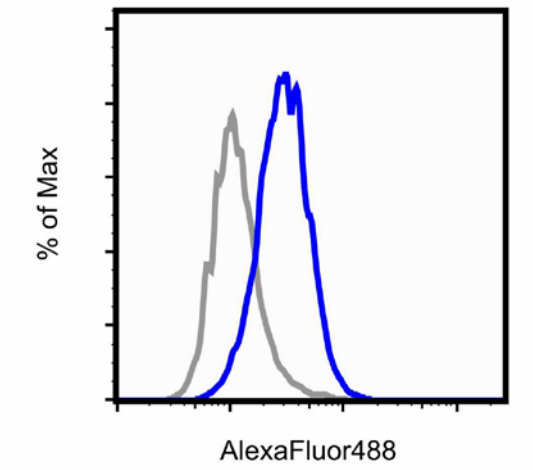

Figure 14 Histogram representing polymersome fluorescence of unmodified SJL/PLP7 cells (grey) and sialic acid modified SJL/PLP7 cells incubated with NeutrAvidin coated polymersomes (blue).

As SJL-PLP7 cells will be utilized in a functional assay after polymersome conjugation, viability of these cells is determined directly after nanoparticle conjugation as well as after 24 h. While amine anchored polymersome conjugation to SJL-PLP7 cells still induces apoptosis, this effect seems to be reversible upon incubation of the T cells in full cell culture medium over a time period of 24 h (Figure 15A + SI Figure 3). The conjugation of polymersomes to sialic acid residues of the T cells, however, not only induce apoptosis directly after conjugation of the polymersomes to the cells, but also significantly induced necrosis of the cells within 24 h (Figure 15B + SI Figure 4). For this reason, only the amine anchored conjugation can be seen as suitable for the biotin-NeutrAvidin mediated conjugation of polymersomes to primary T cells.

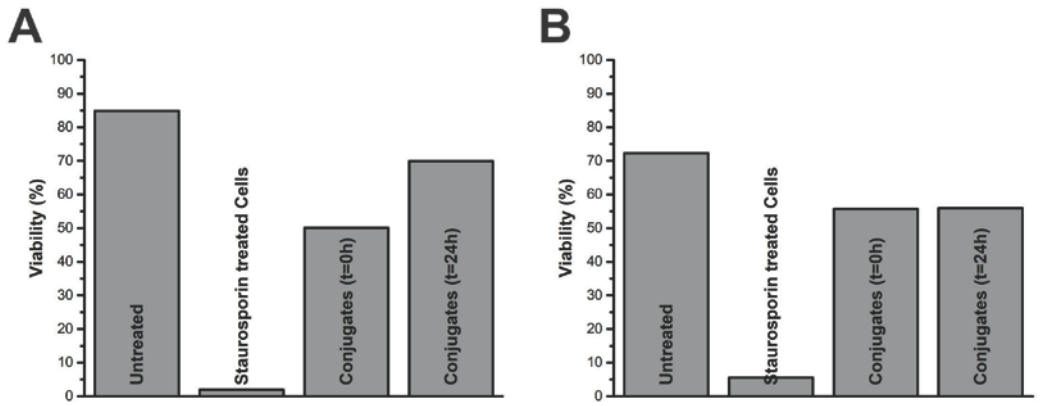

Figure 15 Bar plot representation of the viability of unmodified SJL-PLP7 cells, SJL-PLP7 cells incubated with Staurosporin and (A) NHS-biotin modified SJL-PLP7 cells and (B) sialic acid modified SJL-PLP7 that were incubated with 10,000 NeutrAvidin coated polymersomes per cell after t=0 h and t=24 h as determined in an AnnexinV/DAPI assay.

Thus only the ability of NHS-amine modified SJL-PLP7 cells conjugated to polymersomes to bind to brain endothelium via LFA-1/ICAM-1 interaction was assessed. This assessment was performed qualitatively in an ICAM-binding assay. Therefore, un-/modified T cells were incubated on a glass slide coated with protein A and ICAM/DNER-FC antibody chimeras. The combination of protein A and the ICAM- or DNER chimera coating hereby ensures the correct directional immobilization of the proteins to enable T-cell binding to the modified glass substrate. The binding of the polymersome T cell conjugates was shown to be specific to ICAM-1 over the control protein DNER and showed no significant difference in ICAM-1 or DNER binding compared to unmodified control cells as shown in Figure 16.

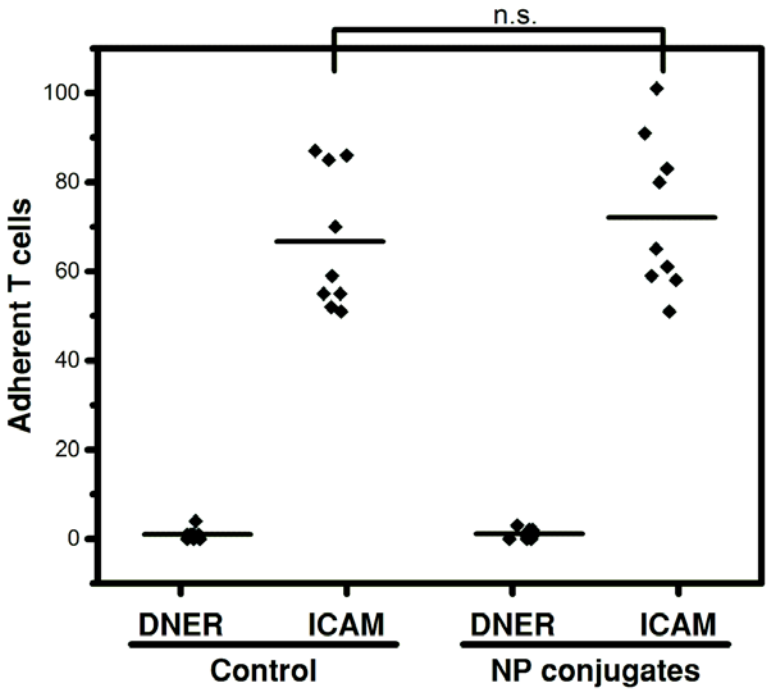

Figure 16 T-cell binding to ICAM-1. Cell count of a binding assay on ICAM-1 and DNER coated wells for unmodified control cells and polymersome T-cell conjugates performed at RT for 30 min under moderate shear conditions. Each dot represents one cell count from the diagonal of a 10 mm x 10 mm / 10 divisions counting reticle using a 20x objective. Each well was counted at 3 different positions. The horizontal bar represents the mean over all counts. The P-value was determined by a *t-test* (ns: P>0.05).

4.3.5. Identification of the surface proteins anchoring the NHS-biotin mediated conjugation of polymersomes to Jurkat cells

Compared to the conjugation of polymersomes to lipid or sialic acid modified cells, the conjugation of polymersomes to NHS-biotin modified Jurkat cells is not targeting specific cellular targets, but happens rather unspecifically at a variety of different proteins on the cell surface. To identify these proteins as well as their biological role, Jurkat cells were conjugated to model polystyrene nanoparticles via a reductive cleavable linker (Scheme 1).

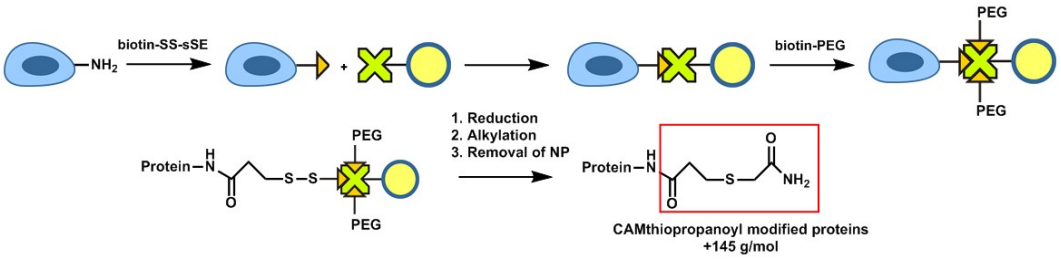

Scheme 1 Tagging of surface proteins conjugating to Fluospheres. NeutrAvidin coated Fluospheres are conjugated to NHS-SS-biotin modified Jurkat cells. Residual binding sites of the NeutrAvidin are blocked by biotin-PEG (2 kDa). Cells are lysed in anionic lysis buffer and particles are separated from the debris by centrifugation. Cell surface proteins are cleaved off the particles surface by reduction with DTT and the reduction is fixed using iodoacetamide. Proteins are digested using Trypsin and the resulting CAMthiopropanoyl tag is identified by LC-MSMS.

After nanoparticle cell conjugation, cells can be lysed to enable the purification of the nanoparticles with the conjugating proteins covalently captured on their surface. Cleavage of these proteins from the nanoparticles was performed using DTT followed by alkylation of the reduced thiol groups with iodoacetamide tagging these proteins with a distinctive CAM-thiopropanoyl modification. This modification enables the precise identification of these proteins by identification of the trypsinated cleavage products by LC-MSMS. Table 1 summarizes the identified membrane proteins with a CAM-thiopropanoyl tag, including the number of specific peptides found for the corresponding protein and the biological function. Generally, proteins identified to anchor the nanoparticle conjugation are rather abundant on the cell surface while some of the proteins are indicators for cellular stress, for instance heat shock proteins and the voltage dependent anion channels. Strikingly, also α4ß1 integrin was found to conjugate to the nanoparticles. Closely related to LFA-1 (also called α4ß2), this integrin is involved in the attachment of the T cells to the brain endothelium via the inflammatory marker VCAM-1. However, as seen from the confocal microscopy images above, only a small percentage of the cell surface is coated with nanoparticles. Thus, the ratio of free α4ß1 integrin to α4ß1 integrin conjugating to the nanoparticles may be relatively high and therefore nanoparticle conjugation to T cells may not hinder the migration of surface modified T cells to the brain parenchyma.

Table 1 Surface proteins of NHS-SS-biotin modified Jurkat cells conjugating to NeutrAvidin coated Fluospheres identified by LC-MSMS

Protein	***Accession Nbr***	***Mw/kDa***	***Specific peptide counts***	***Function***
Glyceraldehyde-3-phosphate dehydrogenase	P68104	50	27	Th1 cytokine production
HSP 90-beta	P08238	83	21	HSP
Cofilin-1	P23528	19	14	Cell polarization
HSC 71 kDA protein	P11142	71	11	HSP
4F2 surface antigen	F5GZS6 (+1)	65	6	Transport activity of LAT2
V-dependent anion-selective channel protein	P21796	31	6	Cell volume regulation and apoptosis
Integrin beta-1	P05556	88	5	Integrin for VCAM-1 binding
Isoform 2 of HSP 90-alpha	P07900-2	98	5	HSP
CD2	P06729	39	5	T-cell adhesion
Tetraspanin	A6NMH8	30	5	Regulates ligand induced NOTCH activity
ATP synthase subunit alpha	P25705	60	4	ATP Synthesis
CD59	A0A2U3TZ	13	4	Inhibitor of membrane attack complex
HLA class 1 histocompatibility antigen	Q5SRN5	41	4	MHC-1 protein
Integrin alpha-4	P13612	115	4	Integrin for ICAM-1 binding

4.4. Conclusions

NeutrAvidin coated polymersomes were immobilized on the surface of T cells that were biotinylated using different surface chemistries. Comparison of the different chemistries revealed that biotinylation on cell surface amine groups and cell surface sialic acid residues worked equally well for polymersome conjugation on Jurkat cells. Biotinylation on cell surface thiol groups or lipids, however, did not result in significant immobilization of NeutrAvidin coated polymersomes upon incubation with the cells. The amine anchored conjugation strategy did not impact cellular key functions. However, a slight decrease in viability was observed for the sialic acid anchored conjugation strategy. Thus, these two conjugation strategies were transferred to the use of primary CD4+ T cells. Here, the amine anchored conjugation strategy showed to be superior towards the sialic acid anchored conjugation strategy in terms of nanoparticle immobilization and long term viability of the conjugates. Finally, anchoring proteins for this conjugation strategy were identified for the case of Jurkat cells using novel cell surface capture methods followed by identification using LC-MSMS techniques. The results, however, revealed that nanoparticle conjugation was mainly occurring on stress related proteins or proteins that are relevant for the cell diapedesis on the level of the brain endothelium. For this reason, polymersome-T-cell conjugates have to be investigated in further studies regarding their *in vitro* diapedesis properties before investigation or application in *in vivo* models.

4.5. References

1. Cheng, H., et al., *Nanoparticulate Cellular Patches for Cell-Mediated Tumoritropic Delivery.* ACS Nano, 2010. **4**(2): p. 625-631.
2. Xu, M., et al., *Mesenchymal stem cells-curcumin loaded chitosan nanoparticles hybrid vectors for tumor-tropic therapy.* International Journal of Biological Macromolecules, 2019. **134**: p. 1002-1012.
3. Vabbilisetty, P., et al., *Chemical Reactive Anchoring Lipids with Different Performance for Cell Surface Re-engineering Application.* ACS Omega, 2018. **3**(2): p. 1589-1599.
4. Wang, H.-Y., et al., *Enhanced cell membrane enrichment and subsequent cellular internalization of quantum dots via cell surface engineering: illuminating plasma membranes with quantum dots.* Journal of Materials Chemistry B, 2016. **4**(5): p. 834-843.

5. Zeng, Y., et al., *High-efficiency labeling of sialylated glycoproteins on living cells.* Nature methods, 2009. **6**(3): p. 207-209.
6. Mahal, L.K., K.J. Yarema, and C.R. Bertozzi, *Engineering Chemical Reactivity on Cell Surfaces Through Oligosaccharide Biosynthesis.* Science, 1997. **276**(5315): p. 1125-1128.
7. Yang, Y., et al., *Enhanced imaging of glycan expressing cancer cells using poly(glycidyl methacrylate)-grafted silica nanospheres labeled with quantum dots.* Analytica Chimica Acta, 2020. **1095**: p. 138-145.
8. Bernardin, A., et al., *Copper-Free Click Chemistry for Highly Luminescent Quantum Dot Conjugates: Application to in Vivo Metabolic Imaging.* Bioconjugate Chemistry, 2010. **21**(4): p. 583-588.
9. Engelhardt, B. and R.M. Ransohoff, *Capture, crawl, cross: the T cell code to breach the blood–brain barriers.* Trends in Immunology, 2012. **33**(12): p. 579-589.

4.6. Supporting Information

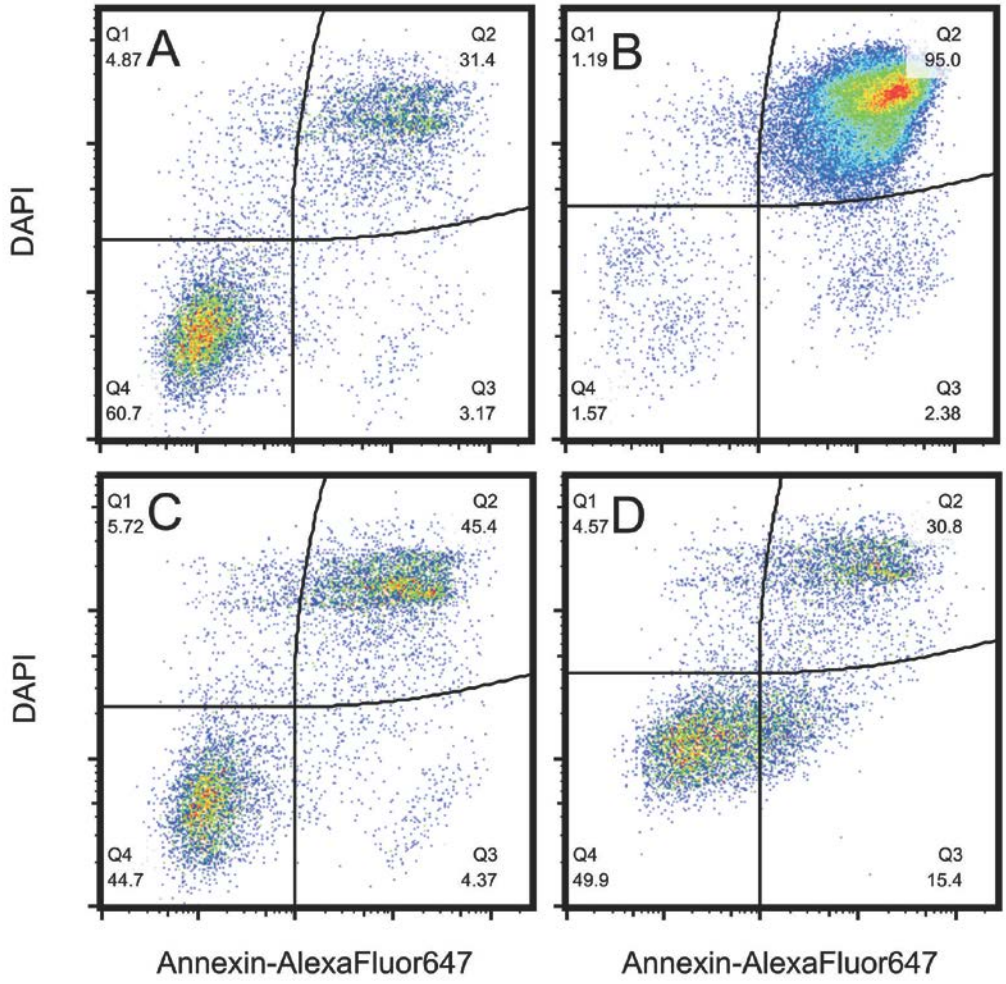

SI Figure 1 Viability assay of (A) unmodified Jurkat cells, (B) Jurkat cells incubated with Staurosporin (24 h) and (C) NHS-biotin modified Jurkat cells (D) incubated with an excess of 10000 NPs/cell NeutrAvidin coated polymersomes. DAPI fluorescence is associated to cell necrosis, Alexa647 fluorescence to cell apoptosis.

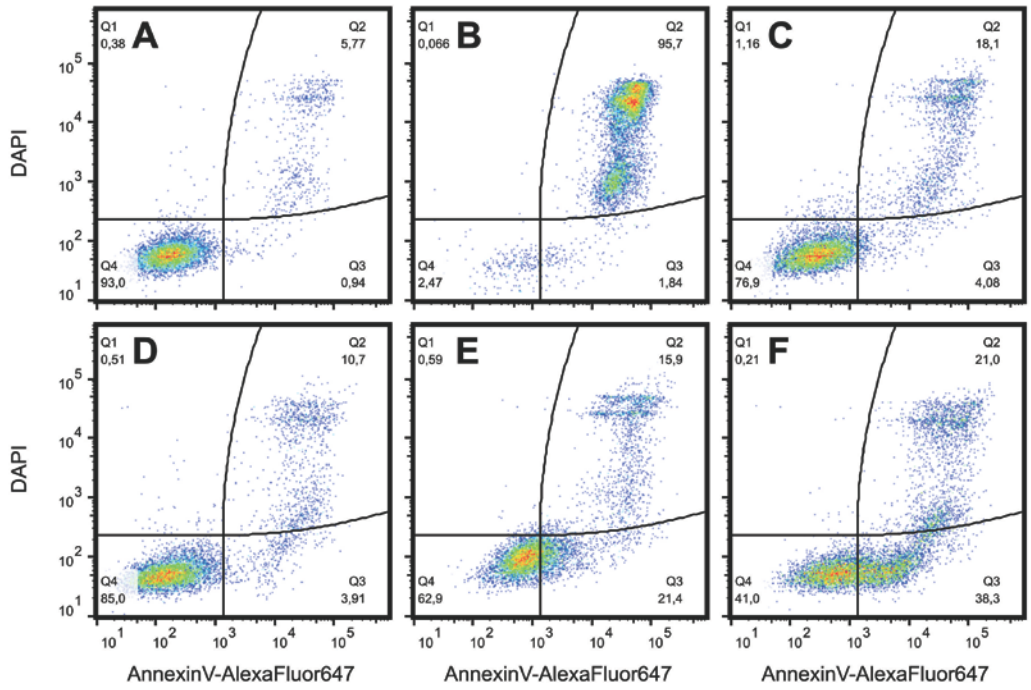

SI Figure 2 Viability assay of (A) unmodified Jurkat cells, (B) Jurkat cells incubated with Staurosporin (24 h), sialic acid modified Jurkat cells after (C) t=0 h and (D) t=24 h and sialic acid modified Jurkat cells incubated with an excess of 10000 NPs/cell NeutrAvidin coated polymersomes at (C) t=0 h and (D) t=24 h. DAPI fluorescence is associated to cell necrosis, Alexa647 fluorescence to cell apoptosis.

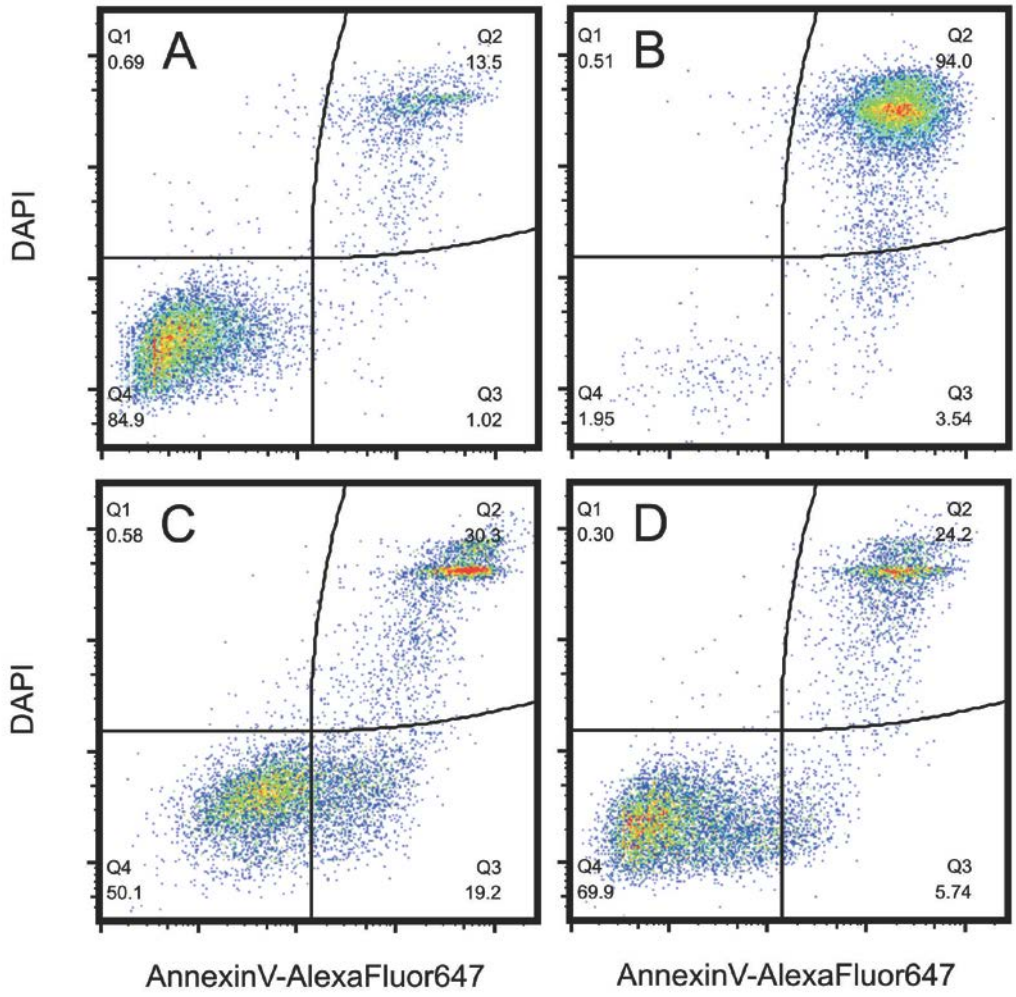

SI Figure 3 Viability assay of (A) unmodified SJL-PLP7 cells, (B) SJL-PLP7 cells incubated with Staurosporin (24 h) and NHS-biotin modified SJL-PLP7 cells incubated with an excess of 10,000 NPs/cell NeutrAvidin coated polymersomes at (C) t=0 h and (D) t=24 h. DAPI fluorescence is associated to cell necrosis, Alexa647 fluorescence to cell apoptosis.

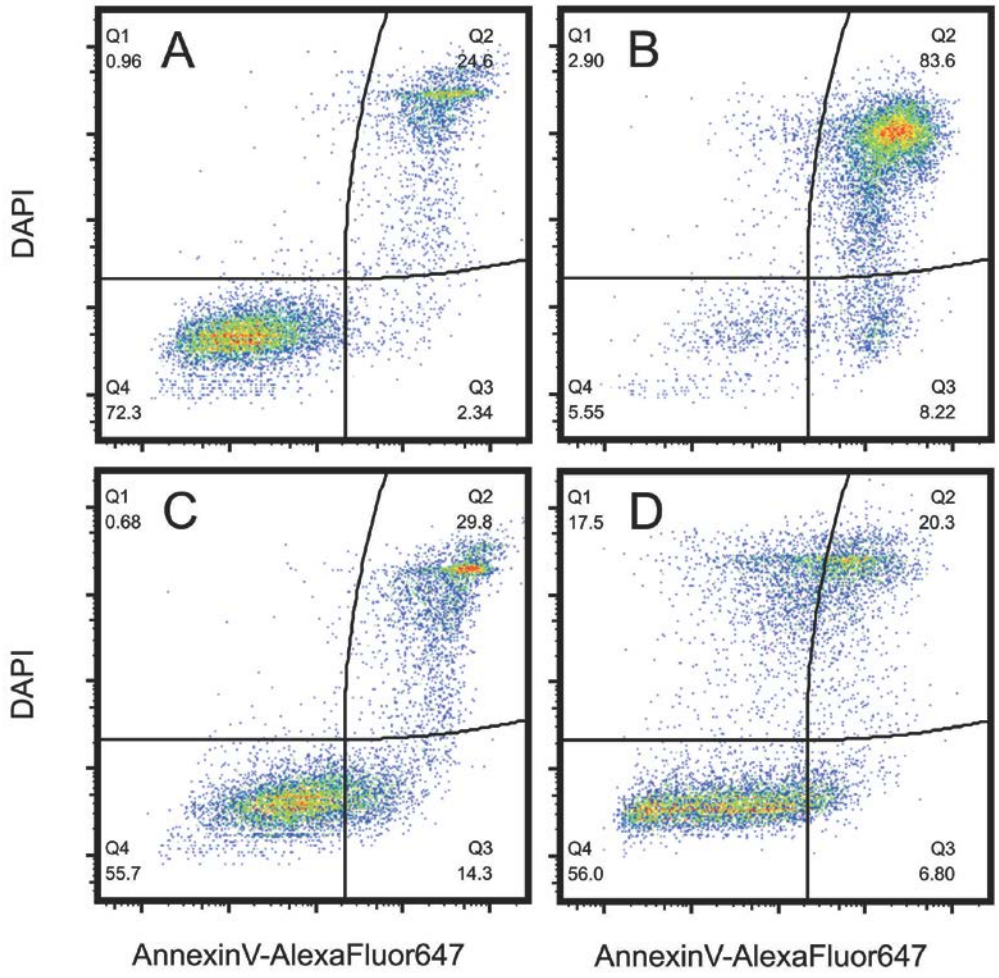

SI Figure 4 Viability assay of (A) unmodified SJL-PLP7 cells, (B) SJL-PLP7 cells incubated with Staurosporin (24 h) and sialic acid modified SJL-PLP7 cells incubated with an excess of 10,000 NPs/cell NeutrAvidin coated polymersomes at (C) t=0 h and (D) t=24 h. DAPI fluorescence is associated to cell necrosis, Alexa647 fluorescence to cell apoptosis.

SI Table 1 Channel values and MESF values of the Quantum bead calibration and the AlexaFluor488 associated fluorescence of unmodified Jurkat cells (control) and Jurkat cells incubated with NHS-AlexaFluor488 before (amine 1-3) and after (biotin1-3) NHS-biotin modification.

Sample name	*Channel value*	*MESF value*
Calibration Beads Blank	0.23	-
Calibration Beads 1	1.09	3179
Calibration Beads 2	5.84	22718
Calibration Beads 3	19.50	95426
Calibration Beads 4	62.91	333766
Control	0.48	1262
Amine 1	38.51	197915
Amine 2	37.15	189879
Amine 3	36.46	185819
Ø Amine-Control	-	189942
Biotin 1	10.62	44825
Biotin 2	11.45	48887
Biotin 3	11.23	47806
Ø Biotin-Control	-	45698
Ø (Amine-Control)-(Biotin-Control)	-	144032

SI Table 2 Channel values and MESF values of the Quantum bead calibration and the AlexaFluor488 associated fluorescence of unmodified Jurkat cells (control) and Jurkat cells incubated with Mal-AlexaFluor488 before (thiol 1-3) and after (biotin 1-3) BMCC-biotin modification.

Sample name	*Channel value*	*MESF value*
Calibration Beads Blank	0.12	-
Calibration Beads 1	0.69	3179
Calibration Beads 2	3.75	22718
Calibration Beads 3	12.39	95426
Calibration Beads 4	41.09	333766
Control	0.27	1110
Thiol 1	5.70	36550
Thiol 2	5.66	36257
Thiol 3	4.64	36110
Ø Thiol-Control	-	35196
Biotin 1	3.96	24081
Biotin 2	3.99	24290
Biotin 3	3.84	23247
Ø Biotin-Control	-	22763
Ø (Thiol-Control)-(Biotin-Control)	-	12433

SI Table 3 Channel values and MESF values of the Quantum bead calibration and the AlexaFluor488 associated fluorescence of unmodified Jurkat cells (control), Jurkat cells incubated with Streptavidin-AlexaFluor488 conjugate (Streptavidin 1-3) and Jurkat cells incubated with DSPE-PEG-biotin and Streptavidin-AlexaFluor488 conjugate (lipid 1-3).

Sample name	*Channel value*	*MESF value*
Calibration Beads Blank	0.13	-
Calibration Beads 1	0.68	3179
Calibration Beads 2	3.71	22718
Calibration Beads 3	12.27	95426
Calibration Beads 4	40.76	333766
Control	0.26	1083
Streptavidin 1	1.50	8037
Streptavidin 2	1.48	7914
Streptavidin 3	1.43	7609
Ø Streptavidin -Control	-	6770
Lipid 1	180.55	1927294
Lipid 2	181.98	1944765
Lipid 3	176.75	1880965
Ø Lipid-Control	-	1916592

SI Table 4 Channel values and MESF values of the Quantum bead calibration and the AlexaFluor488 associated fluorescence of unmodified Jurkat cells (control) and sialic acid modified Jurkat cells incubated with Streptavidin-AlexaFluor488 conjugate (sialic acid 1-3).

Sample name	*Channel value*	*MESF value*
Calibration Beads Blank	0.10	-
Calibration Beads 1	0.32	3179
Calibration Beads 2	1.68	22718
Calibration Beads 3	5.48	95426
Calibration Beads 4	18.16	333766
Sialic acid 1	307.10	9408569
Sialic acid 2	307.58	9425623
Sialic acid 3	307.13	9409635
Ø Sialic acid	-	9414609

SI Table 5 Channel values and MESF values of the Quantum bead calibration and the AlexaFluor488 associated fluorescence of unmodified SJL-PLP7 cells (control) and SJL-PLP7 cells incubated with NHS-AlexaFluor488 before (amine 1-3) and after (biotin1-3) NHS-biotin modification.

Sample name	*Channel value*	*MESF value*
Calibration Beads Blank	0.17	-
Calibration Beads 1	0.72	3179
Calibration Beads 2	3.68	22718
Calibration Beads 3	11.88	95426
Calibration Beads 4	39.71	333766
Control	0.36	1.471
Amine 1	107.29	1143242
Amine 2	113.51	1221042
Amine 3	107.77	1149219
Ø Amine-Control	-	1169697
Biotin 1	89.11	920322
Biotin 2	90.35	935301
Biotin 3	87.04	895396
Ø Biotin-Control	-	915535
Ø (Amine-Control)-(Biotin-Control)	-	254161

SI Table 6 Channel values and MESF values of the Quantum bead calibration and the AlexaFluor488 associated fluorescence of unmodified SJL-PLP7 cells (control) and SJL-PLP7 cells incubated with Mal-AlexaFluor488 before (thiol 1-3) and after (biotin 1-3) BMCC-biotin modification.

Sample name	*Channel value*	*MESF value*
Calibration Beads Blank	0.13	-
Calibration Beads 1	0.71	3179
Calibration Beads 2	3.71	22718
Calibration Beads 3	12.28	95426
Calibration Beads 4	41.00	333766
Control	0.36	1505
Thiol 1	25.80	208246
Thiol 2	25.89	209085
Thiol 3	25.50	205454
Ø Thiol-Control	-	206090
Biotin 1	13.38	97611
Biotin 2	14.19	104461
Biotin 3	13.93	102256
Ø Biotin-Control	-	99938
Ø (Thiol-Control)-(Biotin-Control)	-	106152

5. Conclusions and Perspectives

This work represents a recent review on cell mediated delivery concepts to facilitate the delivery of drugs across biological barriers, emphasizing recent developments, advances and drawbacks (Chapter 1) and addresses three of the major tasks in the field of cell mediated drug delivery that were hitherto unaddressed, namely the use of cells that show antigen independent delivery properties (Chapter 2), the conjugation of modern nanoparticle architectures in form of polymersomes (Chapter 3) and the comparison of different surface chemistries in terms of nanoparticle immobilization as well as cellular key functions (Chapter 4). In fact, Chapter 3 represents the first successful controlled conjugation of polymersomes onto the surface of circulatory cells in significant amounts up to date and addresses the drawbacks for the surface immobilization of this particular nanoparticle architecture.

The conjugation of polymersomes onto the surface of CD4+ T_{EM} cells opens up promising opportunities as a universal drug delivery tool across the BBB. The possibility of polymersomes to entrap both hydrophilic and hydrophobic drugs, as well as macromolecules, therefore, allows the exploration of a great variety of currently overlooked drug candidates acting in the brain parenchyma. As up to 25% of a hydrophilic small-molecule cargo was shown to leak from the vesicle lumen over a time period of 2 days, non-cytotoxic drugs are of particular interest for the cell mediated delivery using polymersome decorated CD4+ T cells avoiding a decrease in cell viability of the polymersome conjugated cells due to a constant local release of the encapsulated drug at the T-cell surface. Especially macromolecules like cytokines and therapeutic antibodies fulfill this criterium and their delivery could be explored in context of autoimmune diseases like Multiple Sclerosis or its animal model, EAE, where antibody-inhibition of LINGO-1 could lead to remyelation of axons or in context of tumor metastases in the brain where delivery of TRAIL could lead to the apoptosis of metastatic tumor cells that are located in close contact to the brain endothelium. Additional co-delivery of glucocorticosteroids like cortison could meanwhile provide anti-inflammatory properties restoring BBB functions.

Nevertheless, the drug delivery potential of this delivery system and the efficacy of the delivered drugs have to be thoroughly investigated *in vitro* and *in vivo* for each disease model before use, as both, pathogenic alterations of the BBB as well as leaking residues of encapsulated drugs might alter the brain migration properties of the T cells. This

alteration might be beneficial for the treatment in case that T cell trafficking is increased for example in autoimmune diseases or detrimental for the treatment in case that T cell trafficking is decreased for example as a result of immunosuppression in the tumor microenvironment.

Markus Schuster

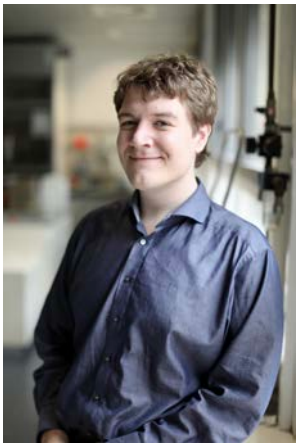

Chemin des Peupliers 6

1028 Preverenges, CH

+41 78 401 30 67

markus.schuster@epfl.ch (professional)

markus.schuster4@gmx.de (private)

Education

Ecole Polytechnique Federale de Lausanne (EPFL)

PhD in Material Science (2016 – Present)

Friedrich-Alexander University Erlangen-Nürnberg (FAU)

Master of Science in Molecular Science (2013-2015)

Friedrich-Alexander University Erlangen-Nürnberg (FAU)

Bachelor of Science in Molecular Science (2011-2013)

Maristenkolleg Mindelheim

Abitur (2011)

Core Experience

Polymers Laboratory (EPFL)

Cell mediated Drug Delivery across the blood-brain barrier (PhD thesis)

PhD thesis supervisor: Prof. Dr. Harm-Anton Klok

- *Preparation and in-vitro evaluation of polymersome conjugated T cells for drug delivery to the brain parenchyma.*
- *Preparation and in-vivo evaluation of nanoparticle conjugated T cells as model system for drug delivery to the brain parenchyma.*
- *Identification of T-cell surface proteins capable of non-/covalent nanoparticle immobilization*
- *Projects were carried out in collaboration with the Theodor Kocher Institute (University of Bern) for neuroimmunobiology (Group of Prof. Dr. Engelhardt) in context of the highly multidisciplinary MSCA-ITN "BtRAIN"* – European Brain Barriers Training Network (H2020-MSCA-ITN-2016, n 675619).

Gmeiner Laboratory (FAU)

Towards the synthesis of novel Almorexant based Orexin-receptor agonists (Master thesis)

Master thesis supervisor: Prof. Dr. Peter Gmeiner

- *Structure-Activity-Relationship (SAR) based design of potential Orexin-receptor agonists.*
- *Organic synthesis and isolation of potential Orexin-receptor agonists with multiple chiral centers*

Technical Skills

Synthetic skills

Organic Synthesis ♦ Polymer Chemistry ♦ Radiochemistry ♦ Bioconjugate Chemistry ♦ Nanoparticle/Polymersome/Liposome Preparation, Formulation and Modification ♦ High Performance Liquid Chromatography (HPLC) ♦ Nuclear Magnetic Resonance (NMR) ♦ Mass Spectrometry (MS) ♦ UV-Vis ♦ Dynamic Light Scattering (DLS) ♦ Size Exclusion Chromatography (SEC)

Life science skills

T-cell isolation ♦ T-cell restimulation ♦ Brain Endothelial Cell Isolation ♦ Cell culture ♦ Proliferation Assays ♦ Viability Assay ♦ Binding Assay ♦ SDS-Gel Electrophoresis ♦ BCA Assay ♦ Flow Cytometry ♦ Confocal Microscopy ♦ Cryo-Sectioning ♦ Immunofluorescence Staining ♦ Fluorescence Widefield Microscopy

IT Skills

MicrosoftOffice13 ♦ ChemDrawBio ♦ Autodesk Inventor Professional ♦ Endnote ♦ Adobe InDesign ♦ CorelDRAW ♦ ImageJ ♦ Imaris ♦ Origin Pro ♦ MestReNova ♦ TopSpin ♦ Kaluza ♦ Attune NxT Software ♦ Flowjo ♦ Zeiss ZEN ♦ NIS-Elements

Languages

German (mother tongue) ♦ English (proficient)

Accredited courses for Soft Skills

Using Vocal Techniques to Teach Effectively ♦ Body Language ♦ Resolving Conflicts

Scientific Publication

Currently N/A